Advanced application of phosphate glass optical fibres in photonics and biophotonics

ScuDo

Scuola di Dottorato ~ Doctoral School

WHAT YOU ARE, TAKES YOU FAR

Doctoral Dissertation

Doctoral Program in Materials Science and Technology (30^{th}cycle)

Advanced applications of phosphate glass optical fibres in photonics and biophotonics

By

Edoardo Ceci Ginistrelli

******

Supervisor(s):

Prof. Daniel Milanese, Supervisor

Dr. Joris Lousteau, Co-Supervisor

Doctoral Examination Committee:

Prof. Amiel A. Ishaaya, Referee, Ben Gurion University of the Negev, Israel

Prof. Kay Schuster, Referee, Institute of Photonic Technologies, Jena, Germany

Prof. Stefano Taccheo , Swansea University, United Kingdom

Prof. Milena Salvo, Politecnico di Torino, Italy

Prof. Davide Janner, Politecnico di Torino, Italy

Politecnico di Torino

2018

Declaration

I hereby declare that, the contents and organization of this dissertation constitute my own original work and do not compromise in any way the rights of third parties, including those relating to the security of personal data.

Edoardo Ceci Ginistrelli
2018

* This dissertation is presented in partial fulfillment of the requirements for **Ph.D. degree** in the Graduate School of Politecnico di Torino (ScuDo).

To my parents, Alessandro and Caterina,
and to my brother Carlo

Acknowledgements

The first acknowledgement is to my supervisor, Prof.Daniel Milanese, whose advice has been fundamental not only in my academic research, but for my whole professional life.

I also need to acknowledge my colleague Dr.Diego Pugliese, who has worked long hours with me in the synthesis lab, and taught me most of what I know about the processing of phosphate glasses. Together we developed the compositions and the processes that made BPh glasses possible. Thanks to Dr. Nadia Boetti who taught me the fabrication process of optical fibres, the main spectroscopic techniques and the critical steps of fibre laser assembly. Many thanks to Prof.Davide Janner, for the fruitful ideas and advice on the surface processing of glasses and on paper writing.

I am grateful for the advice and help of Dr.Joris Lousteau, co-supervisor of this thesis, for all the work on the development of CL glasses and for the support during my visit in Southampton. I would also like to thank Prof.Francesco Poletti, for the hospitality in his research group, Prof. Andy Clarkson and Dr. Callum Smith for the fruitful collaboration in the development of a cane laser.

I wish to acknowledge Prof.Chiara Vitale Brovarone and Dr. Giorgia Novajra, for the fruitful collaboration and their inspiring works on resorbable phosphate glass fibres. I also acknowledge the group of Prof. Antonio Pifferi in PoliMi, The group of Dr.Stavros Pissadakis in FORTH, the groups of Prof.Barolo and Prof.Visentin in university of Torino for the collaborations.

Finally I acknowledge Annarita, Cecilia and Daniele for the work carried out during their master projects, and I wish good luck to Duccio for his future work as a PhD student in this group!

Last but not least I wish to acknowledge all those people who lived with me these last eight years in Torino, making these years simply fantastic.

Abstract

The work of this thesis is focused on two research lines: the first on the development of high power fibre lasers, the second on the development of bioresorbable, inorganic optical devices. The common aspect of these two lines is the use of phosphate glasses as a base material for the fabrication of speciality optical fibres.

Phosphate glasses are extremely interesting materials in virtue of the unique combination of their properties. They have been widely exploited in laser science as active gain media, due to the high solubility of rare earths in the glass matrix, and to the high absorption/emission cross section. Calcium phosphate glasses, on the other hand, have been studied as promising biomaterials due to their solubility in aqueous media, and to the ability of being safely reabsorbed by the human body.

The thesis starts with a literature review on the use of phosphate glasses in the fabrication of optical fibres and lasers. The properties of rare earth doped glasses are reviewed and a detailed description of the quenching phenomena in doped glasses reported and compared to the major results obtained in the literature.

The study of the literature reveals how the issues of heat dissipation, thermal expansion and mechanical stability are still relevant problems in the field of high power lasers. These issues were studied in the course of the thesis. Results obtained on the development of a Nd^{3+}-doped phosphate cane laser are reported in Chapter 5. Cane lasers have the same core/cladding structure that is typical of an optical fibre, but present a much larger diameter. This allows an increased mechanical stability of the device, combined with the easy cooling and good beam quality that are typical for a fibre laser. The development of a first prototype of a phosphate cane laser required the fabrication of a suitable glass (namely CL) that is featured by an exceptional matching of thermo-mechanical properties between core and cladding. A core glass composition (CL1:Nd) and a cladding glass composition (CL1) that present a difference in the glass transition temperature of only 8 °C and identical

coefficient of thermal expansion were fabricated ad-hoc for this scope. The materials were fully characterized and used for the fabrication of a cane with a diameter of 800 μm. Power scaling experiments performed on a 60 mm-long section of the cane show laser emission at 1054 mm, with a maximum putput power of 2.5 W and a slope efficiency of 44% with respect to the absorbed power.

Another issue that emerged from the literature and from the studies of fibre/cane lasers is the interest in developing new fibres with complex geometry. Chapter 4 of this thesis describes work carried on this topic, focusing on the critical step of fabricating and assembling a fibre preform. With the aim to develop rapidly and effectively optical fibre preforms with a wide range of geometries, a project for the the in-house development of an extrusion facility in Politecnico di Torino was kick-started. A first prototype of the facility is available, and preliminary results on the extrusion of phosphate glasses are presented.

The second part of the thesis is dedicated to the development of resorbable optical materials. An overview on the use of calcium phosphate glasses in the biomedical field is given, with particular interest in the use of glass fibres in biomedical applications. Subsequently, the results obtained on the use of resorbable glasses in biophotonics are reported. The idea at the basis of this research is to combine in a single device the two main field of application of phosphate glasses: the biomedical field and the optical one. This becomes particularly interesting as it enables fabricating multifunctional optical devices, which are of interest in optical sensing and photo-therapy. In particular, the bioresorbability minimizes the impact of the therapies, eliminating the need of removal surgery. Chapter 4 reports a detailed description of the design, fabrication and characterization of transparent calcium phosphate glasses. The materials show a window of transparency ranging from 240 to 2600 nm, therefore are able to guide light in the near UV region, and the refractive index can be tailored according to the composition. The glasses proved to be stable against vitrification and suitable for fibre drawing. Single material fibres were fabricated and proved to be soluble in aqueous media, in simulated physiological conditions.

Once the fabrication of the material is complete, resorbable glasses were used for the fabrication of single and multi-mode optical fibres. Step index fibres were fabricated using the rod in tube technique and the attenuation loss was measured by cut-back method. The fibres showed values of attenuation loss between 5 and

15 dB/m in the visible region and from 2 to 5 dB/m in the near infra-red. These values are from one to two orders of magnitude lower than those reported in literature for other resorbable optical devices. These results paved the way towards the application of such fibres for the inscription of fibre Bragg-gratings and for the use in time-domain diffuse optics experiments. Preliminary results on these topics are presented in Chapter 6.

Finally, resorbable hollow fibres were fabricated by drawing a tube-shaped preform. These fibres were used for obtaining a controlled release of a photosensitive drug, that could be activated by the light guided trough the same fibre. Experiments on the controlled release of drugs are still ongoing, and involved the development of a silanization method for phosphate glasses, in order to increase the release time of drugs.

Contents

List of Figures

List of Tables

Chapter 1

Introduction

"Fama est adpulsa nave mercatorum nitri, cum sparsi per litus epulas pararent nec esset cortinis attollendis lapidum occasio, glaebas nitri e nave subdidisse, quibus accensis, permixta harena litoris, tralucentes novi liquores fluxisse rivos, et hanc fuisse originem vitri."

Gaius Plinius Sec.
Naturalis Historia

History of glass is almost as old as civilization itself. According to Pliny the Elder the first glasses were made in the region corresponding to the modern district of Haifa, in the state of Israel, in a valley at the slopes of Mt.Carmel, about in 3000 b.c. Since then a slow but constant research led to the development of technologies, artefacts, and scientific discoveries that still amaze for their complexity and beauty.

Every time one admires a decorated window from an ancient cathedral, or a Murano chandelier, or the lenses from an ancient telescope, it should be remembered how much work was spent to develop a suitable recipe for the fabrication and the processing of the material. Indeed, the optimization of compositions and the development of the materials processing have always been the most secret tasks of glass working. It is not a case if, in ancient history, glass workers were well

rewarded and respected for their job, but they were often prohibited to live outside their workplace and leave their country.

There is still a lot to be discovered about glass, and it is somehow interesting to realize that the deep meaning of the word "glass" is still under debate, with the last contribution to this discussion being published just few months ago (Zanotto and Mauro J. Non Cryst Sol. 2017).

Progress in glass science is still ongoing and in the last two centuries some major improvements have been made. Glass technology has influenced the development of building sciences, optics, microscopy and astronomy. In the last five decades the research has been driven mainly by the invention of laser, and the consequent revolution in photonics. More recently the invention of biomedical glasses has opened new exciting perspectives on unknown properties of vitreous materials. In both cases, researchers explored the formation of glasses beyond the silicate systems, such as phosphates and chalcogenides.

A vitreous system that attracted particularly the interest of glass scientists in the last three decades is based on phosphorous oxide, due to the wide range of properties that can be obtained by opportunely changing the material composition. Phosphate glasses have been used as laser gain materials for the development of lasers and amplifiers, due to the high values of absorption cross sections and the high solubility of rare earth ions. Later, they have been explored as biomaterials, due to their ability to be reabsorbed by the human body.

Another major achievement of this century has been the invention of optical fibres. Thanks to the ability of these devices to transport light, it has been possible to achieve enormous developments in several disciplines, going far beyond the well known revolution in telecommunications. Nowadays optical fibre lasers and delivery fibres are used in several applications, including medicine, defence, and materials processing.

The research performed in this thesis is focused on the study of optical fibres made by phosphate glasses. The properties that are required to a phosphate glass for its use in fibre production have been studied and discussed in detail, leading to the development of new materials and improving the performance of fibre based devices. The fibres developed in this work have been studied for two main fields: the development of rare earth doped glasses for high power lasers and the development of bioresorbable optical fibres for biomedical applications. This second topic of the

research represents the first example, to the author's knowledge, of an inorganic based resorbable optical device.

The list below details the topic of each chapter of the thesis, giving brief description of the main contents:

- **Chapter 1:** Introduction
- **Chapter 2:** Literature review on the state of the art and the properties of phosphate glasses for optical applications.
- **Chapter 3:** Description of the methods and the analyses performed during this research, for the fabrication and characterization of materials.
- **Chapter 4:** Description of the methods used for the fabrication of optical fibre preforms, including the design and implementation of a glass extrusion facility in Politecnico di Torino. The results on the first experiments on the extrusion of phosphate glass hollow structures, and the assembling of optical fibre preforms are reported.
- **Chapter 5:** The results obtained on the development of two glass matrices for high power fibre lasers, with particular attention to the control of their thermo-mechanical properties are reported. The glasses have been used for the fabrication of a first example of a phosphate cane laser. The cane has been used for power scaling experiments and reached a multi-watt power emission, matching the best results obtained so far on phosphate step index fibres.
- **Chapter 6:** The chapter starts with a brief literature review on the state of the art in bioresorbable optical devices and on the use of calcium-phosphate glasses as biomaterials. Subsequently, the concept of glass-based resorbable optics is introduced. Finally, the results obtained on the development of a resorbable phosphate glass suitable for optical applications are reported. A full description of the material design, fabrication and characterization is given. The optical properties of the glass have been analysed and discussed in detail, with particular attention to the influence of the processing on the glass quality.
- **Chapter 7:** Results obtained on the development of bioresorbable single-mode and multi-mode optical fibres for biomedical applications are reported. Proof-of-principle studies for the use of such fibres in time-domain diffuse

optics experiments and inscription of fibre Bragg gratings are described. The fabrication of hollow fibres for the release of drugs and preliminary experiments on the combined release of photosensitive drugs and effective light propagation are described and discussed.

The objective of this thesis is to exploit the extreme versatility of phosphate glasses, that can offer a vast range of properties according to the composition that is chosen. It has been demonstrated that high power fibre lasers are a solid reality in research, and are almost ready for use in industrial applications. Moreover, a first example of a phosphate glass cane laser has been demonstrated, proofing that this configuration is able to combine the compactness of a bulk laser with the advantages, in terms of stability, of a fibre lasers.

Finally, phosphate glasses can be very interesting materials for the development of resorbable optical devices. This topic has recently raised the attention of the scientific community, as it may allow accessing remote areas of the human body in a minimally invasive way. Resorbable phosphate glasses showed a much lower attenuation and a wider window of transparency if compared to polymeric materials that have been used so far in this field.

As a conclusion, despite phosphate glasses have been already studied for decades, they still have not been exploited in all their potential. The feasibility of biomedical and laser devices, with enhanced properties of biocompatibility, efficiency and optical performance is still an unexplored field of research.

Chapter 2

Phosphate glasses in optics: a review

In this chapter the state of the art in the science and engineering of phosphate glasses is reviewed. The chapter starts with an introduction about the structure and properties of phosphate glasses. Subsequently, an extensive review on rare earth-doped phosphate glasses for laser applications is reported.

2.1 Phosphate glasses, structure and properties

Phosphate glasses are vitreous materials based on the presence of phosphorous oxide as a principal glass former. As other vitreous materials they are included in the recent definition proposed by Zanotto and Mauro, stating that glass is a "nonequilibrium, non-crystalline condensed state of matter that exhibits a glass transition" [34]. Phosphate glasses have been explored since the 1950s for specific applications, such as UV transmitting glasses and agents for water treatment [1]. However, the poor mechanical properties and the difficulties in processing have initially inhibited the wide diffusion of such materials.

More detailed studies on phosphate glasses were carried out in the 1960s after the invention of lasers. It was discovered that phosphate glasses doped with rare earth ions are able to store and re-emit a very high amount of optical energy, therefore they became very interesting laser gain media [35]. This is mainly due to the high value of absorption and emission cross sections of rare earth (RE) ions in the phosphate glass network and to the high quantum efficiency [36–38]. Moreover, phosphate glasses allow to host a higher amount of rare earth (RE) ions if compared to silica

and silicate glasses. This was of particular interest for the development of high power solid state lasers. Research performed at the Lawrence Livermore National Laboratories (USA) represents a milestone in this field [39, 40].

Another major achievement in phosphate glass science was the introduction of calcium-phosphate glasses as resorbable biomaterials in 1981 [41]. This achievement followed the invention of bioactive materials by Hench [42, 43] and introduced the concept of bioresorbability [41].

Nowadays phosphate glasses are also studied for a variety of other applications, including their use as solid electrolytes and nuclear waste hosts [44, 45].

2.1.1 Structure of phosphate glasses

The basic building unit of phosphate glasses is the phosphorous oxide tetrahedron, that results from the bonding of the P atom with four oxygens in a sp^3 hybridization. The unit is able to form a maximum of three covalent bonds through three oxygen atoms, defined as bridging oxygens. The fourth oxygen atom is connected to the central P ion trough a double bond, to preserve charge neutrality. In the common Q^i terminology, where i represents the number of bridging oxygens, this is known as a Q^3 structure [1, 46].

The Q^3 structure was thought being the typical state in which the vitreous form of pure anhydrous phosphorous pentoxide (v-P_2O_5) could be obtained [47]. However, four different structures of the phosphorous tetrahedron are possible, where $0 < i < 3$. These different coordination possibilities are displayed in Fig.2.1.a. Further studies have suggested that v-P_2O_5 is made by the formation of large chains of phosphorous tetrahedra, based on a large Q^2 structure. Thus, the Q^2 structure is dominant in the majority of phosphate glasses, with respect to the Q^3 form [48, 1].

An equivalent way to classify phosphate glasses is done considering the oxygen/phosphorous ratio, $\frac{O}{P}$, that determines the number of tetrahedral linkages in the glass structure, trough bridging oxygens. Glasses can be classified in:

- Ultraphosphate glasses ($2.5 < \frac{O}{P} < 3$) showing a prevalence of Q^3 structures,
- Metaphosphate glasses ($\frac{O}{P} = 3$) showing a polymeric structure of Q^2 chains,

- Polyphosphate glasses ($\frac{O}{P} > 3$) showing a the presence of Q^2 chains and Q^1 ions
- Pyrophosphate glasses ($\frac{O}{P} = 3.5$) made in prevalence of isolated pyrophosphate, anions
- Orthophosphate glasses($\frac{O}{P} = 4$) made of isolated Q^0 tetrahedra.

Pure v-P_2O_5 is rarely used in any large scale applications, as it presents poor mechanical properties and low chemical stability, due to a strong hygroscopic tendency. However these properties can be markedly improved by formulating glass compositions combining an opportune amount of different oxides [1].

The addition of oxides to a base glass former unit has effect on the overall glass network. Oxides are generally classified in relation to their effect on the vitreous network [46]:

- **Network formers oxides**: (i.e. silica, boron oxide, phosphorus oxide) these oxides act as building blocks of the glass network,
- **Network modifiers**: (mono and divalent metal oxides, i.e. sodium and potassium oxides, calcium oxide..) can bond to one or two non-bridging oxygens, and have effect on physical, chemical and thermal properties of the glasses,
- **Intermedate oxides** (i.e. alumina) can enter the glass network and bond to bridging oxygens.

A schematic of a typical oxide glass network is portrayed in Fig.2.1.b.

In the specific case of phosphate glasses, alkaline metal oxides are widely used to improve the chemical stability of glasses, increase the solubility of rare earth ions, and preserve transparency in the near UV region [49, 2]. Alumina is often used in phosphate glasses to increase the chemical stability of the network and reduce hygroscopic behaviour [50], whereas calcium and magnesium in concentrations above 30% are used to tailor glass solubility in biomedical glasses [51]. Boron proved to increase the level of cross-linking in the glass network, increasing the mechanical and chemical stability of the glass [52, 53]. The addition of transition metal ions, such as Ag^+ and Cu^{2+}, has been explored for the development of biomaterials with antibacterial properties [49].

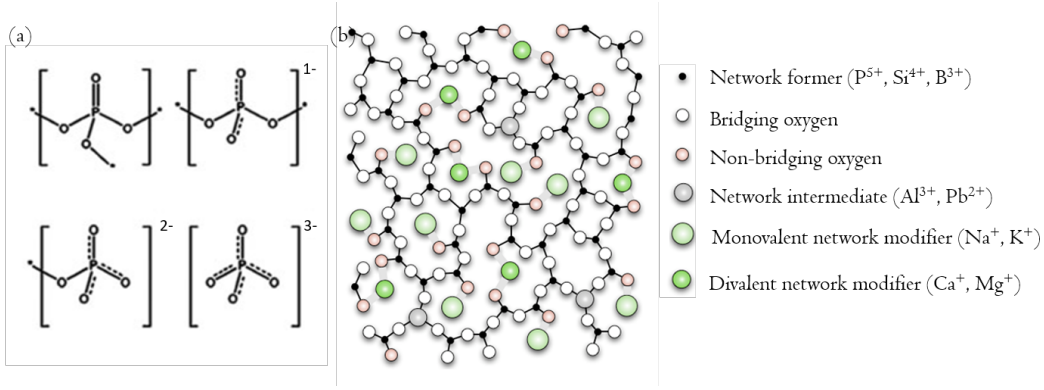

Fig. 2.1 (a) chemical structure of the Q^3, Q^2, Q^1 and Q^0 phosphate tetrahedral sites [1], (b) schematic of the typical network of an oxide glass (Copyright: Creative Commons).

2.2 Phosphate glasses in photonics

In this section, the use of phosphate glasses in photonics is analysed in detail. The optical and spectroscopic properties, the rare earth doping systems and the effect of quenching phenomena due to concentration and water absorption are reviewed and described.

Optical materials have been classified in two categories: active and passive materials. Active materials are those that emit laser radiation once they are excited with an opportune source of energy. Passive materials, on the other hand, do not present any gain effect.

Phosphate glasses are widely appreciated active materials, as they proved to be very good hosts for rare earth-ions. Lanthanide doping of materials, indeed, is the most common and most effective way to obtain laser generation from a glass, due to the peculiar electronic structure of such ions in the trivalent cation form.

Silica, silicate and phosphate glasses are commonly used as hosts for active ions. Silicate glasses chemically and mechanically are more stable and resistant than phosphates. However, they present very low solubility for rare earth ions, and they suffer from photodarkening phenomena [54, 50]. On the other hand, phosphate glasses show several advantages when used as laser gain materials. In the following paragraphs the properties and application of rare earth-doped phosphate glasses are reviewed.

2.2.1 Optical and spectroscopic properties of phosphate glasses

Phosphate glasses are featured by a unique matching of optical properties, including low non-linear refractive index and low onset for photodarkening. Depending on the composition they can be transparent in the near UV region. The following paragraphs describe in detail the main optical properties of phosphate glasses.

Transparency window

The window of transparency of phosphate glasses is delimited, on the lower energy side, by the absorption peak located around the wavelength of 3000 nm (3300 cm^{-1}), related to the vibrational energy of the $-OH$ group [50, 10, 1]. Despite the limit for transparency in the IR region should be defined by the phonon energy of the phosphate lattice, that is located at higher wavelengths, light transmission is not efficient beyond the limit of water absorption [50].

On the high energy side, the window of transparency is delimited by the UV edge of the glass. This limit is defined by the electronic bandgap of the material [2, 55]. The theoretical UV edge of pure $v-P_2O_5$ is 145 nm [56]. However, this value is not reachable in any practical case: the presence of impurities, such as water or transition metals, can heavily affect the transparency in the UV [2, 57]. Typically, metaphosphate glasses present a UV edge transparency limit around $300-350$ nm. This value, however, can be reduced to 240 nm by controlling the processing, composition and the reagents purity [57, 58, 5].

The effect of impurities on the UV edge of silica glasses is displayed in Fig.2.2 as reported in [2]. Ehrt studied the effect of impurities and melting conditions on the UV edge of metaphosphate and ultraphosphate glasses (see Fig.2.2) [59, 3]. Marzouk et al. have confirmed that the UV edge limit of phosphate glasses is due to metal impurities in the glass, that are originated from the fabrication process, in perfect analogy to what happens on silicate glass [60]. The effect of Ti, Pt, Pb and Nb on the UV edge of various phosphate glass compositions was also observed during this research work, as displayed in Fig.2.3.

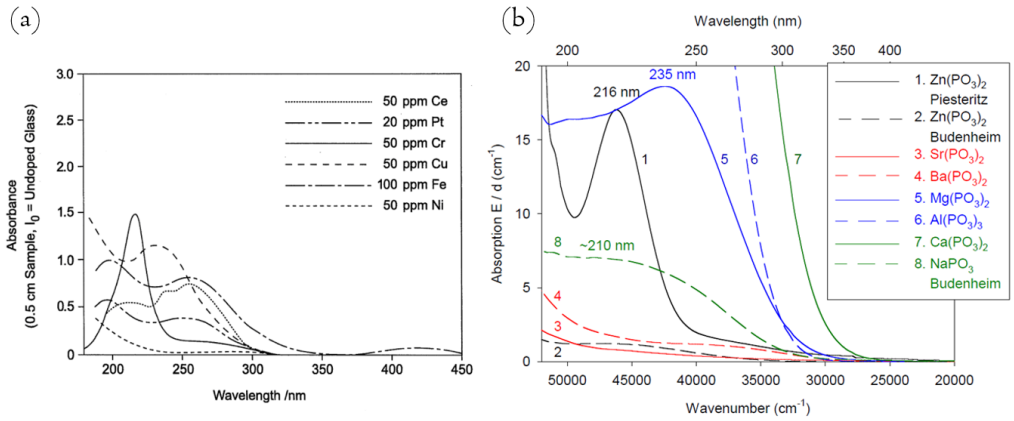

Fig. 2.2 (a) effect of transition metal impurities on the UV edge of silicate glasses as reported in [2], (b) UV edge of different phosphate glasses as reported in [3].

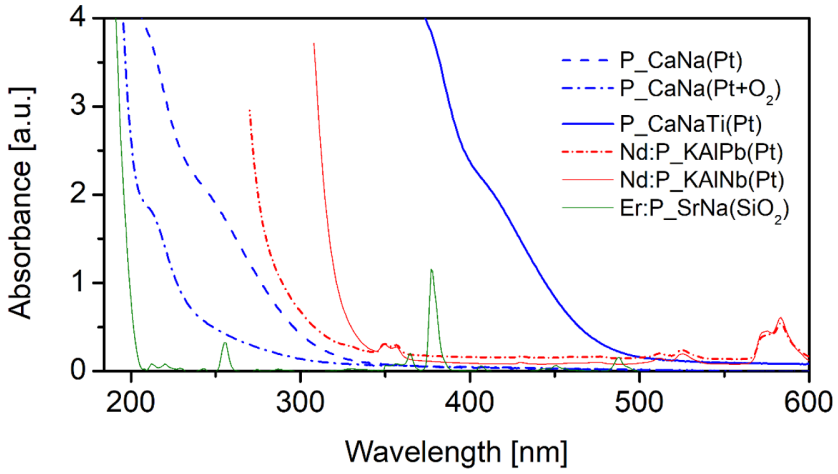

Fig. 2.3 UV edge of different phosphate glasses produced in Politecnico di Torino: The data for Nd:P_KAlPb and Nd:P_KAlNb are reported in [4], data for P_CaNa(Pt+O_2) are reported in [5], data for Er:P_SrNa are reported in [6], data for the P_CaNa(Pt) and P_CaNaTi are from this work.

,

Absorption end emission cross section

The absorption and emission cross sections of silicate and phosphate glasses have been measured and reviewed several times. In general it is recognised that phosphate glasses have larger values of cross section in comparison to silicates [50].

The glass composition has an effect on both absorption and emission cross section values. A comparative study among different compositions of silicate, borate, phosphate and fluoro-phosphate glasses was made by Weber et al. on the emission cross sections of Yb-doped materials. Phosphate glasses showed values of emission cross section about 20% higher than silicate and borosilicate glass [61].

Emission cross sections from $1.9 \times 10^{-20}\,\mathrm{cm}^2$ to $4.0 \times 10^{-20}\,\mathrm{cm}^2$ have been reported for Nd-doped phosphate glasses. On the other hand, values ranging from $0.9 \times 10^{-20}\,\mathrm{cm}^2$ to $3.6 \times 10^{-20}\,\mathrm{cm}^2$ were achieved in silicate glasses [35, 50, 62].

Emission cross section values lower than $3.0 \times 10^{-20}\,\mathrm{cm}^2$ are normally reported for Er-doped silicate glasses [63]. On the other hand values above $7.0 \times 10^{-20}\,\mathrm{cm}^2$ have been reported on Er-doped commercial phosphate glasses [64].

Absorption cross section values around $6 \times 10^{-21}\,\mathrm{cm}^2$ and have been reported for Er-doped silicate glasses, whereas values between $8 \times 10^{-21}\,\mathrm{cm}^2$ and $10 \times 10^{-21}\,\mathrm{cm}^2$ have been measured on phosphates [65, 66].

Absorption cross sections for Nd-doped phosphate glasses are usually between $0.7 \times 10^{-20}\,\mathrm{cm}^2$ and $3 \times 10^{-20}\,\mathrm{cm}^2$, about twice as in silica [4, 65, 67, 11].

Absorption cross sections for Yb-doped phosphate glasses present values around 0.9 to $1.4 \times 10^{-20}\,\mathrm{cm}^2$, whereas silicate glasses show values up to $2.5 \times 10^{-20}\,\mathrm{cm}^2$ [65, 67–69].

Nonlinear refractive index

If a high intensity beam light is launched trough a transparent material, a variation of the refractive index can be observed, according to the following equation [70]:

$$n = n_0 + \Delta n \tag{2.1}$$

Table 2.1 Nonlinear refractive indices of various commercial phosphate and silicate glasses as reported by Adair et al. [29]. Values are reported in 10^{-13} esu units

Glass Label	Type	Producer	Nonlinear Refractive Index
LHG-5	Phosphate	Hoya	1.44
LHG-6	Phosphate	Hoya	1.12
Q-88	Phosphate	Kigre	1.27
Fused Silica	100% SiO_2	Dynail	0.85
LG-650	Silicate	Schott	1.44
BK-7	Borosilicate	Schott	1.30

where n_0 is the linear refractive index, and Δn is the variation dependent on the beam intensity I, according to a nonlinear refractive index coefficient γ:

$$\Delta n = \gamma I \tag{2.2}$$

The measurement of Δn is important in the characterization of glasses for high power lasers, as it is responsible for self focusing effects. This provokes beam distortion and intensity fluctuations in the beam of high power lasers, and may lead to catastrophic failure of the devices if the phenomenon is not controlled. This kind of nonlinearity constitutes a major limitation to the performance of high-power lasers [70].

Non-linear refractive index has been measured on a series of phosphate and silicate glasses in the late 1970s, revealing that phosphate glasses show slightly lower values compared to silicates [71, 70]. The result was later confirmed by Adair et al. using three-wave frequency mixing. The results obtained are displayed in Table. 2.1 [29].

Photodarkening

Photodarkening is a detrimental phenomenon that consist in the lifetime quenching of rare earth ions in a glass matrix, occurring at high population inversions. The phenomenon is also responsible for an increase of the fibres loss, which is associated to an increase of the absorption in the glass. This is responsible for the overheating of the system [72]. It was first observed in silica fibres by Paschotta et al. in 1997 [73]. The mechanism that leads to photodarkening is still not fully understood, and it is currently the strongest limit to the power scaling of fibre lasers. In Yb-doped silica,

it is commonly agreed that it depends on the concentration of rare earth ions, to the formation of colour centres in the glass matrix or to the generation of high-energy photons due to cooperative luminescence [74].

Recently, some strategies have been adopted to mitigate photodarkening in silica fibres, including the use of UV-Vis light and the doping of the glass with P or Ce ions. However photodarkening in silica fibres still remains an unsolved issue [75, 76].

Photodarkening in heavily doped Yb^{3+} phosphate glasses has been studied by Lee et al. It has been observed that phosphate glass optical fibres were substantially immune to photodarkening, whilst silicate fibres undergoing the same test were heavily affected [54].

Modal instabilities in fibre lasers

An issue that has raised recently, and is limiting the power scaling of fibre lasers, is that one of mode instabilities. Mode instability has been observed for the first time by Eidam et al. in single-mode fibre lasers [77]. Its origin is still under debate, and, at the same time, it is not completely clear if the phenomenon is observable only in fibre lasers or also in other configurations [78].

Mode instabilities are related to the presence of refractive index fluctuations within the length of an optical fibre. Such fluctuations create a periodic pattern in the fibre, acting as a fibre Bragg grating. This results in the destabilisation of the beam propagated in the fibre, and in the generation and propagation of higher order modes. The origin of such fluctuation is not clear yet, however, most of the studies tend to assume that the effect has a thermal origin [79].

What can be observed by analysing the output beam of a fibre lasers is that normally stable, high-quality, high-power laser beams undergo severe fluctuations when the output power exceeds a certain threshold power. The effect is that the beam is severely deformed and in some cases may split, with detrimental effects on the quality of the laser beam [78].

In order to avoid this effect, the approach that is commonly attempted resides in increasing as much as possible the threshold power at which mode instabilities arise. This is done by trying to reduce the quantum defect, and reaching saturation of the population inversion. However, it was also found that photodarkening phenomena play a role in the arising of mode instabilities, by increasing the loss of the fibres [80].

The solution of the mode instabilities problem, however, seems to reside in the host materials. Active materials featured by high thermal conductivity, low thermo-optic coefficient and low sensitivity to photodarkening may mitigate this issue [78].

2.2.2 Doping systems in active phosphate glasses

Phosphate glasses have been doped with lanthanide ions, mostly to exploit the emissions in the NIR region. Nd^{3+}, Yb^{3+}, Er^{3+} and Yb^{3+}/Er^{3+} systems have been widely studied for their use in laser emission. A review of the electronic structure and properties of these lanthanide ions is given in the following paragraphs.

The neodymium ion

The Nd^{3+} ion is particularly suited for being pumped with a non coherent light source (i.e. a flash lamp), as its electronic structure is rich of absorption levels in the visible region. For such reason it has been the first rare earth to be explored as an active laser gain media [81].

A less common way to pump neodymium is solar energy. Solar pumped, Nd^{3+}-based solid state lasers have been demonstrated in Nd:YAG [82, 83]. Preliminary studies on the excitation of phosphate glasses for solar lasers have been performed [11, 84, 85]. However, there is no reference to the writer's knowledge, of effective demonstration of a solar-pumped laser action from a phosphate glass.

Nowadays, flash lamp excitation of Nd-phosphate glasses has become less common. More efficient pumping of Nd^{3+} is obtained by directly stimulating the ${}^4I_{9/2} \longrightarrow {}^2H_{9/2} + {}^4F_{5/2}$ transition using laser diodes at 808 nm or at 795 nm [4, 86].

A simplified schematic representation of Nd^{3+} electronic structure is displayed in Fig.2.4. The Nd^{3+} ion is featured by three main emission bands, located respectively at $890-910$ nm, $1050-1100$ nm and $1310-1320$ nm [65]. The strongest transition is the one located at $1050-1100$ nm, related to the ${}^4F_{3/2} \longrightarrow {}^4I_{11/2}$ decay, leading to laser emission located at 1053 nm in phosphate glasses. This emission is related to a four level behaviour of the Nd^{3+} ion, which is particularly advantageous as it allows laser action to occur with a low threshold power.

The third emission band, located at $1310-1360$ nm has been considered of technological interest for use in telecommunications. This emission is related to the

$^4F_{3/2} \longrightarrow {}^4I_{13/2}$ decay and led to laser emission in phosphate glasses at 1358 nm. At last, by exploiting a three-level behaviour of the Nd^{3+} ion in the the $^4F_{3/2} \longrightarrow {}^4I_{9/2}$ transition, laser action in phosphate glasses can be achieved at a wavelength of 906 nm [87].

The ytterbium ion

The Yb^{3+} ion is the most suitable for high power applications. Its simple electronic structure is featured by a lower quantum defect [1] in comparison to neodymium, thus it allows higher efficiency of a laser [65].

A schematic of the electronic structure of the Yb^{3+} ion and the absorption and emission bands are displayed in Fig.2.5. The ion is featured by a strong absorption band with a peak located at 975 nm and broad, overlapping absorption band around 915 nm. Emission peaks are located at 975 nm and at 1032 nm. The absorption and emission peaks are related to the $^2F_{7/2} \longrightarrow {}^2F_{5/2}$ transition, that is commonly used for laser action. Pumping occurs normally at 975 nm using pump diode with a small bandwidth. Lasing occurs typically around 1032 nm [65].

Yb^{3+}-doped phosphate glasses proved to be excellent active media for high power lasers and for single frequency lasers, being able to to achieve high power and high efficiency both in continuous wave and pulsed configuration [88, 89].

The erbium ion

The Er^{3+} ion has recently become of very high interest due to a complex electronic structure, which allows emission at different wavelengths. Er^{3+} ion has been mostly exploited for its emission around 1550 nm, fundamental for the fabrication of erbium-doped fibre amplifiers used in telecommunications [90]. This peak is related to the $^4I_{13/2} \longrightarrow {}^4I_{15/2}$ transition and is obtained from a three-levels behaviour of the Er^{3+} ion under excitation at 980 nm on the $^4I_{15/2} \longrightarrow {}^4 I_{9/2}$ transition.

However, more recently, emissions in the visible have been studied through upconversion phenomena [39, 91]. Indeed, upconversion of Er^{3+} in phosphate glasses leads to green emission (532 nm) from the $^2H_{11/2} \longrightarrow {}^4I_{15/2}$ decay and red

[1] In this context, the quantum defect is considered as the difference of energy (expressed in percentage) between the pump photon and the emitted laser photon of a gain media.

emission (660 nm) from the ${}^4F_{9/2} \longrightarrow {}^4I_{15/2}$ decay [65]. These transitions have been studied for laser emission in fluoride glasses and in crystals [92, 93]. Despite visible lasing is not possible in phosphate glasses, due to the high phonon energy, upconversion in phosphate glass has been studied for potential applications beyond laser emission [94].

Another transition of interest for the Er^{3+} ion is the ${}^4I_{11/2} \longrightarrow {}^4I_{13/2}$ transition, responsible for emission at about 2800 nm. However, this transition cannot be exploited in oxide glasses, due to the presence of a water absorption peak at the same energy [65, 10]. Glasses with high transparency in the near and mid-IR, such as chalcogenides, appear to be more promising for this application [95, 96].

The Yb/Er co-doping of phosphate glasses

Yb^{3+}/Er^{3+} co-doping has been widely exploited to increase the performance of the three-level transition of Er^{3+} at 1550 nm. Indeed, Yb^{3+} act as a sensitizer allowing a highly efficient energy transfer from its excited state to the erbium ion. Phosphate glasses proved to be particularly suitable hosts for this system, in virtue of the high cross section, efficient energy transfer and low backward transfer rates [65, 10].

Efficient energy transfer phenomena are favoured in phosphate glass, with respect to silicates, from the higher phonon energy that increases the ${}^4I_{11/2} \longrightarrow {}^4I_{13/2}$ relaxation probability [97]. Combined with a very good spectral overlap of the Er^{3+}, ${}^4I_{15/2} \longrightarrow {}^4I_{11/2}$ absorption and the ${}^2F_{5/2} \longrightarrow {}^2F_{7/2}$ of Yb^{3+}, the overall efficiency of the Yb^{3+}/Er^{3+} energy transfer can be as high as 95% [39, 98].

Case study: phosphate glasses for inertial confinement fusion research

The leading research on RE-doped phosphate glasses has been performed, in the past, towards the development of the Laser Inertial Confinement Fusion (Laser ICF) at the National ignition Facility in the USA. The final goal of this laser is to produce a confined nuclear fusion for energy production purposes [99].

The facility is composed of 192 high power laser beams working at 1054 nm and amplified trough a series of Nd-doped phosphate glass slabs pumped by flash-lamps. The fabrication of such slabs has been one of the most challenging tasks of modern glass engineering and led to the development to the continuous casting process of

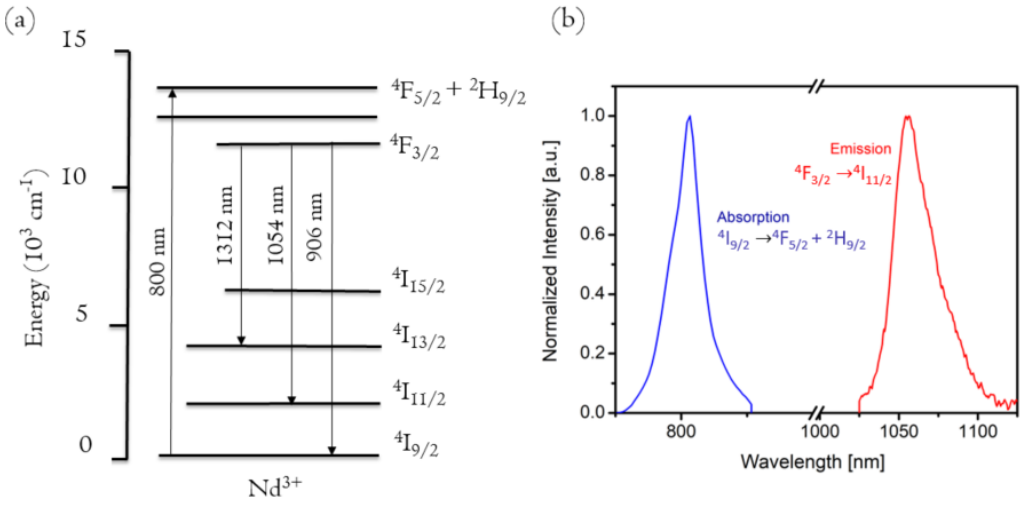

Fig. 2.4 (a) Schematic representation of the energy levels of Nd^{3+} ion (b) absorption and emission peaks related to the $^4I_{9/2} \longrightarrow {}^2H_{9/2} + {}^4F_{5/2}$ and $^4F_{3/2} \longrightarrow {}^2I_{11/2}$ transitions [7].

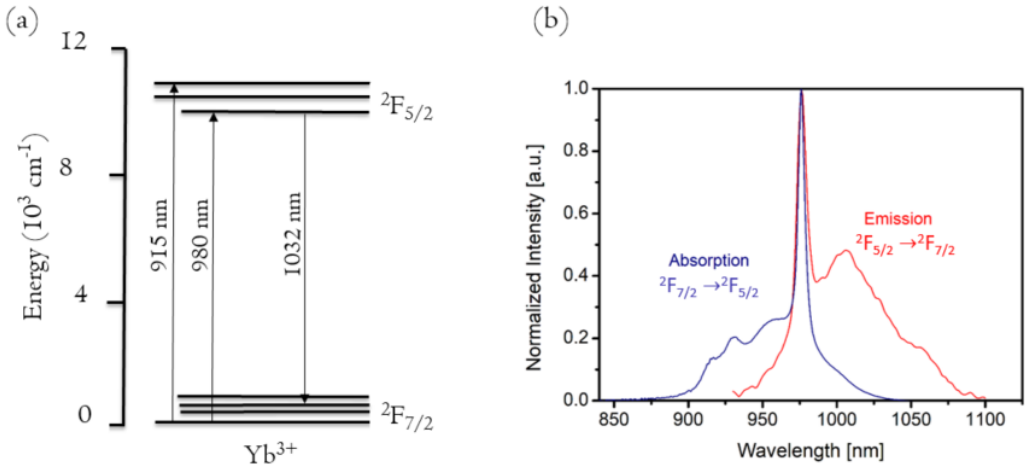

Fig. 2.5 (a) Schematic representation of the energy levels of Yb^{3+} ion (b) absorption and emission peaks related to the $^2F_{7/2} \longrightarrow {}^2F_{5/2}$ and $^2F_{5/2} \longrightarrow {}^2F_{7/2}$ transitions [7].

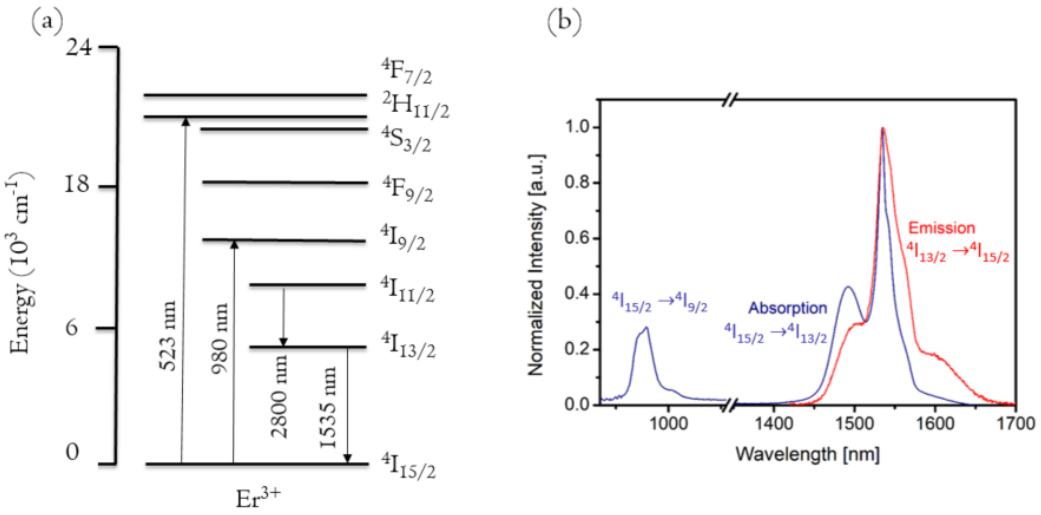

Fig. 2.6 (a) Schematic representation of the energy levels of Er^{3+} ion (b) absorption and peaks related to the $^4I_{15/2} \longrightarrow {}^4I_{9/2}$ and $^4I_{15/2} \longrightarrow {}^4I_{13/2}$ transitions and emission peak related to the $^4I_{13/2} \longrightarrow {}^4I_{15/2}$ transition [7].

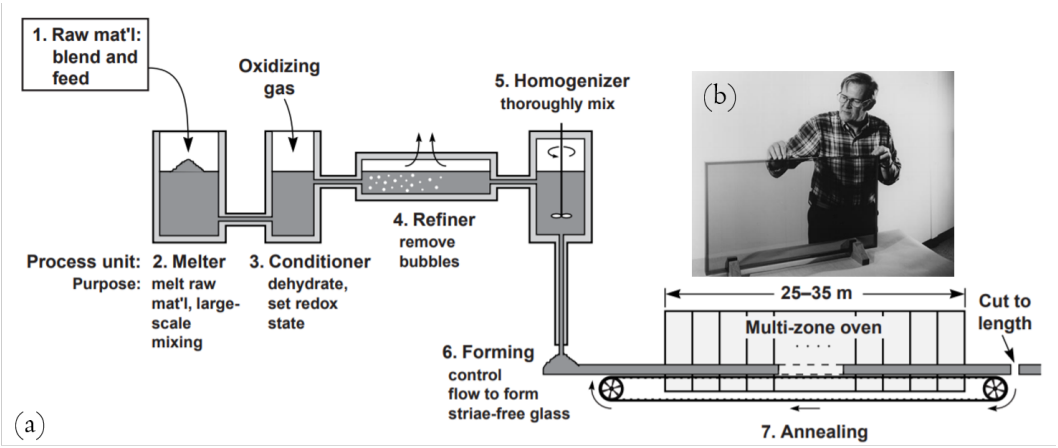

Fig. 2.7 (a) Schematic of the continuous casting process (b) example of a *Nd*-doped glass slab produced trough this method (Adapted from [8]. Copyright: Elsevier).

phosphate glasses. The implementation of this process required at first developing of opportune glass compositions, then refining the materials from impurities and finally cast an homogeneous melt [100, 37, 8].

A schematic representation of the continuous casting process and a picture of a sample slab are displayed in Fig.2.7. The process is made of seven stages, from the mixing of raw materials to the final slab. First the reagents are mixed in form of powders and melt, then three stages of melt processing (conditioning, refining and homogenization). Finally the melt is cast on a tape and undergoes a long annealing process.

The process allows obtaining extremely homogeneous glasses, free from platinum inclusions and with a very low water content [37, 2].

2.2.3 Quenching phenomena in rare-earth doped phosphate glasses

The features described in previous paragraphs show how phosphate glasses are ideal hosts for RE ions, to be used in laser generation and amplification. In particular, the fabrication of giant pulsed lasers for nuclear fusion research has been the first topic to be explored, and has led to enormous advancements in the understanding the behaviour and the processing of phosphate glasses.

Nowadays phosphate glasses are attractive for the fabrication of small, high-gain devices, and in particular compact optical fibre devices featured by high gain per unit-length. The main applications are LIDAR sources, high power lasers and single frequency lasers [101, 86, 102].

Some phenomena, however, are responsible for a degradation of the performance of phosphate glass laser materials. These are:

- Multiphonon relaxation,
- Concentration quenching,
- Nonradiative decay, due to water absorption or impurities

These phenomena lead to the relaxation from the excited states trough non radiative paths, reducing the efficiency of laser emission.

The nonradiative decay rate k_{nonrad} can be expressed as the sum of all nonradiative processes:

$$k_{nonrad} = k_{mp} + k_{conc} + k_{OH} + k_{imp} \tag{2.3}$$

where k_{mp} is the multiphonon decay rate, k_{conc} is the concentration quenching, related to the ion-ion interactions, k_{OH} is the decay rate due to water contamination and k_{imp} is related to the presence of transition metal or lanthanide impurities. While k_{mp} is a constant value defined by the glass host and k_{imp} can be minimized by using extremely pure reagents, k_{conc} and k_{OH} are more difficult to control [9]. A schematic representation of these phenomena, as described by Ehrmann [9] and Layne [103] is depicted in Fig,2.8 The following two paragraphs describe in detail the quenching phenomena due to water absorption and concentration quenching.

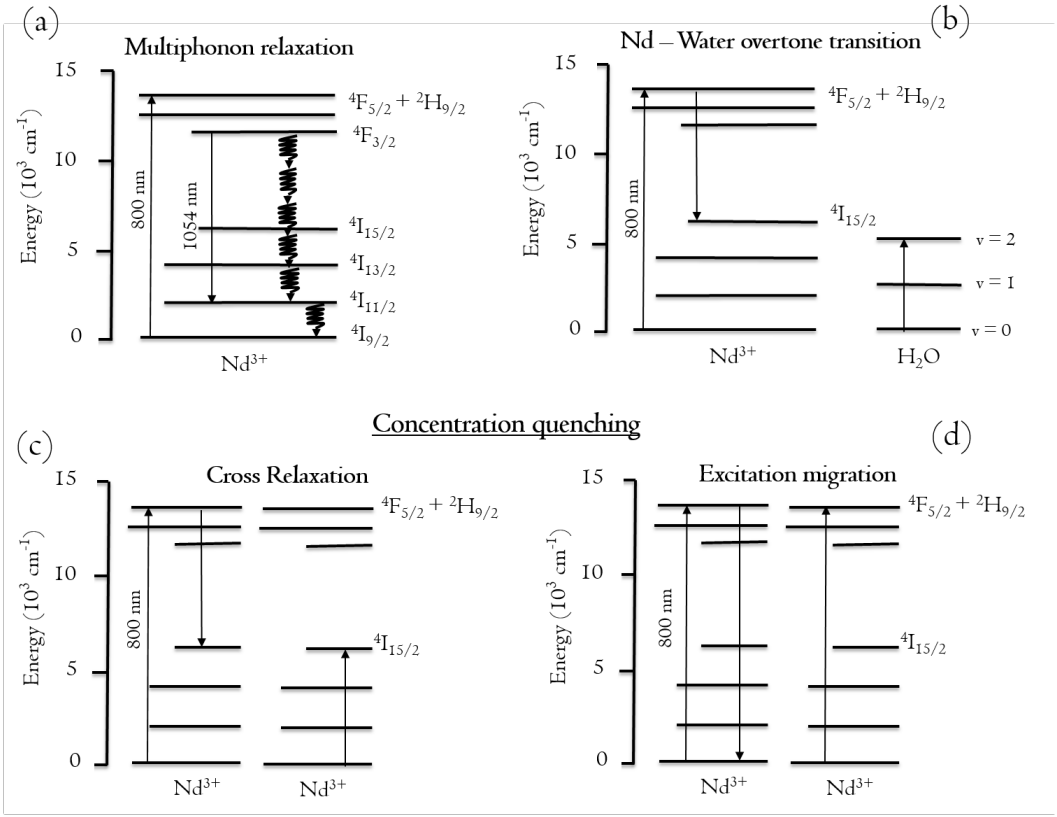

Fig. 2.8 Non-radiative Nd^{3+} relaxation processes in phosphate laser glasses as described in [9]: (a) Multiphonon relazation, (b) Quenching due to water absorption, (c-d) Relaxation phenomena due to concentration quenching.

Quenching phenomena due to water absorption

The presence of $-OH$ groups in the glass matrix is considered detrimental for laser materials. A number of works have correlated the presence of water to a decay of the fluorescence lifetime of rare earths and to an increase of the non-radiative decay rates. This effect is particularly present in phosphate glasses, due to the high hygroscopic nature of such matrix [104, 105].

Fluorescence quenching was first studied in Nd-doped phosphate glasses by Ebendorff et al., more detailed studies were than performed by Ehrmann et al. [104, 9, 106] They discovered that the increase of the concentration of $-OH$ groups in the glass network is responsible of an increase of the nonradiative decay rate, therefore it affects the efficiency of the emission process.

The phenomenon was described using an experimentally derived linear relation between the the decay rate of the ion $(1/\tau_m)$ and the concentration of $-OH$ groups in the glass network. This latter quantity is difficult to measure, therefore the equation is usually written referring to the absorption coefficient of the $-OH$ absorption peak located at $3300\,\mathrm{cm}^{-1}$:

$$1/\tau_m = m_{OH} \cdot \alpha_{OH} + (1/\tau_0) \tag{2.4}$$

where τ_m is the measured fluorescence lifetime of the excited state, α_{OH} is the absorption coefficient of the material at $3300\,\mathrm{cm}^{-1}$. The quantity τ_0 represents the maximum lifetime achievable in absence of water in the glass matrix. Finally, m_{OH} is the slope of the graph.

By considering that the total decay rate $(1/\tau_m)$ is the sum of all radiative decay rates A_{Rad}, plus the energy transfers due to cross relaxation (W_{cross}) and water absorption (W_{OH}) it can be written:

$$1/\tau_m = A_{Rad} + W_{OH} + W_{cross} \tag{2.5}$$

therefore, combining eq.2.4 and eq.2.5:

$$W_{OH} = m_{OH} \cdot \alpha_{OH} \tag{2.6}$$

Eq.2.6 can be compared with the analysis performed on quenching phenomena by Stokowsky and Krashevich [107]. They have defined three quenching mechanisms depending on the rare earth concentration in the medium. The mechanism occurring

for concentrations ranging between 10^{20} and $10^{21}\,\mathrm{cm}^{-3}$ is the most relevant in the practical case [107]. According to this description the energy transfer due to water is described as:

$$W_{OH} = k_{OH} \cdot N_{Nd} \cdot \alpha_{OH} \tag{2.7}$$

Where k_{OH} is a constant and N_{Nd} is the concentration of the donor ion (in this case Nd^{3+}). The combination of eq.2.7 with eq.2.4 leads to the final form of the equation for the energy transfer due to water absorption:

$$1/\tau_m = k_{OH} \cdot N_{Nd} \cdot \alpha_{OH} + (1/\tau_0) \tag{2.8}$$

The constant k_{OH} is considered to be the same for all metaphosphate glasses and is equal to $6 \times 10^{-19}\,\mathrm{cm}^4\mathrm{s}^{-1}$ [106]. This is considered as a material property and is related to the interaction forces between the rare earth ion and the $-OH$ groups. This mathematical relation allows analysing $-OH$ quenching phenomena separately from other nonradiative relaxation processes.

This mathematical description of fluorescence quenching by $-OH$ impurities was experimentally confirmed on Nd-doped glasses [104, 9]. The nonradiative decay rate increased linearly with the concentration of $-OH$ in the matrix, as displayed in Fig.2.9.a. The mathematical description of the water quenching phenomenon can be extended to all rare earth ions. In particular Er^{3+} emission at 1550 nm is heavily affected by water contamination [108]. More recent studies confirmed the linear increase of the nonradiative decay rate as a function of water content. Experiments performed in this research group confirmed this trend also for an Yb/Er doped glass system, as displayed in Fig.2.9.b [10, 109, 6].

The data displayed in Fig.2.9.b allow estimating the values of k_{OH} for the Er^{3+}/Yb^{3+}-ion. By fitting the data with the minimum square method and applying eq.2.8 it can be written:

$$k_{OH} = \frac{Slope}{N_{Er}} \tag{2.9}$$

Where $Slope$ is the value of m_{OH} resulting from the fitting of the data. The resulting values are: $k_{OH} = 2.25 \times 10^{-22}\,\mathrm{cm}^4 \cdot \mathrm{s}^{-1}$ for the P_CaNa glass matrix and $k_{OH} = 2.52 \times 10^{-22}\,\mathrm{cm}^4 \cdot \mathrm{s}^{-1}$ for the P_LiAlBa matrix.

The same calculation was performed on some data reported by Gapontsev et al. on two Er^{3+}-doped glasses featuring a concentration of active ions equal to

$2.9 \times 10^{20}\,\mathrm{cm}^{-3}$ and $1.2 \times 10^{20}\,\mathrm{cm}^{-3}$ [97]. The results show values of $k_{OH} = 3 - 4.5 \times 10^{-22}\,\mathrm{cm}^4 \cdot \mathrm{s}^{-1}$.

The calculated values are quite similar and may be considered an estimation of the k_{OH} constants for the $Er^{3+}$and the Er^{3+}/Yb^{3+} doping systems. However, this is the first estimation of such parameter to the writer's knowledge and the measurements should be confirmed with a more accurate analysis.

Concentration quenching phenomena in active glasses

The concentration quenching is a phenomenon that provokes increase of non radiative decay ratios (decrease of the fluorescence lifetime) in consequence of the interaction between two rare earth ions. A theory that explains this phenomenon was developed by Auzel et al. in the early 2000s [110, 111].

According to Auzel's theory, concentration quenching may occur following two different cases: in the first case, known as diffusion limited, the quenching starts at relatively low concentrations of rare earth ions, and is described by the following equation [110]:

$$\tau(N) = \frac{\tau_\omega}{1 + \frac{9}{2\pi} \cdot \left(\frac{N}{N_0}\right)} \tag{2.10}$$

where $\tau(N)$ is the fluorescence lifetime of the ion at a given concentration N, τ_ω is the theorical lifetime at near-zero concentration (i.e. the radiative lifetime), N_0 is defined as the critical concentration for self quenching.

A second case of the Auzel's theory considers the case of fast diffusion materials, at which quenching occurs at higher concentrations:

$$\tau(N) = \frac{\tau_\omega}{1 + 4.45 \frac{N}{N_{00}} \exp\left(-\frac{\beta \Delta E}{4}\right)} \tag{2.11}$$

where N_{00} is the critical concentration for diffusion quenching, β represents the exponential parameter for multiphonon assisted energy transfers, ΔE is the first excited state energy of the ion under consideration.

The Auzel's theory has been applied widely to analyse the behaviour of rare earth ions in phosphate glasses, leading to the conclusion that eq.2.10 describes in the best way the behaviour of phosphate glasses. In particular concentration

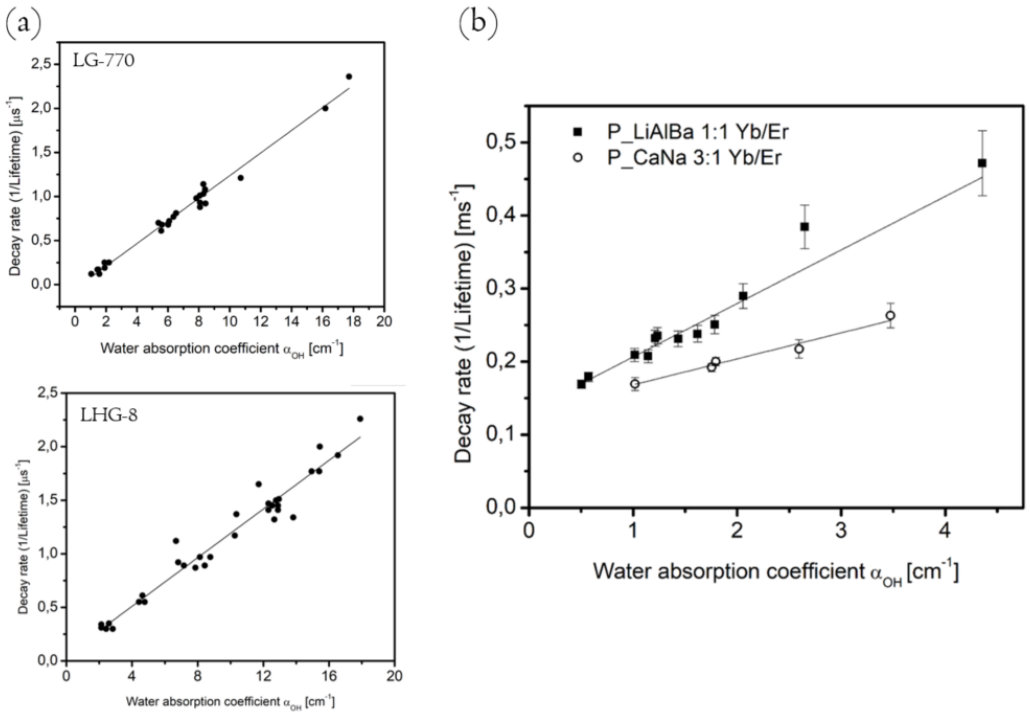

Fig. 2.9 (a) Decay rate of the excited state lifetime in function of the $-OH$ concentration for Nd-doped LG-770 (Schott) and LHG-8 (Hoya) as reported by Ehrmann and Campbell [9], (b) decay rate of the excited state lifetime for two Yb/Er glass compositions developed in this laboratory. Data for P_LiAlBa are reported in [10], data for P_CaNa are from this work.

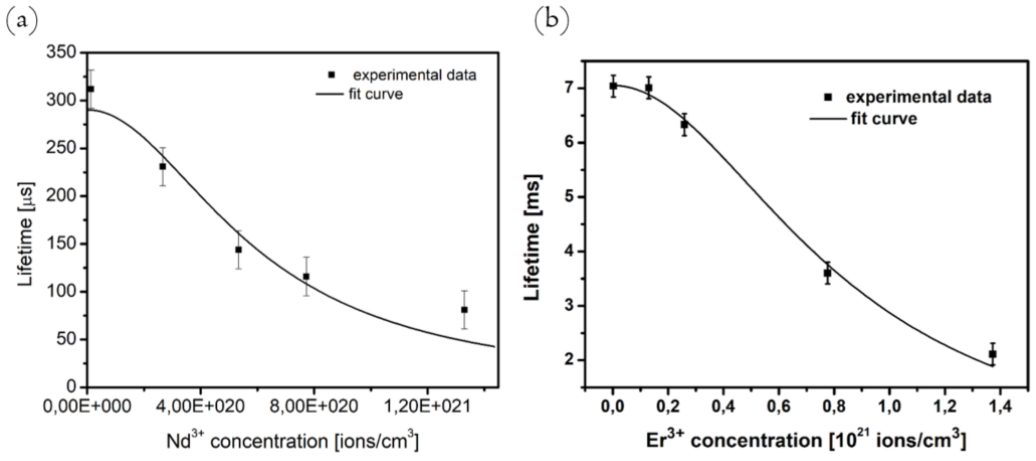

Fig. 2.10 Lifetime decay in consequence of concentration quenching for (a) Nd-doped and (b) Er-doped glasses. The data have been fitted with the Auzel's equation in the case of limited diffusion [10, 11].

quenching studies have been performed on Er-doped glasses [10, 112, 113], on Yb-doped glasses [114] and on Nd-doped glasses [11]. Samples of Auzel's curves for an Er-doped and a Nd-doped phosphate glass are portrayed in Fig.2.10.

In few cases, a deviation of the experimental data towards longer lifetime values was observed at high doping levels [112, 114]. In Er and Yb-doped glasses this may be due to the presence of energy transfer phenomena or re-absorption phenomena in the glasses. However, this was not observed in all cases [10].

A corrected form of the Auzel equation, that takes into account re-absorption phenomena, can be obtained by correcting the τ_ω factor in: $\tau_\omega = \tau_w \cdot (1 + \sigma N l)$, where l is identified as the size of the sample and τ_w is the equivalent of τ_ω in the new form of the equation. The equation is valid only if the condition $\sigma NL < 1$ is verified [111]. However, this form of the Auzel's equation has not been used so far for studying phosphate glasses.

In all cases, the N_0 values that are measured in phosphate glasses are much higher than silicates [10, 11, 113]. This proves that the amount of rare earth ions that can be incorporated in a phosphate glass is at least an order of magnitude higher than those possible for silicate glasses. Moreover concentration quenching effects are much lower in phosphate glasses than in silicates [10].

2.3 Phosphate glasses for fibre lasers

As the diffusion of laser based technologies progressed, from the early 1990s until now the demand of technological advancement was no more driven by the development of giant lasers, but by the need of compact, small and efficient coherent sources. This was the driving force of an increasing research activity performed on phosphate glasses as laser hosts [115, 116, 7].

Industry required solid glasses, that are able be pumped at very high power, minimizing the negative effects due to thermal lensing and material degradation. Particular interest was devoted to the development of phosphate glass optical fibre lasers [117]. The following paragraphs will give an overview on this topic.

2.3.1 Working principle of a fibre laser

A fibre laser is a laser device in whom the gain media is the core of an optical fibre. In the majority of cases the active media is a rare earth doped glass. The first fibre laser was developed by Snitzer at the arising of the laser era and was pumped by means of a flash lamp [81]. Since the invention of high power diode lasers, more efficient pumping can be obtained by directly stimulating the excitation level with an appropriate radiation. This allows obtaining a high power, high quality laser beam starting from a high power, low quality laser emitted from the diode.

There are two possible configurations for a fibre laser, depending on the structure of the optical fibre: single and double cladding. In the case of single cladding (SC) fibres the pump light is launched directly in the active core, that is used to guide both the pump light and the emitted signal. On the other hand, in the case of double cladding (DC) fibres the pump light is confined within the first cladding, whilst the core only guides the generated laser signal. This second configurations presents several advantages, as it allows the pump power to be guided, and absorbed, more uniformly by the active media. This results in a more uniform thermal loading of the fibre and generally a higher slope efficiency [65]. A schematic representation of a double cladding optical fibre, featuring an active core, is portrayed in Fig.2.11.

Recently phosphate glass fibre lasers have attracted interest from industry, as they are able to reach high beam quality and high output power in a compact size [118, 7]. However, phosphate glasses that are suitable for the fabrication of very high power lasers are difficult to obtain, as they require a complex matching of optical, mechanical and thermo-mechanical properties [4, 119]. The following paragraphs will give an overview of the properties of a glass for fibre laser, and the main results achieved so far in this field.

2.3.2 Phosphate glasses for optical fibre drawing

Phosphate glass optical fibres are mainly fabricated via the rod-in-tube technique (see Chapter 3). Glasses suitable for this procedure require a good stability against crystallization and matching of thermo-mechanical properties between core and cladding. Moreover high power regimes require the absence of residual stress at the core cladding interface of the fibre, and a good robustness of the device. Finally the

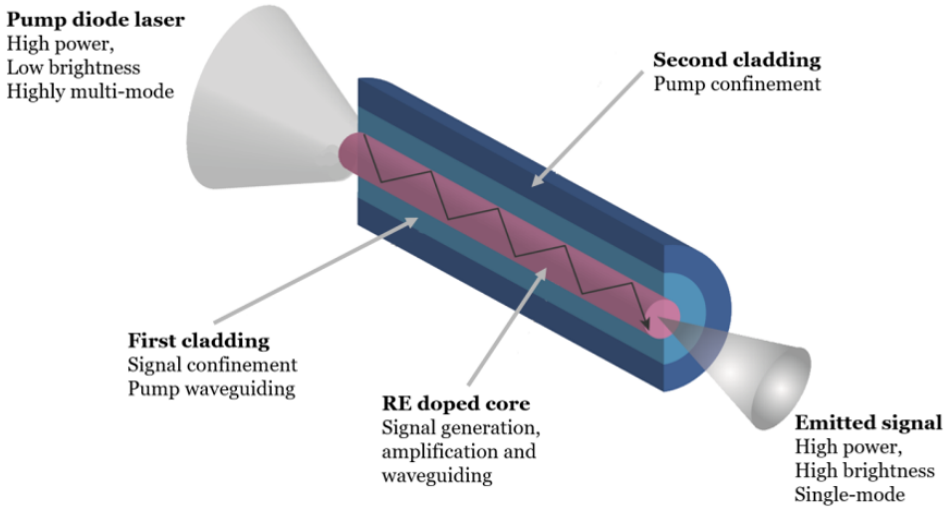

Fig. 2.11 Schematic representation of the structure of a double-cladding fibre laser

refractive index mismatch of core and cladding must be carefully tailored to meet the requirements of laser developing.

Glass thermal stability

The rod-in-tube technique requires that the material is heated above the glass transition temperature in order to reach a viscosity ranging from $10^3\,\mathrm{Pa}\cdot\mathrm{s}$ to $10^4\,\mathrm{Pa}\cdot\mathrm{s}$ [119]. Glasses undergoing this process must be resistant to crystallization. This feature is commonly assessed by measuring the difference between the glass transition temperature and the crystallization temperature. A difference of at least 150 °C is normally requested for avoiding crystallization during the drawing process [5, 32]. The glass composition and the concentration of intermediate oxides has great influence on the glass stability [120].

Core and cladding glass matching

The thermo-mechanical properties of the core and the cladding glasses of an optical fibre should match in terms of glass transition temperature and thermal expansion coefficient. This is necessary to allow the simultaneous drawing of core and cladding

trough the preform drawing technique, and to avoid the presence of residual stress in the fibre [4, 121].

Control of the thermal expansion coefficient

Silicate doped glasses commonly show values of thermal expansion coefficients around 9 to $7 \times 10^{-6}\,\mathrm{K}^{-1}$, whereas commercial phosphate glasses show slightly higher values, between 12 to $7 \times 10^{-6}\,\mathrm{K}^{-1}$. Relatively low values of expansion coefficient are necessary to keep the robustness of an optical fibre. Moreover this limits the effects of fibre misalignment in consequence of overheating during laser operation [4]. An advantage of phosphate glasses is the possibility to obtain glasses that do not change the optical path in consequence of overheating. These glasses are called "athermal" and can be obtained only with materials that present a negative change of refractive index in consequence of heating. Phosphate glasses can show this property and thus they have been used for the development of athermal glasses, particularly interesting for high power lasers [100, 122, 67].

Control of the refractive index

The refractive index mismatch between core and cladding of an optical fibre defines the numerical aperture of the device:

$$NA = \sqrt{n_{core}^2 - n_{clad}^2} \tag{2.12}$$

This value, together with the fibre geometry, defines the modal properties of the laser [123]. In particular, the number of modes supported by an optical fibres at a given wavelength λ is defined by the V-number [65]:

$$V = \frac{2\pi}{\lambda} \cdot a \cdot NA \tag{2.13}$$

The fibre supports only one mode when the V-number is lower than 2.405. Values of numerical aperture as low as 0.07 are requested for single mode regime of optical fibres working in the near IR. On the other hand values of numerical aperture above 0.4 are requested for first/second cladding interfaces [124, 88]. This values can be achieved by changing the composition of the glass. However, great attention must be paid in order to keep unaltered the thermo-mechanical compatibility of the materials.

Table 2.2 Properties of the Nd:LiAlBa core glass developed in Politecnico di Torino between 2012 and 2014. Data are reported in [30, 31, 11, 32, 33].

Properties of the Nd:LiAlBa core glass		
Property	**Value**	**Unit**
Density	2.8 ± 0.05	g/cm^3
Thermal expansion	9.7 ± 0.1	$10^{-6}\,°C^{-1}$
Glass transition temperature	489 ± 3	°C
Crystallization temperature	675 ± 3	°C
Softening temperature	538 ± 3	°C
Young's modulus	60 ± 2	GPa
Tensile strength	$200 - 400$	MPa
Fracture toughness	0.5	$MPa \cdot \sqrt{m}$
Bulk transparency window	$350 - 2700$	nm
Absorption cross section	3 ± 0.2	$10^{-20}\,cm^2$
Refractive index at 1061 nm	1.57 ± 0.01	–
Quenching concentration	8.47	$10^{20}\,cm^{-3}$
Near-zero concentration lifetime	367	μs

Mechanical properties

The mechanical characterization of optical fibres is important to assess the effective employability of the devices on a large scale. Phosphate glasses are known for having lower mechanical resistance if compared to silicate. For this reason a great effort has been spent to improve their toughness and structural strength [125]. A complete mechanical characterization on phosphate optical fibre performed by Sglavo et al. reports values of Young modulus of $E = 60\,GPa$, tensile strength values above $\sigma = 200\,MPa$ and fracture toughness around $0.5\,MPa \cdot m^{0.5}$ [33, 32].

2.3.3 Performance of phosphate fibre lasers

The studies performed so far to achieve the best material, suitable for the production of phosphate glass fibre laser, have led to important achievements in the demonstration of high power, high quality devices. The following paragraphs will give a very brief overview of the main results obtained in recent years.

Nd-doped fibre lasers

Nd^{3+} has always been considered interesting in laser development due to its low lasing threshold. Remarkable results obtained on Nd-doped phosphate fibres include the generation of multi-watt output power from phosphate glass step index fibres, with a conversion efficiency around 45%. These results have been achieved on a 26 cm-long DC optical fibre doped with Nd^{3+} at a concentration of $3.4 \times 10^{20} \mathrm{cm}^{-3}$ and on a 6 cm-long SC cane doped with Nd^{3+} at a concentration of $7.2 \times 10^{19} \mathrm{cm}^{-3}$ (see Chapter 5) [4, 126].

More recent results include the generation of 1.42 W in single mode regime with an efficiency of 34%. The result was recorded on a single mode, DC fibre featuring a core diameter of 5.3 μm [127].

In the last years photonic crystal fibres became also interesting configurations for the development of fibre lasers, due to the large area, single mode behaviour. The record output power of 15.5 W, with a slope efficiency of 55%, on CW fibre laser was obtained using a seven-core, single-mode photonic-crystal fibre [86].

Yb-doped fibre lasers

The record power and record slope efficiencies obtained on fibre lasers have been obtained on Yb^{3+}-based fibres, in virtue to the peculiar structure of the ion. A CW laser featuring a maximum power of 57 W with a slope efficiency of 56.7% was demonstrated in a single mode phosphate fibre, at a wavelength of 1030 nm. The phosphate glass core of the fibre was heavily doped with Yb^{3+} ions at a concentration of $1.42 \times 10^{21} \mathrm{cm}^{-3}$ [88]. This result was preceded by the generation of 20 W emitted power in a single-mode regime featuring a slope efficiency of 25% on the launched power, obtained in the same configuration of the previous experiment [102].

Er and Yb/Er-doped fibre lasers

A record power of 9.3 W in continuous wave regime was obtained on an Yb/Er co-doped fibre laser at the wavelength of 1535 nm in multi-mode regime, featuring a maximum slope efficiency of 29%. In the same work the authors report the generation of 4 W output power in single mode regime [128].

2.4 Conclusion

Phosphate glasses are still under study for the fabrication of compact high power laser devices. Research on this topic is still ongoing, in particular for the development of rare earth doped compositions that are suitable for fibre drawing. The interest in these applications is raised by the increased use of lasers in several fields, such as materials processing, defence and medicine.

Chapter 3

Fabrication and characterization of phosphate glasses

In this chapter, all the fabrication and characterization techniques that were used during the course of this Ph.D. program are described. Particular attention is devoted to the optical characterization of rare earth doped glasses and to the optical fibre fabrication and characterization process. A final section is dedicated to the procedures used for assembling and characterization of high power fibre lasers.

The chapter is divided in four sections, related to the fabrication and characterization of bulk optical glass, the process of optical fibre drawing, fibres characterization and power scaling and characterization procedures of high power lasers.

The processing methods used for the optical fibre preform fabrication and assembly will be presented Chapter 4.

3.1 Phosphate glass fabrication and characterization techniques

The fabrication of an optical device starts form the synthesis of the bulk materials. In this work, phosphate glasses have been used as the base material for all the experiments. In this section the procedures that are used for the fabrication of phosphate glasses on a laboratory scale are described.

3.1.1 Glass synthesis and melting procedure

The definition of the glass composition customized according to the needs, and the choice of the components is usually done according to a preliminary literature review. The glass compositions used in this work will be described in detail in Chapter 5 and Chapter 6.

Once the glass composition has been defined, the glass preparation procedure requires the mixing of the opportune amount of chemical precursors (usually oxides). The main glass former used for the synthesis of phosphate glasses is the phosphorus oxide (P_2O_5). This is normally combined with other oxides acting as network modifiers (Calcium Oxide, Magnesium Oxide, Sodium Oxide, Potassium Oxide,..), network intermediates (Alumina, Lead Oxide..), or other network formers (Silica or Boron Oxide). As most of these reagents, and in particular P_2O_5, are very hygroscopic, the precursors are mixed in a controlled dry atmosphere. The precursors used for this thesis were mixed in a glove box with a humidity level inferior to 0.1% at 25 °C under a flux of dry N_2.

Glass melting procedure

Melting occurs typically at temperatures between 1100 °C and 1400 °C, depending on the composition. This step is extremely critical as it defines the final quality of the material and the reproducibility of results among different glass batches. It is extremely important to control the atmosphere at which the melting takes place, as this influences the final physical properties of the glass. The main parameters that are influenced by the melting atmosphere are:

- **Water content:** In order to obtain a good quality optical glass it is fundamental to minimize as much as possible content of $-OH$ groups in the network. This is mainly achieved by controlling the water content in the furnace, by flowing dry gas during the process [104, 10].
- **Transparency:** In our experience the presence of an oxidising atmosphere in the furnace is fundamental to obtain a clear and transparent glass. This has been correlated to the oxidation state of platinum inclusions in the glass, that tend to aggregate into metallic clusters in the matrix [2]. A clear example of

positive effect of flowing oxygenated gas in the melting furnace is described in Chapter 6, in relation to the melting procedure of the "BPh" glass series.

- **Physical properties:** The fraction of solid material that evaporates during glass melting influences the properties of the glass: as light components tend to evaporate more than heavy ones, a high weight loss during the melt is associated with higher glass density and higher refractive index [1].

- **Glass homogeneity:** A good optical glass should not present striations, bubbles, inclusions or other defects in the bulk. This can be obtained my making the glass melt as homogeneous as possible. In order to obtain this finely grounded components should be mixed carefully before the melting [129]. Stirring of the glass melt has been proposed as a valid alternative procedure for glass homogenization [36].

Definition of the % weight loss during glass melting

Every time a glass is melted, some material is lost due to evaporation. This can be due to the presence of water absorbed on the surface of the reagent's powders, to the evaporation of carbon dioxide from carbonates or to the real evaporation of light components of the glass (i.e. sodium or potassium).

Measuring carefully the material loss is allows assessing the repeatability of the processes, as a well designed fabrication procedure will result in constant weight loss values for different glass batches. The weight loss measurement also allows estimating how much the real composition of a glass resembles the initial reagent's mixture.

The weight loss is measured as the difference between the initial amount of material (the sum of all reagents) and the amount of glass that is finally obtained, expressed in percentage. The final quantity glass takes into account the amount of material that is left in the crucible after the casting. It should be noted that if any gas is released during the melting, i.e. in consequence of the use of carbonates as reagents, this should not be considered as lost material.

The glasses fabricated for this work show typically values of loss between 0.2 to 3.5% for the "BPh" compositions (see Chapter 6) and between 15% to 25% for the "CL" glasses (Chapter 5).

3.1.2 Density Measurements

The density of the glass was measured on bulk samples of glass by the Archimedes principle, using distilled water as an immersion fluid. Cylindrical samples featuring a diameter of 12 mm and 10 mm in height were used for all measurements. According to the Archimedes formula. The density of a non-porous material can be calculated as:

$$\rho = \frac{W_{dry}}{W_{dry} - W_{wet}} \tag{3.1}$$

where ρ is the sample's density, W_{dry} is the weight of the sample in air, W_{wet} is the weight of the sample in water. the density of distilled water is assumed to be $1\,\mathrm{g/cm^3}$. The typical error on the measurement is $\pm 0.01\,\mathrm{g/cm^3}$

3.1.3 Thermal characterization

Thermal characterization is performed to measure the characteristic temperatures of the materials. Having a reliable measurements of the glass transition temperature (T_g), glass crystallization temperature (T_x), glass softening temperature (T_s), and coefficient of thermal expansion (CTE) is fundamental for designing a proper processing of the material and an effective device. As detailed in Chapter 5 there are strict requirements on the T_g and CTE mismatch that can be tolerated during optical fibre drawing. Moreover fibre drawing and extrusion procedures require the use of glasses with a high T_x, in order to avoid precipitation of crystal during the processing. Two analyses were performed in the course of this work: differential thermal analysis (DTA) and dilatometric analysis. The first is used for measuring the transition and the crystallization temperature of a glass, the second to measure the coefficient of thermal expansion and the softening temperature.

Differential Thermal Analysis

DTA, and similarly differential scanning calorimetry (DSC), are very effective techniques used to monitor ongoing thermodynamic transformations, occurring with a change in the specific heat of the sample. A DTA set-up is made of two specimen holders equipped with one thermocouple each. The first specimen holds the sample to be tested, while the second one contains an inert material. The machine is able

to run a specific time-temperature program, defined by the user, and record the temperature difference between the two specimen during the process. A final graph of temperature mismatch against time is given as an output.

A typical DTA graph is displayed in Fig.3.2.a. As it can be seen the T_g is identified by an inflection of the curve (second order transformation) followed by the so called entropic relaxation peak. The crystallization of the glass and the subsequent melting are identified by two peaks of opposite direction (first order transformation) [130, 46].

DTA measurements performed in this work were obtained by using a Netzsch DTA 404-PC model. A constant heating rate of $5\,^{\circ}\mathrm{C}/\mathrm{min}$ was used for all experiments. 200 mg of alumina sealed in Pt-Rh crucible were used as an inert reference. The sample was made weighting about 200 mg of grounded glass sealed in a Pt-Rh crucible. The T_g was defined as the onset of the inflection related to glass transition transformation, whilst the onset of the crystallization peak was defined as T_x (see Fig3.2.a). The typical error on DTA measurements is $\pm 3\,^{\circ}\mathrm{C}$.

Thermal expanison measurements

The measurement of thermal expansion in glasses can provide important information on the characteristic temperatures of the material (T_s, T_g), as well as providing a measurement of the thermal expansion coefficient CTE. The shape of the dilatometric curve is indicative of the presence of residual stress in the glass and the consequent quality of the annealing process [46].

The set-up is made of an inert probe applying a small force on a bulk sample with known dimension. The machine is able to run a specific time-temperature program, defined by the user and the output is a graph plotting the elongation of the sample as a function of the temperature.

The expansion behaviour of a glass is linear, provided that no residual stress is present in the sample; the slope of this line is defined as the coefficient of thermal expansion CTE of the material. When the T_g is reached, an abrupt increase of the sample's CTE can be observed. The softening temperature T_s is defined as the temperature at which the material starts to shrink in consequence of the load applied by the probe. An example of the thermal expansion curve of a phosphate glass is displayed in Fig.3.2.b

Fig. 3.1 (a) the DIL 404-PC fcility used for thermal expansion experiments, (b) the DTA 404-PC used for calorimetry experiments.

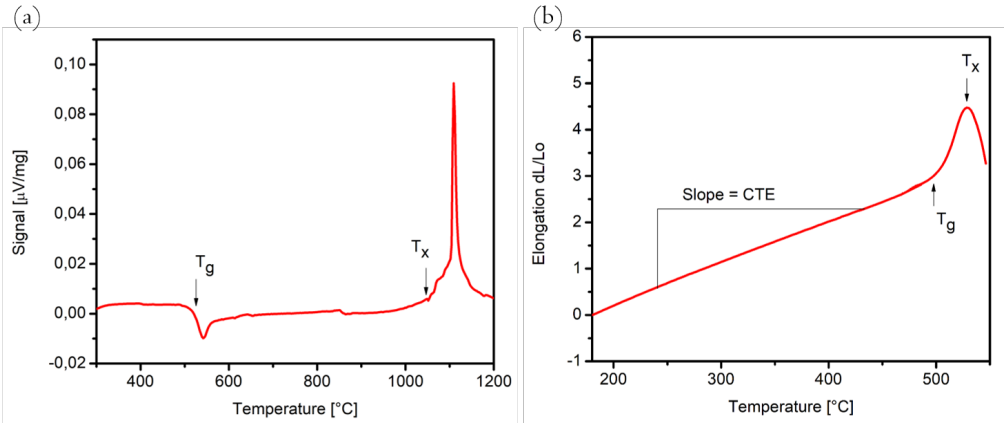

Fig. 3.2 (a) typical DTA curve of a phosphate glass, (b) tipical thermal expansion behaviour of a phosphate glass.

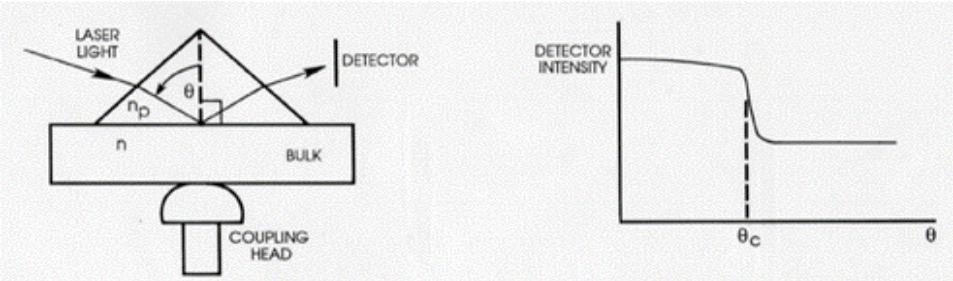

Fig. 3.3 Principle for the measurement of the refractive index by prism coupling technique. Image adapted from Metricon2010 users manual.

Thermal expansion experiments in this work were performed using a Netzsch DIL 404-PC model. A constant heating rate of 5 °C/min was used for all experiments as reported for DTA measurements. 5 mm-long samples with parallel faces were used for the measurements. The CTE was measured by calculating the average slope of the expansion curve between 200 °C and 400 °C, the T_g was estimated as the onset of the slope change of the curve in consequence of glass transition. The typical error on DTA measurements is $\pm 0.1 \times 10^{-6}\,\mathrm{K}^{-1}$.

3.1.4 Optical/Spectroscopic characterization on active and passive glasses

Optical and spectroscopic characterization was carried out on bulk samples of glass. The samples used for all measurements were obtained by slicing a 12 mm diameter rod into 2 mm-thick disks. The disks were optically polished with Alumina suspensions and diamond suspension down to a grain size of 1 μm. This allowed obtaining samples featuring surface roughness values $R_{sq} < 1$ nm for all samples, as measured by AFM and described in Chapter 7.

Refractive index measurement

The refractive indices of all samples were measured by means of a Metricon2010 model prism coupler facility equipped with diode lasers at 5 different wavelengths (633, 825, 1061, 1312 and 1533 nm).

The principle of prism coupling method for the measurement of the refractive index is depicted in Fig.3.3, as described in the user's manual. The laser source is launched though the prism and reflected at the prism/sample interface. When the angle of incidence becomes smaller than the critical angle the beam is no more reflected and the detector signal drops abruptly. This is a direct measurement of the critical angle. The refractive index can be calculated from the critical angle according to the formula:

$$\theta_c = \arcsin(n/n_p) \tag{3.2}$$

where θ_c is the critical angle, n is the refractive index of the sample and n_p is the refractive index of the prism. The theoretical resolution of this machine is $\pm 10^{-4}$,

however due to the inhomogeneities in the glass batches, the typical error considered for refractive index measurements is $\pm 10^{-3}$.

UV-Visible/NIR absorption spectroscopy

The UV-Vis/NIR absorption spectra of the samples were recorded using a dual beam Varian-Cary 500 UV-Vis/NIR spectrophotometer (Fig.3.4.a) at different scan rates in the region between 190 and 3000 nm. The measurements were performed in single beam configuration.

A light beam at a defined wavelength is launched at a normal angle on the sample surface. The amount of incident light is known, and the amount of transmitted light is recorded. The machine's software is able to plot a spectrum of the absorbed light as a function of the wavelength. This allows defining the window of transparency of a glass.

In the case of active materials (rare earth doped glasses) the absorption spectrum of the glass is used to measure the absorption cross section of the active ion, defined as follows:

$$\sigma_{abs} = \frac{\alpha(\lambda)}{N} = \frac{2.303 \cdot A}{LN} \tag{3.3}$$

where $\alpha(\lambda)$ is the absorption coefficient of the material, A is the absorbance, L is the thickness of the sample N is the concentration of active ions per volume unit. The typical error on this measurement is considered $\pm 0.02 \times 10^{-20}\,\mathrm{cm}^2$

Fourier Transformation Infrared Spectroscopy (FTIR)

FTIR spectroscopy is used to perform absorption spectroscopy in the near IR region. It can be performed in transmittance configuration or in the so called attenuated reflectance mode (ATR). This method takes advantage of the use of a Michelson interferometer and an algorithm based on Fourier transformation to provide an absorption spectrum of a sample. It is particularly useful to investigate the absorption spectra of materials in the region ranging from 1 to 12 μm.

FTIR spectroscopy in the transmittance mode is used to perform quantitative analyses on the water content of the glass. This is obtained by measuring the absorption peak, located at 3300 nm, associated to the presence of $-OH$ groups in phosphate glasses [104, 10, 6].

FTIR-ATR is used to perform structural analyses on phosphate glasses, as it allows to investigate the presence of Q^1, Q^2. or Q^3 structures in the glass by identifying the vibrational transitions related to different $P-O-P$ bonds [6].

Emission spectroscopy and lifetime measurements

An important characterization to be performed on rare earth-doped glasses is the measurement of the emission spectrum and the excited state lifetime of the active ion in consequence of the excitation with a laser pump. The emission spectra can be recorded by using a spectrophotometer equipped with a dedicated detector. The lifetime value can be calculated by interpolating the fluorescence decay curve once the excitation source is removed.

In this work, emission spectra from Nd^{3+} doped samples have been measured. The fluorescence spectra were acquired using a Jobin Yvon spectrometer equipped with an InAs cooled single channel detector Hamamatsu P4631-02. Emission spectra of the Nd^{3+} ion were obtained by exciting the samples with a pigtailed laser diode at 785 nm. A schematic of the set-up used is displayed in Fig.3.5.a.

The lifetime was measured by collecting the fluorescence decay curve of a sample excited by a pulsed laser source. The set-up used for lifetime measurements is similar to the one used for collecting the emission spectra. A square-wave signal generator is used to obtain generate a pulsed laser emission from a fibre-coupled diode. The signal is directed on the edge of a glass sample to minimize re-absorption. The light emitted from the sample is directed towards the detector, that is connected to an oscilloscope. A schematic of the set-up is displayed in Fig.3.5.b. The photodetector converts the emitted light signal into an electric signal, allowing the oscilloscope to register it and display the decay curve on the screen. The decay curve is registered and fitted according to a single exponential equation:

$$y = A \cdot \exp(-t/\tau) \tag{3.4}$$

where y is the signal intensity, t is the time, A is a constant and τ is the fluorescence lifetime. Typically, five to eight measurements per sample are taken, and the typical error on the measurement is $\pm 5\,\mu$s.

Fig. 3.4 (a) the UV-Vis/NIR spectrofotometer used for absorption spectroscopy (b) the FTIR facility Alpha Bruker used for IR spectroscopy.

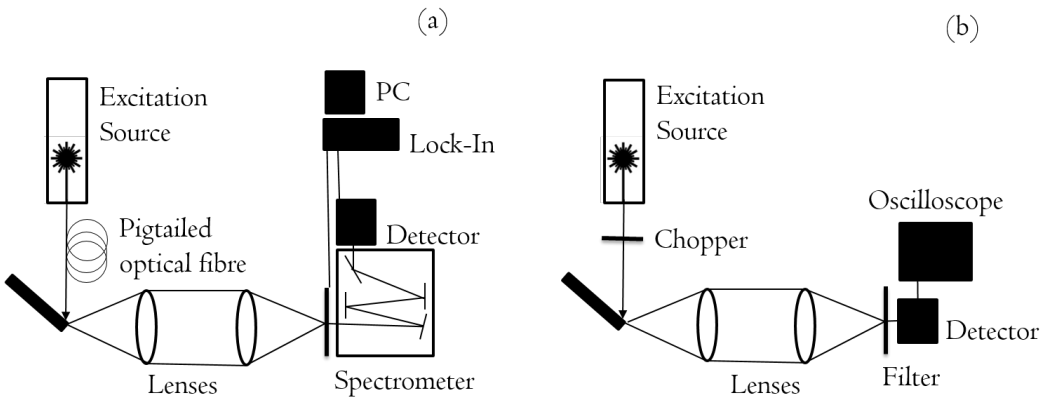

Fig. 3.5 (a) Set-up used for the measurement of the emission spectra, (b) set-up used for lifetime measurements.

3.1.5 Dissolution tests

Dissolution tests are widely used in the in-vitro characterization of biomaterials and they are performed in a variety of ways, depending on the time scale, the dissolution fluid and the parameters monitored. In this work dissolution tests have been performed in order to assess the solubility in simulated physiological conditions of the "BPh" glass series (see Chapter 6). This glass was developed in order to behave both as a biomaterial and as an optical glass.

This test can be performed on any kind of sample, provided that the ratio between the surface exposed to the dissolution liquid and the volume of liquid is controlled. In this work dissolution tests have been performed on single material phosphate glass fibres, single material hollow glass fibres and optical fibres irradiated with high intensity UV light (see Chapter 6 and 7). Phosphate buffered saline solution (PBS) at $pH = 7.4$, $T = 37\,^{\circ}\mathrm{C}$ was used as a dissolution media for all experiments.

The experiments performed on glass fibres were used to monitor the diameter reduction, pH change and the weight loss. Fibres were soaked in PBS with a solution volume/sample exposed area of $0.1\,\mathrm{mm/ml}$. To calculate the exposed area of the fibre sample, fibres with a mean diameter D_f were considered as a single cylinder with the same diameter of the fibre and a length L, corresponding to the sum of single fibres lengths. The total surface area can be thus calculated as a function of the total weight of the fibres, density of the glass and mean diameter [18]:

$$A_{exp} = \pi D_f L = \pi d_f \left(\frac{W}{\rho}\right) = \frac{4W}{\rho D_f} \tag{3.5}$$

where A_{exp} is the surface exposed, D_f is the diameter of the pristine fibre and L its length. W is the total amount of material weighted and ρ the density of the glass.

Monitoring fibres diameter reduction

A first experiment, performed in triplicate according to the standard ISO 10993-14 [131], was set-up for monitoring the diameter reduction of the fibres. The samples were weighted and immersed in PBS. At different time points (3, 7, 14, 21 days) at least three fibres were removed from each container and dried. For each time point at least 15 diameter measurements were performed on the samples, calculating average size and standard deviation. Measurements were performed using an optical

microscope. Refreshing of the medium was performed twice a week to simulate physiological fluid exchange.

Dissolution occurred homogeneously on single materials fibres, while inhomogeneity in the dissolution kinetics was observed on UV irradiated fibres. A detailed discussion of the results is reported in Chapter 7.

Monitoring fibres weight loss and pH alteration

In a second experiment the fibres weight loss and the *pH* change of the solution during fiber dissolution were studied. This test is also conducted in triplicate. the samples were weighed and immersed in PBS in the same conditions as the previous experiment, with the only difference that the size of the experiment was scaled by a factor of 2. *pH* measurements were performed twice a week priorly to PBS refreshment (after 3, 7, 14, 21 days). After 21 days, the PBS solution was removed from the samples; the fibres were washed with bi-distilled water, dried and finally weighed. The weight loss was expressed as a percentage.

3.2 Preform drawing technique for optical fibres fabrication

The optical fibres fabricated for this work were obtained by preform drawing, with the preform being assembled according to the rod-in-tube technique. The steps required for the fabrication and assembling of the preform are described in detail in Chapter 4.

The drawing facility used for the fabrication of optical, hollow and single material fibres has been developed in this laboratory in the past years [124]. It consists in a 4-meter high drawing tower. The top part is equipped with an induction furnace, delivering an amount of power between 150 and 250 W according to the drawing temperature. A graphite ring is used as a coupling medium to obtain a localized heating on the glass preform.

A schematic of the drawing tower facility is represented in Fig.3.6.a. The glass preform is heated in the furnace until a glass drop forms. The resulting glass fibre is attached to a rotating drum, that is spinning at a known velocity. By controlling the

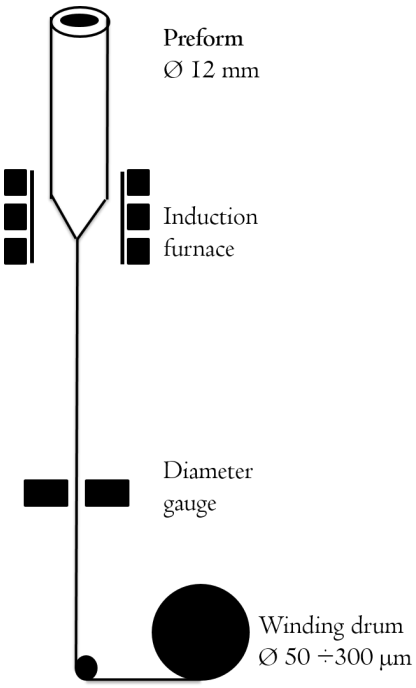

Fig. 3.6 (a) Schematic representation of the drawing facility developed at Politecnico di Torino

drawing speed and the feed speed at which the preform is heated, it is possible to determine the size of the fibre. According to the volume conservation law the flow of material in the tower can be described as:

$$D_p^2 \cdot v_p = D_f^2 \cdot v_f \tag{3.6}$$

where D_p and D_f are the diameters of the preform and the fibre respectively, whereas v_p and v_f are the feed speed of the preform in the furnace and the drawing speed. The final diameter of the fibre is thus given by:

$$D_f = \sqrt{(D_p^2 v_p)/v_f} \tag{3.7}$$

this equation is used to control the size of the drawn fibre with a tolerance of $\pm 3\,\mu$m.

3.3 Characterization of optical fibres

Two main reasons make necessary the full characterization of an optical fibre after the fabrication. The first one is related to a quality control procedure, carried out to assess the effective outcome of the glass and preform processing. The second reason is related to the assessment of the fibre properties, such as the ability to emit or amplify laser light or the ability to perform simultaneous actions, such as guiding light and fluids in the same time (see Chapter 7). In this section the standard procedures that are used in our laboratory for the quality control of optical fibres are described.

3.3.1 Morphological characterization

Optical miscroscopy is the most straightforward method for assessing the good quality of the fibre. An optical microscope (Nikon Eclipse 50i) equipped with a camera and connected to a PC through a dedicated software was used for all measurements.

Optical microscopy allows assessing that the fibre was effectively drawn at the right dimension. Moreover the presence of defects, such as interface inclusions, crystallization or incomplete adhesion of the core/cladding can be easily identified.

3.3.2 Near-Field imaging

Near field imaging is used to investigate the modal properties of optical fibres and to assess the ability to guide light. Light is coupled to a cleaved end of the fibre sample, and the output facet is observed using an IR camera equipped with an opportune magnifying lens. A schematic of the set-up is displayed in Fig.3.7.a.

Typically a laser light at 1300 nm was used to investigate the properties of RE doped fibres, as this wavelength does not interact with the Nd^{3+} ions. In the case of the BPh glass (see see Chapter 7), near field pictures were also taken by illuminating the fibre with a 600 nm laser light in order to assess the modal properties of calcium-phosphate optical fibres in the visible range.

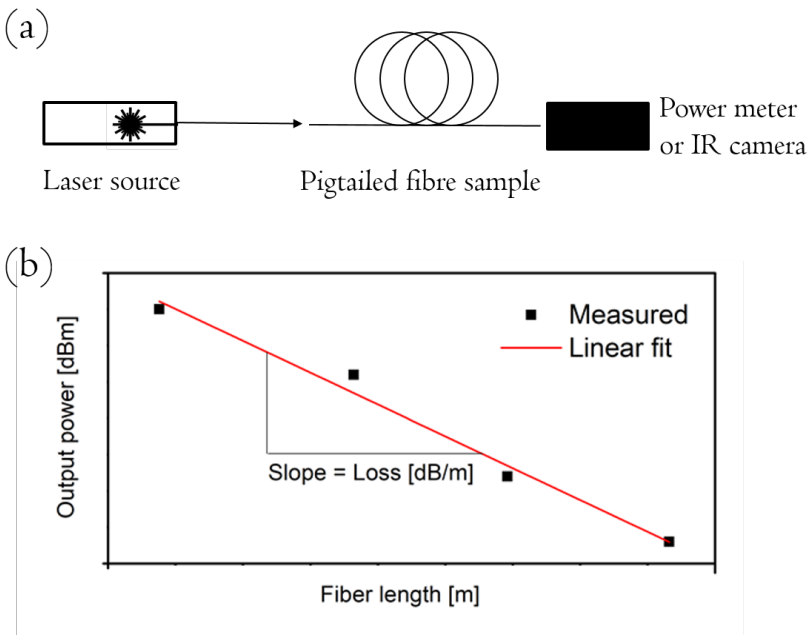

Fig. 3.7 (a) Schematic representation of the set-up used for near-field imaging and (b) sample graph used for cut-back measurements.

3.3.3 Cut-back technique

The cut-back technique is used to assess the fibres loss due to the attenuation of the beam. These losses are related mainly to defects at the core/cladding interface and inhomogeneities in the glass structure. Bending also causes optical losses on the fibres, in the case of very low values of numerical aperture.

The technique consists of launching a known power of laser light into a sample of optical fibre and measuring the power received at the output facet by means of a power meter. The measurement is taken starting from a long section of optical fibre that is progressively cut back in shorter samples.

A graph displaying in logarithmic scale the signal registered by the power meter as a function of the fibre length can be obtained. If the fibre is free of defects, the graph displays a straight line, whose slope is the loss of the fibre (see Fig.3.7.b). Typically the value is reported in dB/m units. A reasonable estimation of the error in this measurement is about 10%

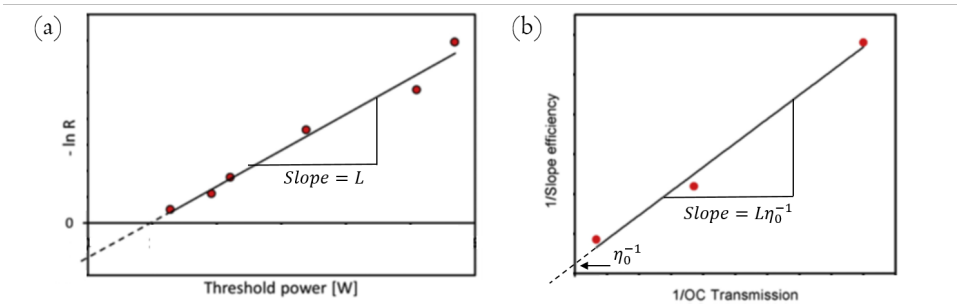

Fig. 3.8 (a)Sample graph used for the Findlay-Clay analysis, (b) sample graph used for the caird analysis

3.4 Assembly and characterization of a fibre/cane laser

The fabrication of high power lasers is a major application of phosphate glasses in photonics. The assembly of a fibre/cane laser device based on a phosphate glass requires a set-up that can be described in three stages, as detailed below. Fig.3.9 displays a schematic of the set-up used in this work for the development of a Nd^{3+} laser.

- **Stage 1** can be defined as the "pump coupling stage". This is made of the high power laser pump diode (or diodes) and the optical system that allows to couple light into the active media (f_1 and f_2 in Fig.3.9). In this work the diode used for the pumping of Nd^{3+} ions operates at the wavelength of 795 nm and provides a maximum output power of 20 W. The beam is guided trough a silica optical fibre featuring a core of 200 μm and a numerical aperture (NA) of 0.22. The optical system used to couple light in the active media defines the size of the spot that is focused on the active input facet. Different sets of lenses were used according to the needs.

- **Stage 2** is the proper laser cavity. It is made of a RE-doped active optical fibre and two aligned mirrors (m_1 and OC in Fig.3.9). The first mirror is transparent at the pump wavelength, but prevents the generated laser signal to be reflected into the pump diode. The second mirror is an output coupler (OC), and is featured by high reflectivity at the pump wavelength. A defined amount of signal (ranging from 5% to 95%) is allowed to be transmitted by the OC and constitutes the output signal of the laser.

- **Stage 3** is an optical system that allows separating the generated laser signal from the residual pump. This stage consists in a lens (f_3) collecting the laser signal and the resudual pump and a dichroic mirror (m_2) with high transmittance at the pump wavelength and high reflectivity at the signal wavelength. The signal can thus be reflected and sent to a diagnostic tool, such as a powermeter, a camera or a beam profiler. The residual pump can be sent to a beam dump or to a power meter to estimate the effective absorbed power.

3.4.1 Power scaling experiments on rare earth doped fibre lasers

Power scaling experiments are used to determine the maximum power and efficiency achievable by a laser. Experiments are conducted in order to optimize the set-up parameters, such as the pump spot size and the OC transparency. In particular performing experiments with different output couplers, measuring both the variation of the threshold power and the slope efficiency as a function of the OC transparency allows performing further analyses of the laser performance. In this work the estimated value of the resonator loss and the intrinsic slope efficiency of the laser have been measured according to the methods developed by Findlay-Clay and Caird [132, 133].

The power scaling experiments in this work were conducted on a Nd^{3+} doped cane laser. The active medium was pumped with increased power and the emitted signal power, the lasing threshold, the launched power and the residual pump power were monitored all along the test. This measurement was repeated for different output couplers and the slope efficiency was calculated both with respect to the absorbed pump power and to the launched pump power.

3.4.2 Estimation of the resonator loss and the intrinsic efficiency of a laser

The resonator loss can be measured according to two different methods: the Findlay-Clay analysis and the Caird analysis. Both method have been used in this work and they are described in the following paragraphs.

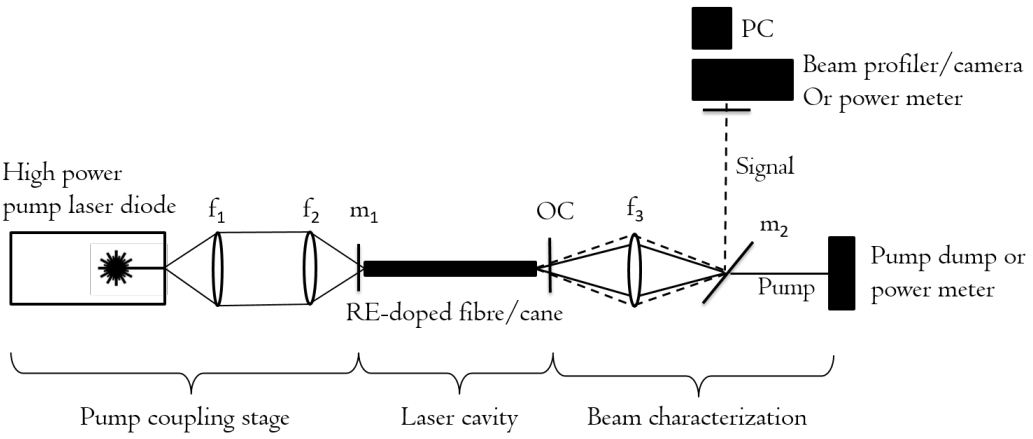

Fig. 3.9 set-up used for laser tests on phosphate glass fibres and canes

The Findlay-Clay analysis

The Findlay-Clay analysis is a method used for estimating the loss of a resonator based on the value of the lasing threshold [132]. The lasing threshold is defined as the excitation level where the optical gain of the active media is exactly balanced by the round trip loss of of the light in the resonator. The losses can be separated into two factors: one due to the resonator's mirrors (controlled by the experimenter) and one due to the medium (i.e. insertion losses, scattering and absorption) that is not generally controllable.

By assuming that the optical loss of the medium is constant when the laser is operating close to the threshold point, the following equation can be written [132]:

$$g_{th} = a_0 - \frac{1}{2l}\log(R_1 R_2) \tag{3.8}$$

where g_{th} is the gain at the threshold point, a_0 is the optical loss value, assumed to be constant and R_1, R_2 are the reflectivities of the resonator's mirrors.

As it is difficult to obtain a laser working in a stable condition at the threshold point, some assumptions can be made to rewrite the eq.3.8 in a more convenient way: the threshold power P_{th} can be assumed to be $P_{th} = 2g_{th} \cdot l$, where l is the cavity length. R_1 can be assumed equal to 1, as its value is normally above 95%. The loss of the resonator can be redefined as $L = 2a_0 \cdot l$. This allows rewriting the former equation as:

$$P_{th} = K\,(L - \log R_2) \tag{3.9}$$

where K is constant. This allows the experimental determination of the value L.

Practically, the estimation of the losses is done by measuring different values of the threshold power P_{th} of the laser using different output couplers (corresponding to different R_2 values). The results are then plotted on a graph having $\log R_2$ as the ordinate and the threshold power as the abscissa. The value of L can than be extrapolated from the slope of the linear graph obtained.

An example of a typical Findlay-Clay graph is displayed in Fig.3.8.a.

The Caird analysis

The Caird analysis is another method that allows estimating the cavity loss of the laser, in addition to the Findlay-Clay method it also provides an estimation of the so called "intrinsic slope efficiency" of the laser. This is a limit value that estimates the maximum slope efficiency that can be obtained from the laser [133].

According to this method a linear relation between the inverse slope efficiency of the laser and the inverse output coupling can be written as:

$$\eta_s^{-1} = \eta_0^{-1}\left(1 + LR_2^{-1}\right) \tag{3.10}$$

where η_s is the slope efficiency of the laser and η_0 is the intrinsic slope efficiency. The other parameters are defined as in the previous paragraph. In bulk lasers the intrinsic slope efficiency is generally considered to be a material's property, being dependent on the pumping efficiency, the quantum defect and the absorption and emission cross-sections:

$$\eta_0^{-1} = \eta_p \cdot \frac{\lambda_p}{\lambda_s} \cdot \frac{\sigma_e - \sigma_a}{\sigma_e} \tag{3.11}$$

where λ_p and λ_s are the the pump and signal wavelengths, σ_a and σ_e are the excited state absorption cross-section and the emission cross section.

An example of a typical Caird graph is displayed in Fig.3.8.b.

3.5 Conclusion

In this chapter the fabrication and characterization techniques that were used along this Ph.D. project were described. A variety of methods have been applied in order to

characterize novel bulk materials, with multiple functionalities and enhanced optical properties. The materials have been used for the fabrication of optical devices, such as optical fibres, cane and fibre lasers, whose performance has been tested. In the following chapters the results obtained during this work will be reported in detail.

Chapter 4

Fibre preform fabrication

In Chapter 3 all the steps leading to the fabrication of an optical fibre, from the raw material up to the complete device, have been discussed. However, the key steps related to fibre preform fabrication and assembly have not been yet analysed in depth. The methods used for obtaining a preform affect the overall quality, functionality and performance of a specialty optical fibre.

Chemical vapour deposition (CVD) is the gold standard process used for the fabrication of common step-index silica optical fibres [50]. This method is used to obtain the purest materials. However, it is very complex to extend the use of CVD to soft glasses and to specialty optical fibres with a microstructured section. For such a reason, the rod-in-tube and the stack-and-draw processes are preferred for fabricating soft glass specialty optical fibres. This brings to the necessity of obtaining soft glass preforms featuring the desired profile requested for fibre fabrication. Typically, this involves providing hollow profiles with a very good shape uniformity and excellent surface quality.

Significant attention has been given in selecting an efficient method for the fabrication of hollow profiles to be used as the cladding of a step-index fibre or the preform of a hollow fibre (e.g. a photonic-crystal fibre (PCF)). This step is becoming increasingly important as the development of complex shape, asymmetrical and microstructured optical fibres progresses. As an example, recent research in the field of optical fibre fabrication, demonstrated that fibres featuring asymmetrical sections could greatly increase the slope efficiency of high power lasers, by improving the pump power absorption, mitigating non-linear effects and facilitating heat sinking

[134]. However, the high cost and intrinsic difficulties of preform manufacturing and materials processing are still a limit to the wide diffusion of such devices. Some innovative fabrication techniques, such as additive manufacturing or laser machining, have been proposed for manufacturing preforms, however they are available only for silica glass. Moreover, it seems very difficult to extend the application of additive manufacturing techniques to soft glasses, such as phosphates, as there is no evidence that a sufficient material homogeneity and surface quality can be obtained [135, 136].

In this chapter three methods used for fabricating cladding components of phosphate glass optical fibres are reviewed: coring or drilling, rotational casting and extrusion. Particular attention is devoted to the development of an extrusion facility in our laboratory in Politecnico di Torino, discussing the advantages and peculiarities of this technique.

4.1 Coring and/or drilling of a preform

Coring is the most straightforward technique for fabricating glass preforms and it is still the commonly used when a large amount of material is available. A cylindrical billet can be obtained by drilling a bulk glass cylinder using a coring diamond bit, typically mounted on a large vertical drill. Then, the resulting cylinder can be made hollow by drilling a hole of the desired size using a diamond bit. This technique is easy to implement and requires a small investment in terms of machining facilities. It offers discrete versatility, as the internal holes can be placed anywhere in the cylinder's section.

As a drawback, this technique allows fabricating only cylinder-shape holes. More complex machining can be performed, i.e. cutting and milling, for obtaining non-cylindrical external shape. However, this becomes very expensive in terms of time and material waste. Another drawback is related to surface quality: machining methods are not able to give a sufficiently smooth surface for optical fibre drawing, thus, polishing of all the surfaces is mandatory. This step is very complex, expensive and time consuming, as it involves the polishing of small and curved surfaces, requiring most of the times skilled manual labour. The final result is usually excellent in quality, but it comes at an excessive price. This limitation has been so far a true bottleneck to the large scale diffusion of PCFs and other microstructured fibres.

4.2 Tube fabrication by rotational casting

The rotational-casting technique has been applied for the first time to fluoride glasses. Later, its use in the fabrication of phosphate glass tubes was introduced by our research group in 2013 [32, 12, 137]. This technique involves casting a glass melt into a pre-heated, cylindrical mould. With the aid of an engine, the mould spins at a speed around 3000 rpm creating a hollow structure. A schematic of the set-up developed in the laboratories of Politecnico di Torino and examples of preforms obtained by rotational casting are depicted in Fig.4.1.a.b.c. This method has the advantage of yielding the best internal surface quality observed so far on optical fibre preforms, but is very limited in terms of the shapes that can be obtained.

4.2.1 Fiber drawing process with rotational casting preforms

Rotational casting are limited by the wall thickness and the diameter aperture that can be obtained. In the practical case, the facility of our laboratory allows the fabrication of centred tubes with an internal/external diameter ratio from $1/2$ to $1/4$. However, not all diameter ratios can be obtained with all glass compositions: casting temperature and viscosity play a decisive role in the process and only small adjustments can be made on such parameters once glass composition is fixed. Only small adjustment in the internal diameter size (in the range of 0.3 to 0.5 mm) can be achieved by varying the rotation speed.

Since it is complex to modify the diameter ratio of a glass tube during the drawing of an optical fibre, and this modification is limited, only fibres or canes with almost the same diameter ratio of the tube can be drawn. This means that only some core/cladding ratios are achievable on optical fibres made by rotational casting. Fibres with a smaller core size can be obtained by multiple stretching steps, using multiple cladding tubes. Repeated heating cycles on the preforms, however, are undesirable, as they favour the crystallization of the glass. Moreover, this process is very time consuming and not free of risks. Fig.4.2 depicts the typical steps required for the fabrication of a single mode fibre. Two tubes obtained by rotational casting, with a typical diameter ratio of $1/4$ are used for the process. The same method can also be used for the fabrication of double cladding fibres (See Fig.4.3.d).

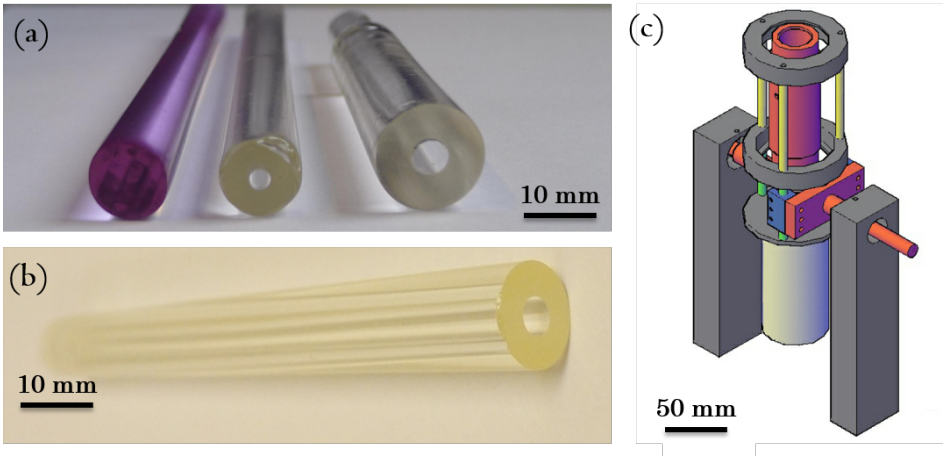

Fig. 4.1 (a) Example of a Nd^{3+} doped core rod and two different cladding preforms obtained by rotational casting, (b) example of a first cladding glass preform obtained by rotational casting, (c) scheme of the apparatus used for rotational casting (adapted from [12])

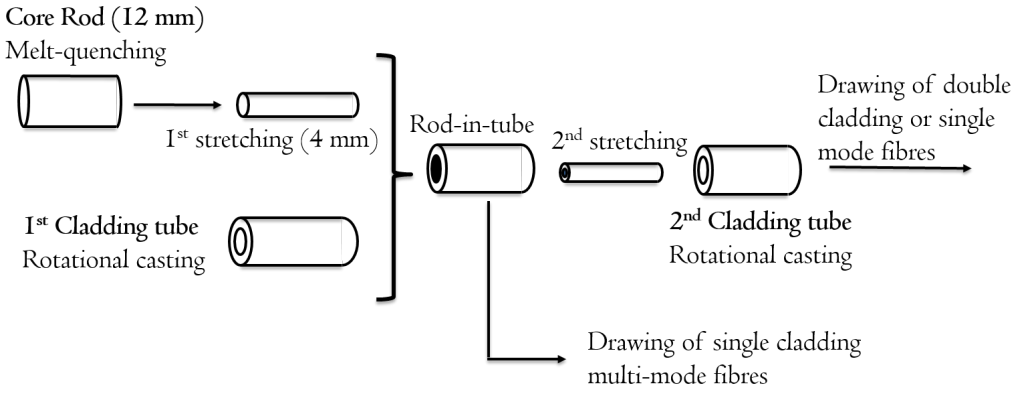

Fig. 4.2 Procedure for fibre preform fabrication, with tubes obtained by rotational casting.

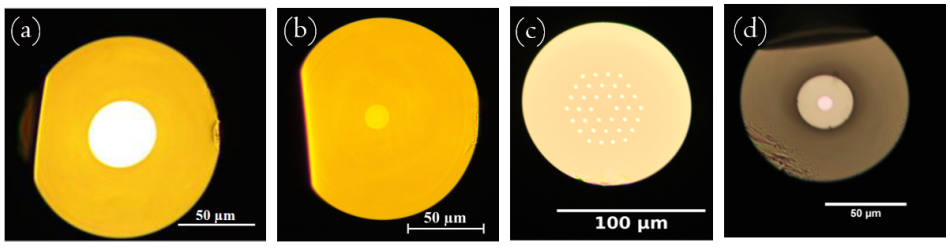

Fig. 4.3 Examples of optical fibres fabricated at Politecnico di Torino with preforms obtained through rotational casting technique: (a) multi-mode single cladding fibre [13], (b) single-mode single cladding fibre [5], (c) all solid photonic-crystal fibre [14], (d) single mode double cladding fibre [15].

Fabrication of all solid PCFs has been also demonstrated using rotational casting (see Fig.4.3.c), however, limitations on tube diameter ratios prevent from designing more efficient structures than those already reported [13, 5, 14, 15].

Nevertheless, the final results were usually good and a well centred fibre with an excellent core/cladding interface was obtained (see Chapter 5). Fig. 4.3.a.b portrays some typical fibres developed for this thesis. The fibre in Fig. 4.3.b was designed to operate in single-mode regime at 1500 nm and manufactured using two tubes obtained by rotational casting. The fibre depicted in Fig.4.3.a was designed to operate in the visible/near-infrared region in a multi-mode regime. As detailed in Chapter 6 these fibres show values of attenuation loss that are some of the lowest reported in literature for phosphate glasses.

Possible defects on preforms obtained by rotational casting

The external surface quality of a tube obtained by rotational casting is not sufficiently good to be used for fibre drawing and it needs polishing. This happens because the glass melt is put in direct contact with the cold metallic surface of the mould.

Inappropriate annealing or mould preheating can lead to fractures of the tube, low rotation speed or high viscosity may lead to inhomogeneous core diameter size or to a tube that is only partially open.

Other defects may occur when using multiple preforms for fabricating single mode fibres. In this case two virtually identical tubes are coupled and bond together as a thick cladding component. However, fluctuations in the glass composition may lead to having slightly different preforms. In this case clear inhomogeneities will be visible at the interface between the tubes.

4.3 The extrusion of phosphate glasses

In this Section, the details and the advantages of the extrusion technique, compared to other preform fabrication procedures, are discussed. The results obtained in the design and implementation of an extrusion facility in Politecnico di Torino are reported. Details on the extrusion of the glass compositions developed for this thesis (CL1, see Chapter 7, BPh, see Section 6) are discussed.

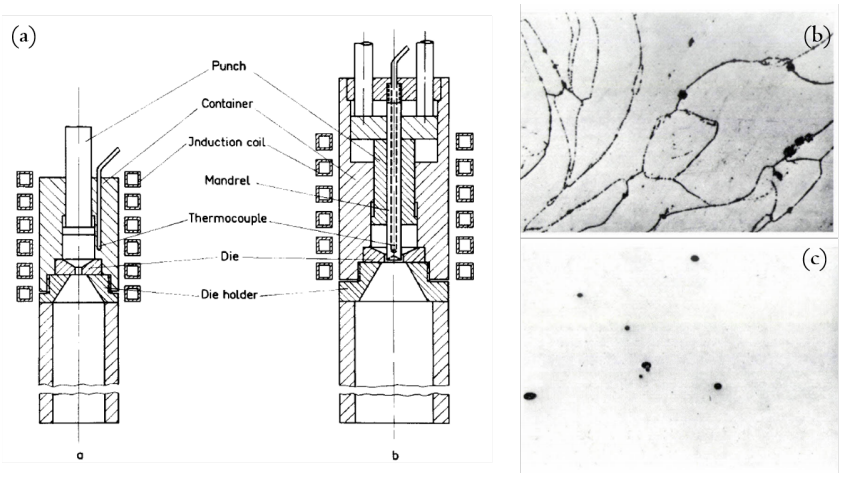

Fig. 4.4 (a) The extrusion facility developed by Roeder, (b) grain boundaries after extrusion of calcium alluminate glass powders (c) inclusions in a borosilicate glass after extrusion of powders (adapted from Roeder [16] Copyright:Elsevier)

Extrusion of glass has been explored due to its potential, that allows obtaining optical fibres preforms with a complex shape. It is particularly interesting for the processing of glasses with tendency to crystallize and with a steep viscosity curve, therefore, such as phosphate glasses. As the extrusion die is kept at constant temperature, fluctuation in the viscosity of the material is prevented, limiting the presence of thermal striations and consequent undesired refractive index variation. Moreover, as the process occurs at higher viscosity if compared to traditional techniques, the risk of crystallization of short glasses is decreased.

4.3.1 State of the art on the extrusion of glass

The first experiments on the extrusion of glass were performed by Roeder [16, 138] in 1971 using glass powders. A schematic of the set-up used is depicted in Fig.4.4.a. Roeder had noticed that extrusion could take place at viscosities up to $10^7\,\mathrm{Pa}\cdot\mathrm{s}$, a higher value than that required for conventional forming techniques. He found this method interesting for forming glasses with a very short working range and strong tendency to devitrification. Nobody at that time had proposed the fabrication of microstructured optical fibres, especially using soft glasses.

The employment of extrusion in optical fibres manufacturing became interesting for the fabrication of optical fibres preforms. In the last decades the scientific

interest in developing fibres with very high non-linear effects for the generation of supercontinuum sources has opened new perspective in the processing and manufacturing of soft glasses and microstructured optical fibres [139, 140]. Germanate and tellurite glasses have been widely employed in this field and extrusion proved to be an excellent tool for the processing of optical fibres preforms [141, 142].

Despite many attempts, the extrusion process is not yet optimized or widespread. In particular, to the author's knowledge, very little literature is available on the extrusion of phosphate glass, and so far no phosphate glass based optical fibre, fabricated by employing this technique, has been characterized [143]. The following paragraphs in this chapter are dedicated to the development and optimization of an extrusion facility for the processing of phosphate glasses.

4.3.2 Extrusion experiments at ORC

The extrusion of several glasses has been carried out during the development of the facility to set up and optimize the process. Some of these experiments were preformed using an already existing extrusion facility in the group of Compound Glass and Fibres at the Optoelectronics Research Centre - University of Southampton. In this campaign, the extrusion of silicate and phosphate glasses was carried out.

The extrusion facility at ORC consists of a punch, which works in displacement control mode. The system was obtained by modification of a mechanical press featured by a maximum load of 10 tons and a minimum speed of $10\,\mu\mathrm{m/m}$. The main body of the furnace is electrically heated and insulated with a refractory. Temperature is detected by four thermocouples, on the main body and on the extrusion die.

Extrusion experiments were performed using two different configurations for the extrusion dies. The first one, namely "standard" is a non-recyclable system of three components, developed at ORC by the Compound Glass and Fibres research group [17]. This die was used for the extrusion of n-BK7 glass. Another type of die, namely "Type A" designed by the same group, was exploited for the extrusion of phosphate glasses from the CL1 composition (see Chapter 7). This new configuration has the advantage to be recyclable, allowing multiple use of the same components. A section of the design of the die is visible in Fig.4.6.

A summary of the extrusion experiments performed at ORC is reported in Table 4.1. As an example Fig.4.7.a-b portrays some silicate tubes (Schott BK7)

Table 4.1 Summary of the extrusion experiments performed at ORC

Glass Label	**Die [mm]**	**Extrusion speed [mm/min]**	**Max. load [kN]**	**Temperature [°C]**	**Final dimension [±0.1 mm]**	**Final quality**
n-BK7	standard $d_1 = 9$ $d_2 = 4.5$	0.12	3.07	770	$d_1 = 10$ $d_2 = 4.5$	very good
n-BK7	standard $d_1 = 13$ $d2 = 10$	0.15	2.0	740	$d1 = 13.8$ $d_2 = 10$	good surface striation
n-FK5	standard $d_1 = 12$ $d_2 = 9$	0.12	2.5	680	$d_1 = 12.5$ $d_2 = 8.9$	bad metal contaminated
n-FK5	standard $d_1 = 9$ $d_2 = 4.5$	0.2	2.5	708	$d_1 = 10$ $d_2 = 4.5$	bad metal contaminated
CL_1	type A $d_1 = 9$ $d_2 = 3$	0.08-0.18	2.6	683	d1=9.4 $d_2 = 3.3$	good slightly bent
CL_1	type A $d_1 = 9$ $d_2 = 3$	0.05-0.12	1.84	680	$d_1 = 9.4$ $d_2 = 3.3$	very good

extruded by using this facility. The activity that was carried out was fundamental to achieve sufficient experience for designing the new facility in Politecnico di Torino.

4.3.3 The extrusion facility in Politecnico di Torino

The extrusion facility developed in Politecnico di Torino is mostly inspired by the first one developed by Roeder in the '70s. The set-up comprises a punch that applies a load on a glass billet. The billet is heated at the extrusion temperature, until the glass viscosity reaches values between $10^{5.5}$ and $10^{7}\,\mathrm{Pa}\cdot\mathrm{s}$. As pressure is applied, the glass billet is forced to flow through an orifice that replicates the final shape of the

preform. This facility is for extruding bulk glass billets, whereas Roeder's machine was designed for powder extrusion. Unlike our method, the powder extrusion led to the occurrence of grain boundaries and external inclusions. Such defects are deleterious in the fabrication of optical components (see Fig.4.4.a.b).

A schematic of the facility is visible in Fig.4.5.a.b. The punch is connected to a screw jack that applies the load on a bulk glass billet with a diameter of 25 mm. The flow through the extrusion die is performed in displacement control. This solution was preferred over an hydraulic press as it allowed a very precise control of the extrusion speed, down to a lower limit of 0.02 mm/min, which is necessary in case of extrusion at high viscosity.

The furnace is made of a metallic tube that holds the extrusion die (AISI 316 or AISI 310), able to carry a load of 3000 N. The die is inserted in an alumina tubular furnace heated by a symmetrical array of heating elements. The furnace can reach a maximum temperature of 800 °C and is designed to provide a circular temperature distribution, reaching the maximum value on the extrusion die. The facility was completely designed and developed during this Ph.D. research activity, and is currently in use for the fabrication of fibres preforms.

4.3.4 Extrusion experiments at PoliTo

This section reports on the first extrusion experiments performed on the new facility in Politecnico di Torino. After the set-up of the machine, a campaign of experiments was carried out to understand and validate the processing parameters. Two types of extrusion dies were designed and tested, namely "Type A" and "Type B". The processing details of the most meaningful extrusion experiments are reported in Table4.2 and commented in the following paragraphs.

Extrusion experiments with "type A" dies

The extrusion of the CL1 cladding glass was performed in order to obtain a first cladding tube to be used for fabricating a DC optical fibre. The extrusion was carried out using a "type A" die featuring a diameter of 9 mm equipped with a 1.8 mm pin at a speed of 0.1 mm/min. In this case the hole in the tube was not perfectly centred and straight, due to a movement of the pin during extrusion. The same problem

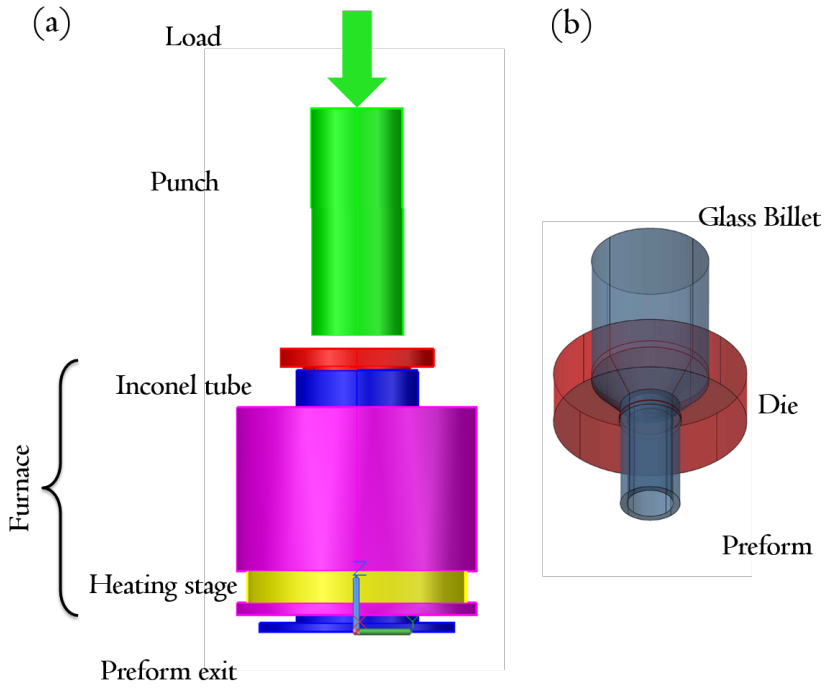

Fig. 4.5 (a) scheme of the extrusion furnace developed in Politecnico di Torino, (b) detail of the extrusion process

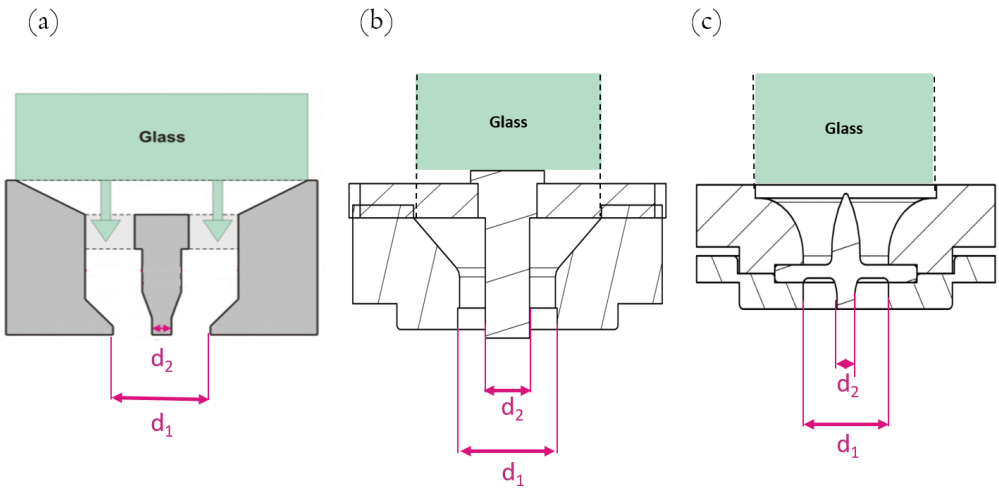

Fig. 4.6 Type of dies used for extrusion experiments: (a) Standard type (adapted from [17]), (b) type A, (c) type B. The values of d_1 and d_2 are reported in Tables 4.1 and 4.2

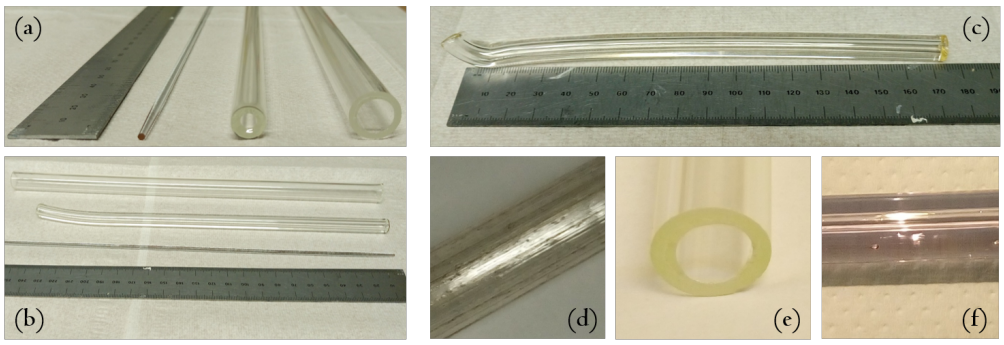

Fig. 4.7 (a,b) Schott BK7 tubes manufactured by extrusion at the Optoelectronics Research Centre-University of Southampton. (c-f) Examples of preforms showing defects: (c) a bent preform, resulted from extrusion with excessive feed speed, (d) preform contaminated with metal oxides, resulting from incompatible glass/die materials, (e) off-centred tube, resulting from a wrong design of the die, (f) surface defects on the glass, resulting from poor polishing of the die surface.

raised during the extrusion of a glass (namely E23) developed as a second cladding composition for the CL1, and featuring the same thermal properties (see Fig.4.7.e).

The employment of "type A" dies in the new extrusion machine presented several problems, due to the minimal mechanical tolerance that is required to maintain the pin centred using this configuration. The components tended to remain caught in their position, creating several difficulties during the cleaning and the maintenance of the machine. Therefore, a new "type B" designed was proposed. This new die was designed to maintain a perfect centring of the die, favour a regular flow of the glass thanks to a curved profile of the funnel, and more importantly adapt better to the machine, in order to be easily removed at the end of extrusion process.

Extrusion experiments with "type B" dies

Experiments with an extrusion die of "type B" (Fig.4.6.c) allowed eliminating the problem of not centred pins, moreover they were much easier to handle and clean, and, over all, they adapted better to the new machine. However, the new configuration seems to be responsible, in some cases, of the presence of surface bubbles, maybe due to the presence of the pin holder in the final part of the die. Another drawback of the "type B" die is due to the curve profile of the funnel, which increases the friction between glass and metal, and requires higher pressures and temperatures. This has

Table 4.2 Summary of the most meaningful extrusion experiments performed with the facility developed in PoliTo

Glass Label	**Die [mm]**	**Extrusion speed [mm/min]**	**Max. load [kN]**	**Temperature [°C]**	**Final dimension [±0.1 mm]**	**Quality and comments**
CL1	Type A $d_1 = 9$ $d_2 = 1.8$	0.03-0.04	2.2	617	$d_1 = 9.5$ $d_2 = 1.5$	new die good slightly off-center
CL1	Type A $d_1 = 9$ $d_2 = 1.8$	0.02-0.1	2.3	617-620	$d_1 = 9.5$ $d_2 = 1.5$	used die good heavily off-center
CL1	Type B $d_1 = 9$ $d_2 = 2$	0.02-0.03	2.5	618-620	$d_1 = 9.5$ $d_2 = 1.5$	bad heavy swelling
E23	Type A $d_1 = 9$ $d_2 = 6$	0.05	2.2	623	$d_1 = 9.2$ $d_2 = 5.8$	good sligtly off-center
E23	Type B $d_1 = 12.6$ $d_2 = 7.6$	0.04	2.1	610	$d_1 = 12.8$ $d_2 = 7.8$	good small surface defects
BPh1	Type B $d_1 = 12.6$ $d_2 = 1.8$	0.05	1.5	530-535	$d_1 = 12.8$ $d_2 = 1.5$	very good
BPh1	type B $d_1 = 12.6$ $d_2 = 9.6$	0.02	2.0	544-553	$d_1 = 12.8$ $d_2 = 8.5$	bad severe surface inhomogeneities
BPh4	type B $d_1 = 12.5$ $d_2 = 9.6$	0.05	2.0	546	$d_1 = 12.7$ $d_2 = 9$	bad severe surface crystallization

been responsible in some cases of heavy swelling phenomena, that led to the failure of the process.

An extrusion experiment with the "type B" die were carried out on CL1 glass matrix, replicating the geometry of an analogue experiment performed with a "type A" die. The experiment failed in consequence of the heavy swelling and distortion of the material. Better results were obtained with the E23 glass, allowing the extrusion of a 12.8 mm preform with an internal diameter of 7.6 mm. Small surface defects were visible on the external surface of the glass.

More experiments were performed using the BPh matrix. Details on the composition and properties of this glasses are reported in Chapter 6. An extrusion process was implemented for fabricating preforms suitable for single mode fibre drawing in just one step. overcoming the limitations of rotational casting. A "type B" die was designed in order to implement a single-stage fabrication method for single-mode optical fibres operating in the NIR window. In this case the same 12 mm diameter funnel used for the extrusion of the large core fibre was used. The die was equipped with a new 2.2 mm diameter pin. Extrusion was carried out at a temperature of 535 °C and a feeding speed of 0.1 mm/min. A 9 cm long tube of glass featuring an external diameter of 12.8 mm and an internal diameter of 2 mm/min was obtained.

Further experiments performed on the extrusion of thin tubes with the BPh glass failed, in consequence of the crystallization of the material and the presence of bubbles. This may be due to the excessive friction between die and glass, that requires extruding at high temperature and pressure, increasing the risk of crystallization. However, the structure of the die may also favour the formation of bubbles in the glass, possibly inducing the presence of turbulent flow

Possible preform defects arising during extrusion

The experiments performed allowed analysing an overview of the defects that have been observed. Fig.4.7.c-f depicts how these defects appeared on the fabricated preforms, and they can be related to several causes:

- **Swelling:** when extruding a preform, a difference between the dimension of the die and that of the extruded profile can be observed. This is a known effect called swelling. However in some cases this phenomenon is uncontrolled and may lead to preforms with inhomogeneous dimension.

- **Bent preforms:** This defect is related to a swelling phenomenon: the preform does not follow a straight line but tends to pigtail around a central axis. This effect is normally observed if the extrusion speed is too high and/or if the viscosity is too high (low temperature). (Fig.4.7.c)
- **Incompatible glass/die materials:** This defect was observed during the extrusion of a glass containing fluorine using a stainless steel die. Reaction between the metal and the glass melt was observed, resulting in heavy oxidation of the metal. Heavy contamination of the glass due to oxide inclusion has lead to complete failure of the process. (Fig.4.7.d)
- **Off-centred holes:** This defect is normally related to an inhomogeneous load distribution on the billet or to slightly off-centred die. It can be solved with opportune design of the extrusion orifice. (Fig.4.7.e)
- **Surface defects:** Normally these defects are related to a poor surface quality of the die, resulting in the contamination of the surface with oxide particles and consequent isolated defects. In some other cases also scratches and vertical striations can be observed.

4.4 Chapter Conclusion

The main aim of this chapter was to give an overview of the fabrication processes available for phosphate glass fibre preforms. The techniques employed to fabricate optical fibres during this research activity have been reported and discussed. Particular attention was devoted to the description of the extrusion process, since an extrusion facility was designed and implemented in Politecnico di Torino, as a part of this PhD program. The advantages of the extrusion technique have been described and the extrusion of some sample preforms has been reported.

This technique proved to be effective in the rapid and cost effective fabrication of complex profiles. Tubes with an external to internal diameter ratio above 0.8 have been successfully manufactured, featuring wall thickness below 1 mm. Tubes featuring a length between 9 and 30 cm have been obtained.

The studies that were carried out allowed the extrusion of useful profiles for the fabrication of single cladding and double cladding optical fibres. However,

the fabrication of more complex structures and asymmetrical profiles was still not possible at this stage of development. The extrusion of thin profiles also proved to be challenging, due to the high load and needed and the small tolerances on die fabrication. Further studies are ongoing for the optimization of the machine design, and for obtaining a more precise control of the temperature distribution in the furnace.

Optimized extrusion processes allows avoiding several stages of preform machining and polishing, dramatically reducing working time, material waste and thus decreasing the overall costs of preform manufacturing.

Chapter 5

Nd-doped phosphate glasses for fibre/cane lasers and amplifiers

This chapter is dedicated to the research activity on the development of Nd^{3+}-doped phosphate glasses for short-length fibre lasers and amplifiers. The design, fabrication and characterization of a Nd^{3+} doped cane laser and a Nd^{3+} doped fibre laser for high-power applications is discussed. All the steps related to the fabrication of the bulk glass, cane and fibre preforms and fibre drawing are described in detail. The power scaling experiments performed on the cane and fibre lasers are also reported. The results presented in this part have been obtained in collaboration with the research groups of prof. F. Poletti and prof. W. A. Clarkson during a six months secondment at the Optoelectronics Research Centre - University of Southampton (UK). Many of the data and images presented in this section have been published recently in a journal paper [4].

5.1 Development of the "CL" and "Nd:CL" glass matrices

Nd^{3+} was the first lanthanide ion to be used as a laser emitter. Embedded in a silica glass matrix, it was used by Snitzer as the first glass based laser. Although at the time (it was 1961, and the ruby laser had been demonstrated just one year before) Snitzer himself didn't realize the revolutionary importance of this invention, it happened

that this device was the first fibre laser in history [81]. In the following decades laser science grew enormously: again Snitzer in 1961 had published a description of the physical behaviour of modes in optical fibres [123] followed soon by the invention of the fibre amplifier in 1964 [144].

The Nd^{3+} ion has the advantage to require a low energy threshold to emit laser radiation. Therefore, it is convenient for the fabrication of lasers featuring a medium/high output power, in the range of a few watts. Moreover, the low threshold and the large bandwidth of the emission peak at 1054 nm make the Nd^{3+} convenient for the fabrication of optical amplifiers around the wavelength of 1 μm.

Phosphate glasses were soon employed as hosts for active ions. As reported in Chapter 2, these materials are particularly well suited for compact high-power laser devices as they offer high solubility of rare-earth ions [50, 145, 36, 146, 85]. Moreover, they show low photodarkening, low non-linear effects and a mature and large-scale manufacturing technology [10, 147, 124, 148, 149]. Phosphate based fibre lasers and amplifiers have been developed in the past, however their performance has been limited in terms of power and efficiency by the high thermal load [150, 151, 144]. This is due to the low thermal conductivity of the material, responsible for inducing severe mechanical stress to the device [100, 86, 102, 31]. Thermal dilatation occurring in consequence of overheating causes misalignment of the optical set-up, beam distortion and fracture at the core/cladding interface of the fibre.

Commercially available compositions for the development of phosphate glass lasers are often not suitable for the fibre/cane drawing process. This happens as they do not present sufficient stability against crystallization, and they do not maintain the vitreous state during forming processes. The work presented in this chapter aims to develop e new glass composition that may overcome these limitations.

The "CL glass" matrices, developed in this work, are meant for the fabrication of optical fibres with a large diameter (known as canes) to be used for high power laser applications. These devices are advantageous for the fabrication of short length, high power lasers and amplifiers, as they benefit from a high threshold for the insurgence of non linear effects and a simple heat sinking configuration. The thermal compatibility between the core and the cladding of a device becomes critical when fabricating a cane laser, as an increase of the interface stress both during the drawing process and the laser activity can be experienced.

In order to reduce the interface stress two sets of glasses, the CL1 and the CL2 series, were developed. Each glass matrix is made of a Nd doped core glass (CL1:Nd and CL2:Nd) and a cladding glass (CL1 and CL2). The glasses were designed to maintain an optimal matching of thermal expansion coefficients, increase stability against crystallization and provide sufficient refractive index mismatch for effective light guiding. As it is reported in detail in Section 5.1.2 the CL1 series proved to be more suitable for the development of laser devices and was selected for the following experiments [152].

5.1.1 Fabrication of CL1:Nd, CL2:Nd, CL1 and CL2 glasses

Two phosphate glass hosts, named CL1 and CL2, were ad hoc developed for this research. The main features that were taken into account for developing these compositions were:

- Minimizing the thermal expansion coefficient (CTE) of the glass to reduce the deformation of the final device;
- Matching CTE of the core and the cladding glass to minimize residual stress at the core/cladding interface of the fibre;
- Reach high stability against crystallization, to allow the cane and fibre drawing processes;
- Obtain suitable refractive index contrast and combined with an enhanced thermo-mechanical compatibility.

Based on these assumptions, two compositions were developed: (CL1: 65%P_2O_5, 7%K_2O, 6%Al_2O_3, 6%B_2O_3, 6%SiO_2, 5%PbO and CL2: 65%P_2O_5, 7%K_2O, 7.5%Al_2O_3, 6%B_2O_3, 7.5%SiO_2, 2.5%Nb_2O_5). Two core and two cladding glasses named respectively CL1:Nd and CL2:Nd were obtained by doping the glass host with respectively $7.2 \times 10^{-19}\,\mathrm{cm}^{-3}$ and $7.5 \times 10^{-19}\,\mathrm{cm}^{-3}$ of Nd^{3+} ions, corresponding in both cases to the addition of 0.3 mol% Nd_2O_3 in the glass host. 4.7 mol% La_2O_3 were also added to the core glasses to increase the refractive index. The two relative cladding compositions, named respectively CL1 and CL2, were fabricated by doping the glass hosts with 2 mol% La_2O_3 and 3 mol% SiO_2 respectively, in order to

compensate the change in the thermal properties provoked by the addition of Nd_2O_3 and La_2O_3 in the core glasses.

High purity chemicals (99+%) were mixed in a glove box according to the planned compositions in order to minimize the water content in the glasses. The batched chemicals were melted at a temperature of 1400 °C for 1 h in a vertical furnace under a dry atmosphere (air, water content < 3 ppm) and cast in a preheated mould. The cast glasses were annealed around the transition temperature, T_g, for 12 h to relieve internal stresses and finally cooled down slowly to room temperature. The core glass compositions (CL1:Nd and CL2:Nd) were cast in a cylindrical mould with a diameter of 12 mm to obtain 100 mm-long rod preforms (see Chapter 3 and 4).

The cladding glass compositions (CL1 and CL2) were shaped in the form of a tube by rotational casting at a rotation speed of 3000 rpm, as explained in detail in Chapter 4. One more batch of CL1 cladding glass was cast in a 25 mm diameter billet to be used for extrusion, as explained in Chapter 3.

The external surface of the core rods and of the cladding tubes was polished carefully with SiC papers of different grits and 1 μm diamond paste. 1 mm thick slices of glass were cut from each preform and polished to optical quality, in order to be used for the spectroscopical characterization of the glasses.

5.1.2 Properties of Nd:CL1 and Nd:CL2 glasses

In this paragraph the properties of the bulk CL1, CL2, CL1:Nd and CL2:Nd are reported and discussed. In absence of further specification, all the measurements were performed according to the procedures described in Chapter 3.

Physical and thermal properties

The thermal and physical properties of the CL1 and CL2 glass are reported in Table 5.1. As a comparison, the same properties are reported for the Schott LG-770 and the Kigre Qx/Nd glasses. The density of the glasses was measured through the Archimede's principle using distilled water. The characteristic temperatures of the glass (transition temperature T_g, crystallization temperature T_x, softening temperature T_s) and the CTE were measured using DTA and Dilatometry, performing a continuous heating ramp at a constant rate of 5 °C/min.

Table 5.1 Physical and thermal properties of the CL1 and CL2 glass matrices in comparison to commercial Nd-doped Schott LG-770 and Kigre Qx/Nd

Glass Label	T_g [$\pm 3\,^{\circ}$C]	T_x [$\pm 3\,^{\circ}$C]	ρ [$\pm 0.01\,g/cm^3$]	CTE [$\pm 0.1 \times 10^{-6}\,K-1$]	τ_m [$\pm 10\,ms$]
CL1:Nd	522	790	3.01	8.1	326
CL2:Nd	593	958	2.80	7.1	350
CL1	530	808	2.91	8.3	n.a.
CL2	610	1000+	2.67	7.4	n.a.
LG-770	461	n.a.	2.56	13.4	350
Qx//Nd	506	n.a.	2.66	8.4	353

Thermal analysis reveals a stability parameter ΔT above 250 °C for all the manufactured materials, proving that they are stable against crystallization and suitable for cane drawing. Dilatometry showed values of CTE lower than those exhibited by the most common glasses available and comparable to those reported for the athermal Qx/Nd glass fabricated by Kigre [67, 66]. The difference in terms of thermal expansion between the fabricated core and cladding glasses is only $0.2 \times 10^{-6}\,K^{-1}$ for the CL1 glass matrix and $0.3 \times 10^{-6}\,K^{-1}$, these values are within the measurement error. Overall this results matches the required criteria in Section 5.1.1 is promising for the fabrication of optical fibres and canes.

Refractive index

The refractive index of the glasses was measured at 633, 825 and 1061 nm by prism coupling technique (Metricon, model 2010). The values are reported in Table 5.2 and compared to those reported in literature for the Schott LG-770 and the Kigre Qx/Nd commercial glasses [66, 67].

The refractive indices of the manufactured glasses are higher than the ones reported for commercial compositions. This is desirable for high-power laser applications, as it facilitates fabricating thermally compatible, low refractive index glasses for the manufacturing of double-cladding optical fibres.

CL1:Nd glass showed the highest value of refractive index at the laser wavelength, thus resulting an advantageous core composition for the fabrication of the canes. The coupling of the CL1:Nd core glass to the relative cladding CL1 leads to a NA value of 0.16.

Table 5.2 Refractive index of the CL1:Nd, CL2:Nd, CL1, CL2 glasses in comparison to the commercial Schott LG-770 and the Kigre Qx/Nd glasses.

Glass label	**Refractive Index** [± 0.001]		
	633 nm	825 nm	1061 nm
CL1	1.549	1,5432	1.540
CL2	1.543	–	1.533
CL1:Nd	1.557	1,552	1.548
CL2:Nd	1.551	1,543	1.540
LG-770	1.507	–	1.450
Qx/Nd	1.536 (n_c)	–	1.530

UV-Vis/NIR absorption Spectroscopy

The absorption spectra were measured on the core samples to identify the Nd^{3+} characteristic peaks. The measurement was performed at room temperature for wavelengths ranging from 300 to 900 nm using a double beam scanning spectrophotometer (Varian Cary 500). The absorption cross section was calculated according to the formula reported in 3 and plotted as a function of the wavelength. The values of absorption cross section measured at the excitation wavelength of 800 nm were respectively $2.3 \times 10^{-20}\,cm^2$ and $2.0 \times 10^{-20}\,cm^2$ for the CL1:Nd and the CL2:Nd glasses, both comparable with those reported in literature and in commercial glasses [147]. The value measured for the CL1:Nd is higher than that observed in CL2:Nd. This suggests that the CL1:Nd may offer a more favourable environment for the exploitation of the ${}^4F_{3/2} \longrightarrow {}^4I_{11/2}$ transition. on the other hand the CL2:Nd glass offers higher absorption cross section at 580 nm, thus suggesting that the ${}^4G_{5/2}$ level is favoured in this matrix.

Emission spectroscopy and lifetime measurements

Emission spectra were obtained by exciting the sample with a monochromatic light at 785 nm, emitted by a fibre pigtailed laser diode (Axcel B1-785-1400-15A). The two normalized spectra are reported in Fig. 5.2 and do not show any relevant difference between the two glasses. Both peaks are centred at the wavelength of 1054 nm, as typically observed in Nd-doped phosphate glasses.

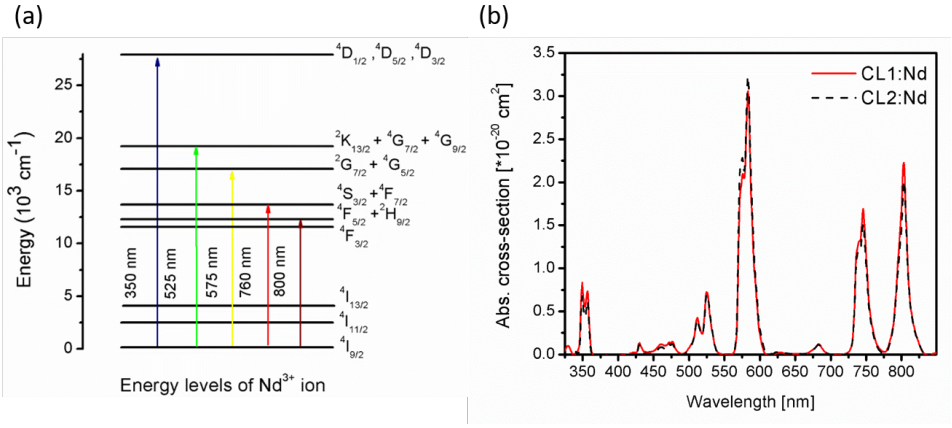

Fig. 5.1 (a) Energy levels of Nd^{3+} ion; (b) absorption spectra of the CL1:Nd and CL2:Nd glasses (adapted from [4])

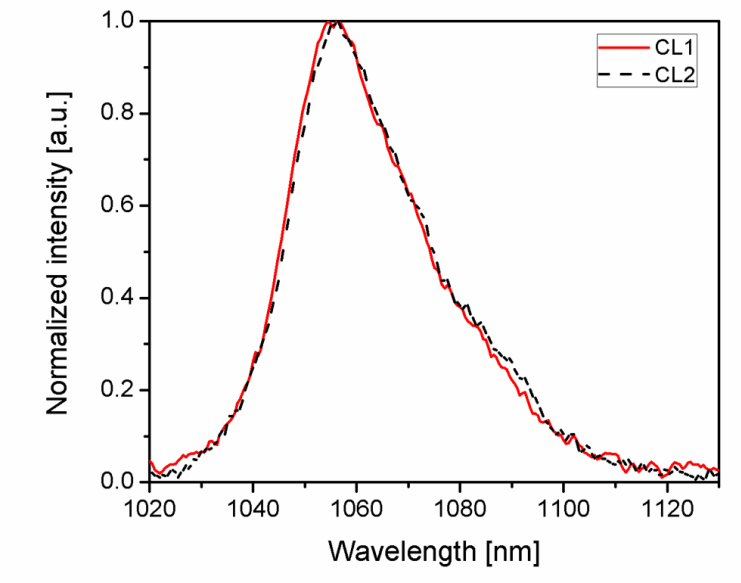

Fig. 5.2 Normalized emission spectra of CL1:Nd and CL2:Nd glasses centred at 1054 nm (adapted from [4]).

The fluorescence lifetime τ_m of Nd^{3+}:$^4F_{3/2}$ level was obtained by exciting the samples with light pulses of the 785 nm laser diode, recording and fitting the decay traces by a single exponential according to the procedure described in Chapter 3. The detector used for this measurement was a Thorlabs PDA10CS. Estimated error of the measurement was $\pm 10\,\mu$s. The values measured are $326\,\mu$s for the CL1:Nd glass and $350\,\mu$s for the CL2:Nd glass and match with our previous measurements on similar glasses and with those reported in literature for commercial compositions [67, 66]. Despite a longer lifetime is generally preferred for laser action, in this case the CL1:Nd composition still seems to be more adapt to the fabrication of fibre/cane lasers, as it presents higher absorption cross section and higher refractive index.

5.2 Fabrication of Nd:CL based cane and fibre lasers

This paragraph reports on the fabrication and characterization of Nd^{3+} doped optical fibres and canes. Optical fibres with two different diameters ($200\,\mu$m, $300\,\mu$m) and a $800\,\mu$m diameter cane were fabricated by preform drawing according to the procedures reported in Chapter 3. All the devices are based on the CL1:Nd/CL1 core/cladding structures, as this glass matrix presents slightly higher refractive index, higher absorption cross section and lower viscosity when melt, facilitating the materials processing. The canes and fibres were used for laser emission and power scaling tests performed at the Optoelectronics Research Centre - University of Southampton (UK).

5.2.1 Fabrication and characterization of CL1:Nd/CL1 cane

The final preform was fabricated by the rod-in-tube method and stretched by cane drawing. The core rod was obtained by stretching the 12 mm diameter rod obtained by melt-quenching into a thinner cylinder with a diameter of 3 mm. The cladding tube was manufactured by rotational casting, as explained in Chapter 4.

The core stretching and the cane drawing were both carried out using the drawing facility as described in Chapter 3. Canes presenting a diameter of $800\,\mu$m and a core/cladding diameter ratio of $1/3$ were fabricated. Fig.5.3.b portraits the typical cross-section of the $800\,\mu$m-diameter cane. No significant defects in size, shape or

in the core/cladding interface could be observed at the optical microscope, proving the good control on the fabrication process.

The loss of the cane was estimated while preparing the laser experiment set-up by launching a laser beam at the wavelength of 1030 nm in the 6 cm specimen used for laser experiments. A proper cut-back measurement for estimating the fibre's loss could not be performed due to the little amount of material available. The loss value at this wavelength was between 3 and 6 dB/m. Although this is a rough estimation, it appears compatible with the values measured on optical fibres. Moreover, it's not very dissimilar from the values measured by the Caird and the Findlay-Clay analyses at the signal wavelength (see Section 5.3.2).

5.2.2 Fabrication and characterization of CL1:Nd/CL1 optical fibres

The optical fibres were obtained by drawing the same preform into two different diameters. The same core rod used for the fabrication of the cane laser served as core of the optical fibres. The cladding tube was obtained by extrusion of a 25 mm billet into a 9 mm tube with an internal diameter of 3.5 mm. The extrusion was performed at the Optoelectronics Research Centre - University of Southampton.

The rod-in-tube procedure was used for fibre drawing. A typical cross section of the cleaved fibre (in this case 300 μm diameter) is reported in Fig.5.3.a. The dimensions of the fibres are reported in Table 5.3.

The cut-back method was used to measure the loss of the fibre at 1500 and at 980 nm, showing values of attenuation loss comparable to those measured for the laser canes. The 200 μm optical fibre shows loss values that are markedly lower than those of the 300 μm one, despite the fibres were made from the same preform in the same drawing process, it is possible that some contamination or some defects at the core cladding interface appear in higher concentration on the surface of the thicker fibre.

Table 5.3 Properties and performance of the CL1:Nd optical fibres

External Diameter [μm]	200	300
Core diameter[μm]	50	75
Numerical aperture	0.16	0.16
Loss @980 nm [dB/m]	3	6.5
Max % slope efficiency	26 (Fresnel Laser)	32 (50% OC)

5.3 Laser emission and power scaling experiments

This paragraph describes the lasing tests performed on the fibres and the cane fabricated with the CL1 glass matrix. The data reported are the results of joint experiments performed at the Optoelectronics Research Centre with the group of prof. W. A. Clarkson. Many of the measurements reported were performed in collaboration with my colleague Callum Smith and are part of a joint research on high power lasers.

The lasers operated at an emission wavelength of 1054 nm and were pumped by a multi-mode fibre-coupled diode laser operating at 795 nm, with a core diameter of 200 mm and a Numerical Aperture (*NA*) of 0.22. A laser cavity was implemented by aligning appropriate mirrors close to the facets of the active gain medium. At the pump input facet a mirror with high transmission at 795 nm and high reflection at 1054 nm was positioned, whilst at the other end an output coupler (OC) mirror featuring high reflection at 795 nm was placed. Several output couplers with different reflectivity at 1054 nm (from 50 to 95 %) were tested. The laser signal was split from the residual pump by means of a mirror with high reflection at 1054 nm and high transmission at 795 nm, angled at 45° with respect to the beam direction. The residual pump beam was sent to a beam dump, while the 1054 nm was sent to diagnostics. A representation of the apparatus is visible in Fig.5.4.

The characterization on the cane laser was completed by performing the Caird and the Findlay-Clay analyses (see Chapter 3) [132, 133].

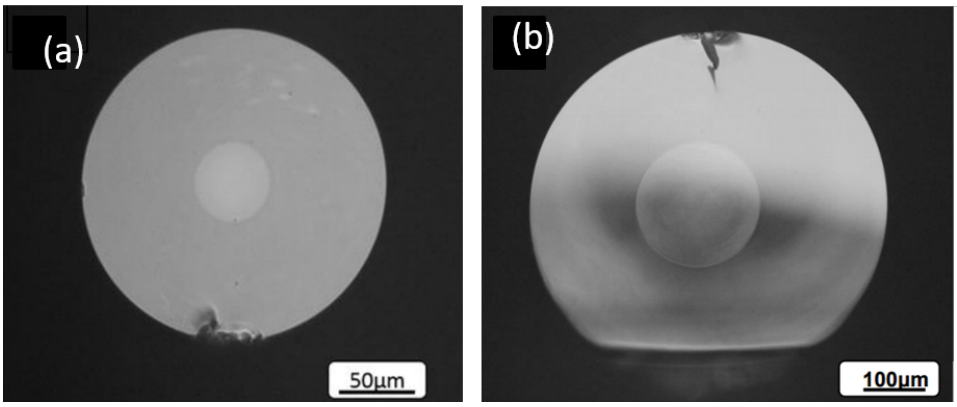

Fig. 5.3 Typical cross-section of the fabricated 300 μm optical fibre (a) and 800 μm cane (b).

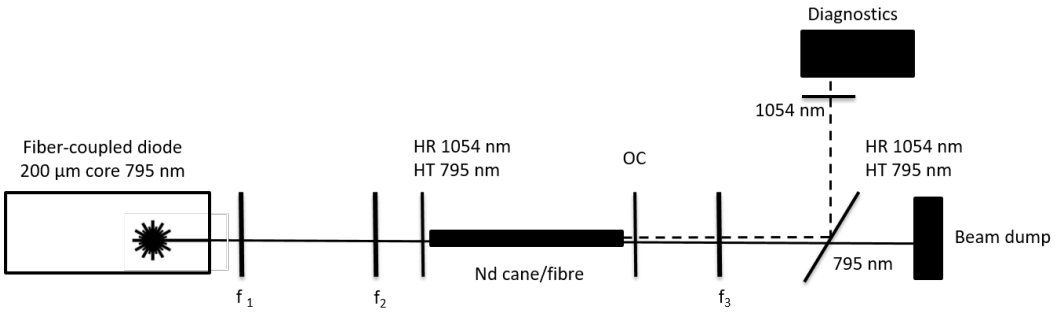

Fig. 5.4 Set-up used for the laser experiments (adapted from [4]).

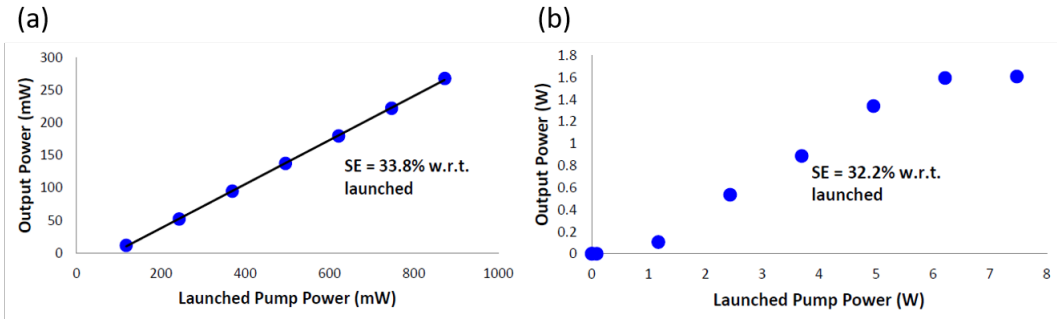

Fig. 5.5 Slope efficiency measurements on the 300 μm CL1 optical fibre obtained with 50 % output coupler (90% transmittance at 1054 nm) for the chopped (a) and the continuous wave (b) regime.

5.3.1 Power scaling experiments on optical fibres

The power scaling experiments were performed at first by cooling the fibre in a water bath. This was done in order to obtain a cladding pumped laser by exploiting the refractive index mismatch between water and glass. However, this configuration failed as misalignment occurred in consequence of overheating. The fibre was thus blocked on a V-groove support and two layers of graphite sheet were used to facilitate heat sink. A low-index silicone coating applied on the optical fibre, acting both as a protection and as a second cladding on the fibre. However, the system was not efficient when operating in a cladding pumping configuration. The tests were thus performed in an "almost core pumping" configuration, using a pump spot size that is about 10% larger than the core of the fibre. This was found to be the most efficient solution for power scaling experiments.

The experiments were first conducted limiting the pump power with a 90 % chopper placed right before the resonator cavity. This was a safety measure implemented to avoid overheating and damage to the instrumentation. This also allowed measuring maximum slope efficiency achievable in ideal heat sinking conditions. Once the system was perfectly aligned the chopper was removed and the experiment was run in continuous wave regime. The results of the slope efficiency measurements for the 300 μm are reported in Fig.5.5 both for the chopped and the continuous wave configuration. Results reported in mW in the chopped configuration should be considered as an average value of power for a CW laser that is obscured for 90 % of the time. I.e., a time slot of 1 s and a power of 100 mW are equal to a 0.1 s of 1 W emission and 0.9 s of obscured set-up.

The highest slope efficiency was obtained on the 300 μm fibre using a 50 % reflectivity OC. As it can be noticed, a higher slope efficiency is achieved in the chopped configuration 33.8 % with respect to the launched power. However, overheating effects soon raised in continuous wave regime, leading to a decrease of the slope efficiency to 32.2 % and heavy roll-over effects. Similar results were obtained on the 200 μm fibre, measuring a maximum slope efficiency of 26 % in continuous wave regime in Fresnel lasing configuration.

It was concluded that the silicone coating prevents heat dissipation from the fibre. Therefore, it was not considered as a suitable method to obtain a DC configuration on following experiments. Methods for reducing overheating of the fibre, such as

coating the device with conductive materials and implementing cladding pumping configuration, are possible only using a double cladding fibre. This evidences the necessity of developing a new low-index glass composition to be used for the fabrication of second cladding components.

5.3.2 Power scaling experiments on the $800\,\mu$m cane

A cladding pumping condition was set up on the cane laser experiment by launching the pump beam trough two lenses acting as a 1:2 imaging system. This resulted in creating a 400 mm diameter pump spot with a *NA* of 0.11 at the front face of the cane. In order to obtain effective heat sinking and provide a low index media acting like a second cladding, the cane was immersed in distilled water during all the experiment.

Slope efficiency measurements were performed using different output couplers ranging from 50 to 95 % reflectivity, with the maximum efficiency being observed with the 50 % OC. A slope efficiency of 30 % with respect to the launched pump power and 44 % with respect to the absorbed pump power was observed, with a maximum measured output power of 2.5 W. The maximum output power was achieved for a launched pump power of 19.0 W, corresponding to an absorbed pump power of 12.5 W. No sign of roll-over or decrease of efficiency were observed, showing that the emitted power is limited by the maximum pump power available.

It was calculated that the absorbed pump power was approximately 65 % of the launched pump power. This assumption was made after estimating that the loss at the glass/water interface, for a 975 nm beam launched in the same configuration of the pump beam, is about 10 dB/m. The plot of the output power as a function of the absorbed pump power is reported in Fig.5.6

Lasing activity occurred at different wavelengths around 1054 nm, in accordance with the Nd^{3+} emission peaks. The beam was analysed with an optical spectrum analyser and a beam profiler, the lasing spectrum and the beam shape at the maximum emitted power are reported in Fig.5.7. The laser output proved to be highly multimodal, as expected from the relatively large numerical aperture and the large core size.

The cane loss for the signal radiation was estimated using the Findlay-Clay analysis and the Caird analysis. Both methods require the use of different output couplers in order to estimate the resonator loss on the basis of the threshold pump

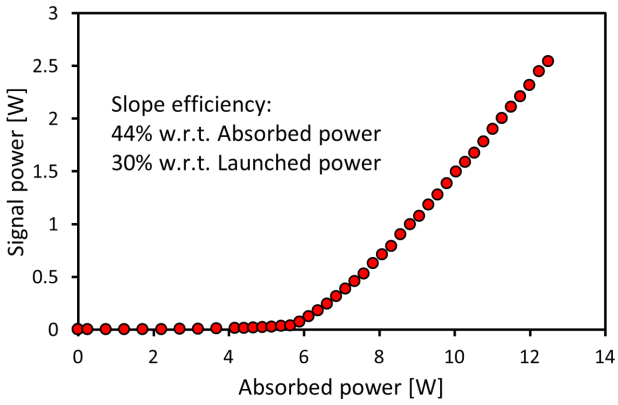

Fig. 5.6 Output power as a function of the absorbed pump power for the CL1 cane laser (adapted from [4]).

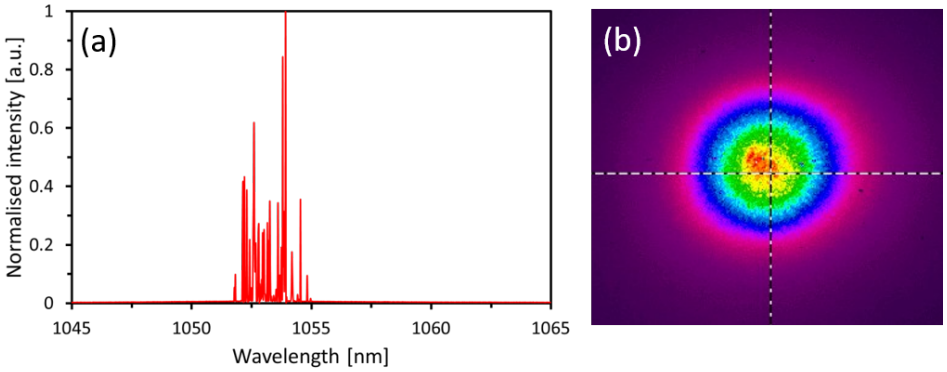

Fig. 5.7 Lasing wavelength (a) and beam profile (b) at the maximum output power for the CL1:Ns 800 μm cane (adapted from [4]).

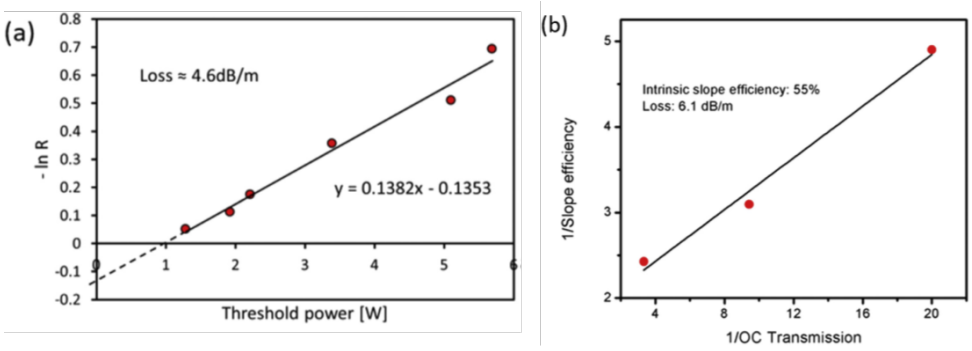

Fig. 5.8 Resonator losses estimated from the threshold pump power (Findlay-Clay analysis) (a) and from the slope efficiency (Caird analysis) (b) for various output couplers (adapted from [4]).

power R (Findlay-Clay) and the slope efficiency (Caird). These two methods provide a good estimation of the efficacy of the active media (see Chapter 3). The Caird analysis, in particular, also provides a value of intrinsic slope efficiency of the laser, often considered as a property of the material. The results for the CL1 cane laser are reported in Fig.5.8.a.b. A loss value of $4.6\,\mathrm{dB/m}$ is measured using the Findlay-Clay method, whilst the Caird analysis results in a loss of $6.1\,\mathrm{dB/m}$ and an intrinsic slope efficiency value of 55 %. The two methods led to comparable loss values, slightly higher than those obtained on other phosphate glass fibres. Further reduction of the loss may be attained during manufacturing by improving the glass homogeneity. The estimated intrinsic slope efficiency matches the maximum efficiency values achieved on multi-core phosphate photonic-crystal fibres, although it is still lower than that achieved on silicate fibres.

5.4 Chapter conclusion

The whole process of the fabrication of a laser device, from raw materials to power scaling tests, has been reported and discussed in this chapter. The critical aspects and their influence on the final result have been pointed.

Glass homogeneity influences the beam quality and the loss, the glass thermal and mechanical properties influence the drawing processes and finally the overall efficiency of the device. The synthesized materials combine good efficiency and optical properties with low thermal expansion, excellent resistance against crystallization and suitability for cane drawing.

The glasses were processed through rotational casting, extrusion and cane drawing without showing any sign of damage or degradation. It was demonstrated that matching the thermal properties of the core and cladding glasses facilitates the cane drawing process and minimizes the interface stress. This results in a higher slope efficiency of the laser. The preliminary results on laser emission of the cane laser proved a good power scaling ability, showing a slope efficiency of 44 % with respect to absorbed pump power and a maximum emitted power of 2.5 W. Results obtained with the Caird analysis show that a slope efficiency up to 55 % can be achieved in ideal pumping conditions.

The development of a second cladding composition for the CL1 glass matrix has been considered as an extension of this study. As it was mentioned in Chapter 4, the E23 glass developed within other research projects in this group seems to be suitable for this scope. Further research work is ongoing towards the fabrication of DC fibres and aim to increase the efficiency of the device. Nevertheless, the results obtained are promising and pave a way towards a development of small size, high power glass based lasers.

Chapter 6

Resorbable calcium phosphate glasses for biophotonics

In this chapter the results on the study and development of resorbable, inorganic glasses are reported and discussed. A new material that combines the biological properties of calcium-phosphate glasses (CPGs) with excellent optical properties has been synthesised. A full characterization of the material is reported.

The chapter starts with an introduction section, where an introduction the use of standard optical fibres in biomedicine is reported, the concept of resorbable optics is introduced and the recent research in this field is reviewed. Subsequently, the main applications of phosphate glasses as biomaterials are introduced.

The second part of the chapter is related to the activity performed during this Ph.D. program, related to the development and full characterization of a resorbable optical material and its suitability for optical fibre fabrication.

Many of the results reported have been recently published [5, 28, 27]. Unpublished data and results will be object of future publications.

6.1 Optical fibres in biomedicine

The invention of laser and the possibility to couple and guide laser light in optical fibres, led to a true revolution in many medical procedures, ranging from surgery to diagnostic, sensing and monitoring. Optical fibres are particularly attractive in

biomedicine due to their small size and immunity to electromagnetic fields, which makes their use compatible with most diagnostic techniques, such as MRI and PET. Moreover standard optical fibres are non toxic, inert to biological environment and thus biocompatible. Optical fibres have been used in medicine for several decades, with perspective application in endoscopy, sensing and surgery [153, 154].

Huge research effort has been spent on the development of fibre-optic based biosensors, both using a fibre Bragg-grating and evanescent wave approach. These structures have been used for the detection of several substances, including DNA and dangerous bacteria. [155, 156].

Fiber based technologies are also used for diagnostics and imaging in biomedical applications. Raman and diffuse optics imaging techniques are the most studied in this field. Research performed in the last decade has produced relevant results in the use of such techniques for the diagnostics and imaging of several kinds of diseases [157–159].

A new and intriguing research line in biophotonics is dedicated to the development of devices that can be resorbed by the human body once their functionality has expired. These instruments may find applications in emerging fields such as deep-tissue photodynamic therapy, optogenetics and biosensing. Different biomaterials have been proposed for such applications, in the next paragraphs, the most recent results in this field are reviewed.

6.1.1 Introduction to resorbable optics

Bioresorbability is intended as the ability of a material to be destroyed by the human body without leaving any harmful residual, minimizing the tissue reactions or enhancing a positive response, such as stimulating tissue regeneration. Bioresorbable materials are of high interest for various biomedical applications, and have been studied in the past decades as they eliminate the need for follow-up removal surgery (see Chapter 8). Some of them, such as resorbable stitches, are commonly employed in everyday surgical procedures, others, like resorbable scaffolds for bone tissue regeneration, are still under study and they are now being tested. The possibility to leave a device in place after its functionality has expired, without the need for retrieval, expands the range of applicability of optical tools in clinics and further diminishes the impact of minimally invasive methods.

The first work dedicated to the fabrication of a biodegradable optical fibre is reported by Dupuis et al. in 2006 using hydroxy-propyl cellulose [160, 22]. A section of the fibre developed is portrayed in Fig.6.3.a. In 2009, Manocchi et al. developed an agarose-gel based waveguide slab (see Fig.6.3.b) [23]. However, neither cellulose nor agarose experienced great success as resorbable optical materials. Silks and hydrogels soon became the most studied materials for such applications [161].

Silk based optics

Silk-fibroin is a natural material that is extracted from spider silks. It has been used for the development of fibre and planar devices with multiple functionalities. In particular, a multifunctional device that aims to combine enhanced imaging of malignancies, therapeutics, and feedback about therapeutics in a single resorbable device was developed in 2012 by Tao et al. [162]. Other studies by the same research group have led to the improvement of silk based devices, by improving the production processes and reducing the loss (see Fig.6.3.c) [24, 163]. More recently a non-regenerated silk based optical fibre was developed and characterized, proposing the use of non-regenerated silks as a more environment-friendly approach to silk production [164].

Silk based optical devices generally show loss values between 25 and 100 $\mathrm{dB/m}$. This makes them suitable only for the transmission of light on a very short distance [24, 162]. Moreover this material is of scarce availability, as it is produced naturally from animals.

Hydrogel based optics

Silks however are not the only materials studied for resorbable optics. PEG-hydrogels proved to be particularly interesting materials and are object of intensive study. As these are completely synthetic materials, they offer lower batch-to batch difference and higher scalability of the production process to industrial quantities. Moreover, they offer the possibility to tailor the stiffness and the refractive index of the material, according to the production procedures [165].

Hydrogel based optical fibres (see Fig.6.3.d) are currently studied and are very much of interest due to their flexibility and relatively lower loss guiding compared to

silks. Proof-of-principle studies for the fabrication and use of hydrogel optical fibres in strain sensing applications have been recently published [166, 25]. Hydrogels proved to be particularly interesting for the fabrication of implantable waveguides to be used would healing trough a method named Photochemical Tissue Bonding (PTB). This method involves the use of a photosensitizer and a light source in order to induce collagen cross-linking in biological tissues [167].

Introduction to resorbable optical glasses

One of the scopes of this research work is to develop an optical quality phosphate glass that is also bioresorbable and suitable for the fabrication of optical fibres.

Calcium-phosphate glasses have been studied for long time as potential biomaterials, thanks to their ability to be dissolved in physiological conditions. They have promising features for their use in biomedical optics. The following section will give an overview of the use of phosphate glasses in biomedicine and introduce to the use of resorbable calcium-phosphate glasses in photonics.

6.2 Phosphate glasses in biomedicine: an overview

The pioneering work performed in the field of biomaterials by prof.Larry Hench led, in the early 1970s, to study in a new way the interaction between materials and tissues [168, 42]. The development of soluble phosphate glasses in 1981, introduced the concept of bioresorbability for a ceramic material, leading to an important progress in biomaterials science [41].

Phosphate based glasses have been studied in virtue of their versatility in tailoring the dissolution kinetics according to the composition, in a range of time going from few days to various months [169]. This capability allows the controlled release of a variety of ions that are embedded in the glass matrix, enabling the therapeutic use of these materials [170]. In particular the Ag^{+} and Cu^{2+} ions have been widely studied for their antibacterial properties, while Ti^{4+} is considered interesting as it is known to increase bioactivity [171–173].

Table 6.1 Overview of the main applications of phosphate glasses in hard and soft tissue engineering and relative references

Phosphate glasses in tissue engineering

Application	Implant	Development	References
Peripheral nerve growth	Micro fibres, Hollow Fibres, nano fibres, fibre bundles	Ongoing clinical trial	[18, 180, 178]
Spinal cord repair	Phosphate glass/collagen composite	Animal test	[181]
Ligament repair	Fibres, fibres composite	In vitro studies	[182]
Bone tissue engineering	Microspheres, composites composite scaffolds	Animal studies	[26, 176, 174]
Antibacterial materials	Bulk, scaffolds	In vitro studies	[171, 172]

6.2.1 Phosphate glass based biomedical devices

The properties of biocompatibility, bioresorbability, bioactivity and the variety of possible compositions that can be obtained make phosphate glasses interesting materials in tissue engineering. They have found applications both as a matrix for composites and as the main material for bone scaffolds [174–176]. The use of phosphate glass micro-spheres has been proposed for targeted treatment of cancer, trough radiotherapy or for bone tissue engineering [26, 177].

The literature on this topic is vast. Giving a complete review of all the work that has been performed is not the scope of this work, as extensive review papers are available on the fabrication and use of silicate and phosphate glasses for biomedical applications [49, 178, 179].

In this section an overview of the principal research lines on the use of phosphate glasses for biomedical applications is given. Particular attention is devoted to review the works of Novajra, Vitale Brovarone et al. on the study of phosphate glass fibres for the stimulation of neural axon growth, as this topic is closely related to the research pursued for this thesis.

Bone tissue engineering

The field of bone tissue engineering is probably the most developed line of research related to the biomedical use of phosphate glasses. A variety of methods has been proposed for the development of phosphate glass based scaffolds in the last decade [175, 176]. Particular effort was devoted to the developemnt of bioresorbable composite materials, mostly embedding phosphate glass fibres and particles in a resorbable polymeric matrix, this topic led to interesting results due to the very good matching between the mechanical properties of the composite and the human bone [183, 184].

Phosphate glasses have also been used in combination with collagen, hydroxyapatite or chitosan and proposed for the fabrication of bone scaffolds [185, 174, 186].

Soft tissue engineering

The open structure of the phosphate glass network allows the release of biologically active ion during the glass dissolution. The effect of such ions has been extensively studied. In particular, the antibacterial effect of Ag^{+} and Cu^{2+} ions was extensively studied by Knowles et al. in a series of works. It was found that concentrations of Ag^{+} ranging from 3% to 5% were bactericidal for *S. Aureus* and *E. Coli*, and reduced the proliferation of *C. Albicans* and *P. Aeruginosa* [187, 188]. The effect of copper on the proliferation of *Streptococcus Sanguis* was studied by the same group, proving the effective antibacterial effect of Cu^{2+} in a phosphate matrix [189].

The group guided by prof.Knowles also studied the potential use of *Fe* loaded phosphate glass fibres for repair of bone-ligament interface. In-vitro tests showed that a content of 3% of Fe^{3+} ions stimulates cell reproduction [182, 190].

Other applications of phosphate glass fibres in soft tissue engineering include muscle tissue engineering and spinal cord repair [178].

Phosphate glass fibres for neural axon growth

A work of particular interest for the research performed in this thesis was carried out by Vitale Brovarone, Novajra et al. and related to the application of phosphate glass fibres and hollow fibres to stimulate neural axon growth.

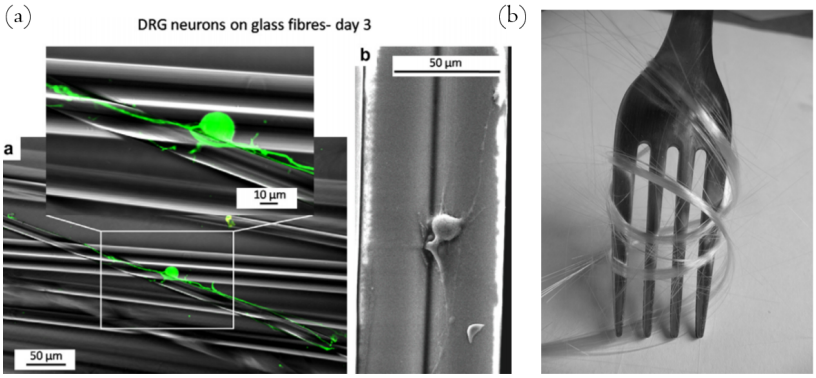

Fig. 6.1 (a) picture of neural cells growing on the surface of phosphate glass fibres, reprinted from [18] (b) a bundle of phosphate glass fibres developed for neural growth. The picture shows the flexibility of the material. Adapted from [19]. Copyright: Elsevier

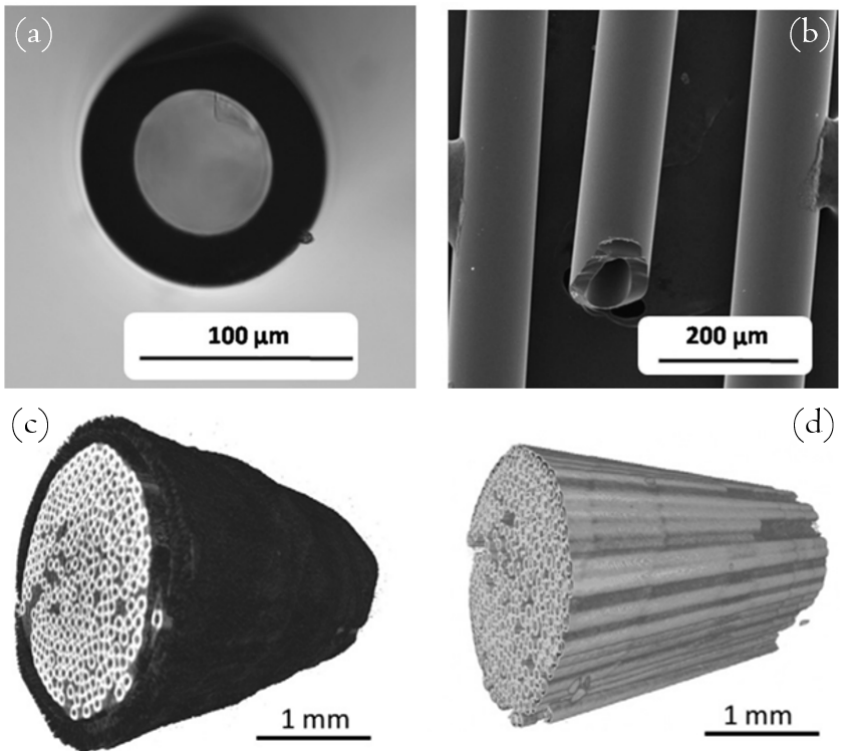

Fig. 6.2 (a) Cross section and (b) SEM of a phosphate glass hollow fibre. Adapted from [20]. (c-d) Side view of the nerve guide developed using hollow fibres. Adapted from [21]. Copyright: Elsevier

In a preliminary work the authors optimized a calcium-phosphate glass composition, containing in various concentrations of TiO_2 to optimize the dissolution time and increase glass stability. The materials proved to be stable enough for fibre drawing and were soluble in different aqueous media with low pH alteration. Single material fibres were obtained featuring different diameters and proved to be flexible end easy to handle [19].

Subsequently the fibres were used as a support for the growth of neurons. The materials proved to be reliable supports for cell adhesion and favoured a directional cell growth. This work has provided a reliable proof of the in-vitro biocompatibility of phosphate glass fibres, assessing their functionality in biological environment [18]. Fig.6.1 portrays the fibres produced for this work and the neural cells used for in-vitro testing.

The authors also explored the use of hollow fibres to increase the efficacy of the system. Hollow fibres are able to transport a liquid, potentially containing growth factors to stimulate neurons. The possibility of obtaining hollow fibres and the ability to carry and release a liquid were tested and later release tests with growth factors were explored. The authors finally succeeded in fabricating a nerve guide using the hollow fibres [20, 21]. A picture of the hollow fibres developed and the fabricated nerve guide are portrayed in Fig.6.2.

6.3 Glass based resorbable optics

In this chapter resorbable calcium-phosphate glasses (CPGs) are proposed as a new material for resorbable optics. CPGs proved to be a true contender as a biomaterial for the production of resorbable devices, thanks to the possibility of tailoring its dissolution kinetics, bioactivity and antibacterial activity by changing the composition.

The scope of the following paragraphs and of the next chapter is to demonstrate that the biological/biomedical properties of calcium phosphate glass can be combined with the optical properties of phosphate glasses. This results into the synthesis of a material that is at the same time resorbable and suitable for optical application, therefore of interest in biophotonics (see Fig.6.4).

Four glass compositions have been synthesised and characterized in terms of optical and mechanical properties, as well as in the in-vitro dissolution kinetics.

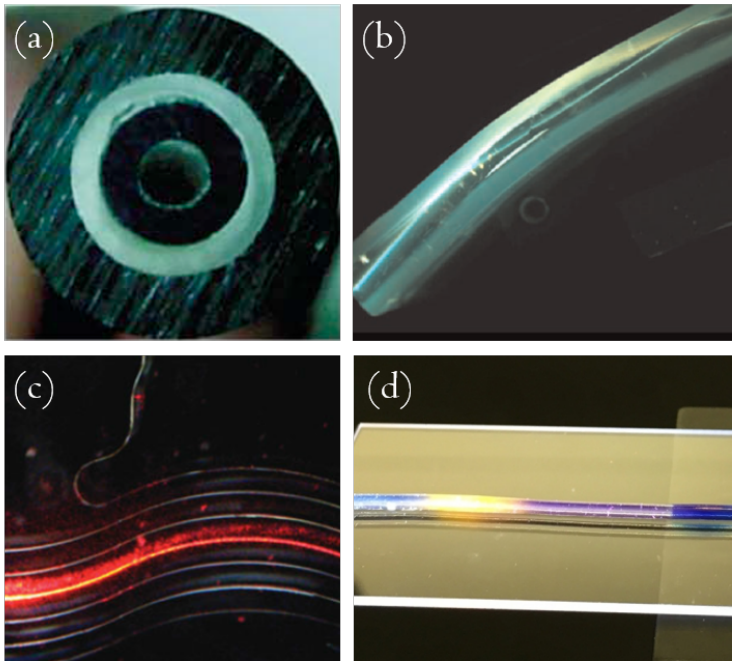

Fig. 6.3 (a) The first cellulose based degradable optical fibre [22]. (b) Agarose-gel based waveguide [23]. (c) Silk printed optical waveguide [24]. (d) Hydrogel based optical fibre [25].

The trends in the variation of the refractive index, Young's modulus and dissolution kinetics were correlated to the composition of the glass. The possibility to tailor the refractive index of the glass according to the composition allowed fabricating multi-mode and single-mode step index optical fibres, used for preliminary studies in sensing and TD-DOS imaging. Hollow fibres were also drawn and used for drug release experiments.

6.3.1 Development of the "BPh" glass matrix

The glasses presented in this section, named BPh, are inspired from the calcium-phosphate composition proposed by Burnie in 1981 [41]. This composition has been widely studied and is considered a promising biomaterial (see Chapter 8). Experiments on fibre drawing from such glasses have been performed and led to good results for their use in favouring neural axon growth. As detailed in Section 6.2 both plain and hollow fibres have been tested for this scope [21, 18].

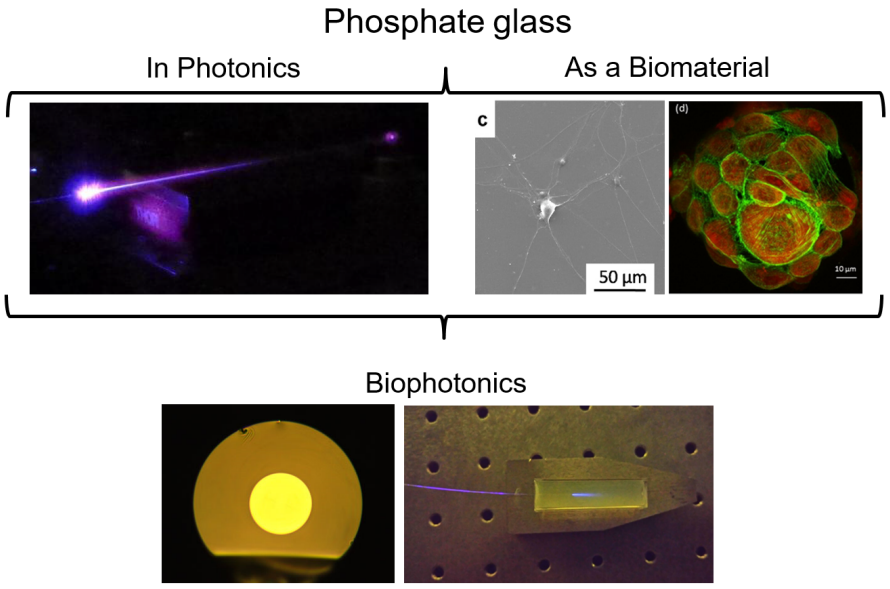

Fig. 6.4 Schematic showing the combination of optical and biomedical properties obtained in a calcium phosphate glass for biophotonic applications [18, 26].

For the first glass fabrication experiments, the composition developed by Vitale-Brovarone et al. [19] was used. The glass (namely Ti-CPG) was processed according to the conditions reported in Table 6.2. However, it was observed that the presence of Ti oxides gives a blue-violet colour to the glass, which is undesirable for guiding visible light.

The BPh glass series has been designed with the intention to obtain a transparent biomaterial. For such reason the composition and the production process were carefully studied in order to obtain a clear and homogeneous CPG. All metallic ions with biomedical functionalities that are used in resorbable phosphate glasses have been removed, to avoid the presence of absorption bands in the visible and near-infrared window. Silica, magnesium oxide and boron oxide were added to the standard sodium/calcium/phosphate composition in order to stabilize the glass against devitrification and to improve mechanical properties.

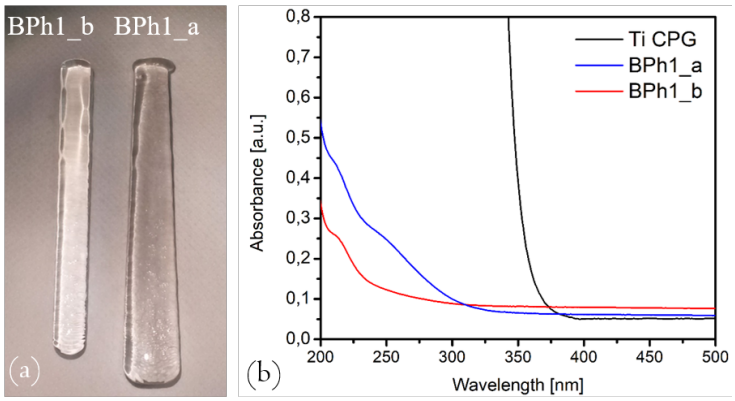

Fig. 6.5 (a) Two resorbable CPGs featuring the same composition (BPh_1) that were melt in oxidising and non-oxidising atmosphere, respectively. (b) UV-Vis spectra of the two BPh1 glasses in comparison to the spectrum of a Ti containing CPG for biomedical applications [19]

6.3.2 Fabrication of the BPh1÷BPh4 glasses

The BPh compositions designed for this work were developed with the aim to obtain a robust but soluble glass, non-toxic and suitable for fibre drawing. The materials were synthesized by conventional melt-quenching method using chemicals ($50\%\ P_2O_5 - (30-x)\%\ CaO - (3+x)\%\ MgO - 11.5\%\ Na_2O - 2.5\%\ B_2O_3 - 3\%\ SiO_2$) with high purity level ($99+\%$). Four different glasses, named BPh1÷BPh4, were obtained increasing the MgO molar concentration, ranging from 3 to 23 mol%, in substitution of CaO, ranging from 30 to 10 mol%. The chemicals were weighted and mixed within a dry box in order to minimize the hydroxyl ions ($OH-$) content in the glass. The batched chemicals were melted at a temperature of 1200 °C for 1 h under controlled atmosphere; the melt was cast into a preheated brass mould, then annealed at a temperature around the transition temperature, T_g, for 12 h to relieve internal stress. The obtained glasses were cut and optically polished to 1 mm-thick samples for optical and spectroscopic characterization. Other samples with thickness of 12 and 5 mm were respectively used for density and CTE measurements.

An additional batch of BPh1 glass was manufactured and used for the fabrication of a tube by rotational casting technique and subsequently for drawing a hollow fibre.

A batch of calcium-phosphate Ti-CPG, was fabricated to be used as a control for glass characterization. A second hollow fibre, identical to the one fabricated using

the BPh1 glass, was obtained from this material. Samples from the two hollow fibres served for the characterization of the dissolution kinetics.

Definition of the procedure of glass fabrication

The melting procedures tested for obtaining a clearly transparent glass, suitable for optical applications, are summarized in Table 6.2. Fig.6.5.a depicts two samples of glass featuring the same composition, but obtained in different melting conditions. The glass labelled "BPh1_a" was the first one to be produced, by melting the glass in a Pt crucible in a vertical furnace. The material shows a grey colour and scarce transparency. The glass labelled "BPh1_b" was the best result obtained after several attempts and it was achieved by controlling carefully the furnace atmosphere. It was found that optimal results in terms of glass transparency may be obtained by melting the glass in oxidising atmosphere, using a flow of dry air ($N_2 + O_2$, water content < 3 ppm) to the furnace during the process.

Uv-Vis absorption spectroscopy (see Chapter 3) was performed on two samples from the BPh1_a and BPh1_b batches in order to assess the origin of the grey colour of the glass. Fig.6.5.b depicts the absorption curves of the two samples. As a comparison, the same analysis was performed on a sample of Ti-CPG glass. The glass containing titanium is completely opaque at wavelengths inferior to 380 nm, whilst the BPh1_a and BPh1_b are both transparent in the near UV, up to 320 nm (BPh_a) and 260 nm (BPh_b) respectively. The BPh1_a glass shows the presence of two broad peaks located at 214 nm and 248 nm, these are almost invisible in the BPh1_b sample.

The peaks observed in the BPh1_a sample can be correlated to the presence of Pt inclusions in the glass [2]. These impurities are very common in almost all glasses, as they are introduced from the melting crucibles. Pt can be included in the glass melt in the form of particles or in ionic form. It has been observed that the variation of the melting conditions has influence on the oxidation state of platinum in the glass. It can be concluded that the oxidising atmosphere contributes to the change in the state of platinum impurities, leading to an improvement in the optical properties of the glass.

Table 6.2 Different composition and processing methods tested to obtain a clear glass

Glass label	**Composition [mol%]**	**Furnace atmosphere**	**Melting temperature** [°C]	**% weight loss**	**Colour**
Ti-CPG_a	50P2O5–30CaO 9Na2O–3SiO2 3MgO–2.5K2O 2.5TiO2	Nitrogen 10 l/min	1400	40%	Violet
Ti-CPG_b	50P2O5–30CaO 9Na2O–3SiO2 3MgO–2.5K2O 2.5TiO2	Air 3 l/min	1200	5%	Violet
BPh1_a	50 P_2O_5 – 30 CaO 3 MgO –11.5 Na_2O 2.5 B_2O_3 – 3 SiO_2	Air 3 l/min	1200	5%	Gray
BPh1_b	50 P_2O_5 – 30 CaO 3 MgO –11.5 Na_2O 2.5 B_2O_3 – 3 SiO_2	Air 5 l/min	1200	4%	Clear

Table 6.3 Thermal and physical properties of the BPh1÷BPh4 glass series in comparison to the Ti-CPG: glass transition temperature T_g, glass crystallization temperature T_x, coefficient of thermal expansion CTE, softening temperature T_s and density ρ.

Label	MgO [mol%]	T_g [±3°C]	T_x [±3°C]	CTE [$\pm 0.1 \times 10^{-6}\,K^{-1}$]	T_s [±3°C]	ρ [$\pm 5 \times 10^{-3}\,g/cm^3$]
BPh1	3	435	658	12.6	467	2.606
BPh2	8	435	628	12.2	461	2.600
BPh3	15	442	632	12.0	471	2.598
BPh4	23	444	625	12.2	477	2.589
Ti-CPG	n.a.	435	672	11.9	464	2.589

6.3.3 Properties of the "BPh" glasses

A full characterization campaign was conducted on the BPh1÷BPh4 glasses in order to assess the behaviour of the material. The procedures used for the analyses are reported in Chapter 3.

Physical and thermal properties

The values of density, characteristic temperatures and thermal expansion of the glass are reported in Table 6.3. The transition temperature (T_g), crystallization temperature (T_x), softening temperature (T_s) and the coefficient of thermal expansion (CTE), were measured by DTA and dilatometry. This allowed assessing the thermal stability parameter $\Delta T = T_g - T_x = 200 \pm 6\,^{\circ}\mathrm{C}$, demonstrating that the glasses are stable against devitrification. The T_s values are also close to the transition temperature and far from the onset crystallization temperature, suggesting that the glass presents a rather steep viscosity curve, suitable for fibre drawing and extrusion.

It is worthwhile noting that the variation in the MgO molar content has little effect in changing the bulk density of the glasses. A decrease of the thermal stability and a limited increase of the glass transition temperature can also be observed with increasing the MgO content in the glass. However, these changes are not significant. It can be concluded that the variation of the MgO content has almost no effect on the physical and thermal properties of the glass. This is desirable for manufacturing optical fibres.

Refractive indices

Fig.6.6.a reports the variation of the refractive index of the glasses at 633, 980, and 1312 nm as a function of the MgO content. The refractive indices were measured by the prism coupling method, except for the value at 980 nm, which was calculated using the Cauchy's equation [191] on the basis of the experimental data. The refractive index values appear to decrease linearly with increasing MgO molar content in substitution to CaO in the composition of the glass.

With the aim to fabricate a step-index optical fibre where the core is made from glass BPh1, all the BPh2, BPh3 and BPh4 are possible candidates as cladding glasses. It can be noticed in Fig.6.6.a that it is possible to tailor the refractive index mismatch

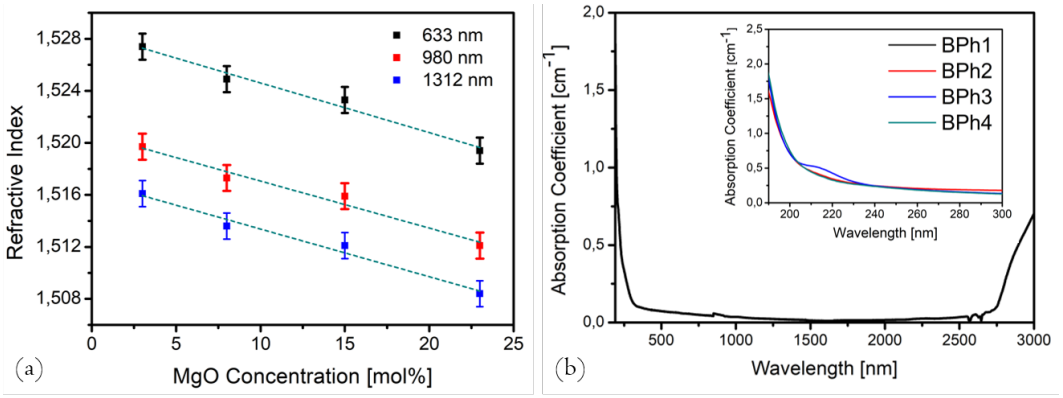

Fig. 6.6 (a) Variation of the refractive indices of the BPh1÷BPh4 glasses as a function of the MgO concentration; (b) Window of transparency of the BPh1 glass in the 190 to 3000 nm region. Detail of the UV-edge of all BPh glasses is reported in the inset.

between two compositions by choosing adequately the amount of MgO content in the glass, interpolating the refractive index data. A low MgO content allows fabricating single-mode optical fibres with small NA values. On the other hand, increasing to a maximum level the content of MgO allows obtaining cladding glasses featuring high NA values for multi-mode optical fibres. Both these approaches were exploited in order to fabricate single-mode fibres for sensing applications (see Section 7.5.1) and multi-mode fibres for time-domain diffuse optics experiments (see Section 7.5.2).

Absorption spectroscopy

The transparency of the BPh1÷BPh4 glasses was assessed through UV-Vis/NIR measurements. A typical spectrum is presented in Fig.6.6.b for BPh1 glass. In the inset of the same figure the absorption spectra of all the glasses in the wavelength region between 190 and 300 nm are reported, in order to show the UV edge of the different compositions. It can be observed that all glasses show a similar transparency window ranging from 240 to 2500 nm covering the near UV, visible and NIR wavelengths. Such window is broader than that reported for polymeric waveguides [22, 165] and most common bioglasses [192], which are usually opaque under 400 nm. This opens the prospect of using different light wavelengths, from UV to NIR regions, for various biomedical applications. The relative transparency of the glass in the near UV is also a requested feature to induce significant changes in the refractive index under intense UV irradiation [193]. This effect has been exploited in the manufacturing fibre Bragg Gratings and results are reported in 7.5.1.

6.3.4 Dissolution behaviour CPG fibres

The solubility of the material was assessed by performing a dissolution test in simulated physiological conditions. Phosphate-buffered saline solution (PBS) with $pH = 7.4$ at the temperature of 37 °C was used as a dissolution media. The tests were performed according to the procedure reported in [19]; details are reported in Chapter 3.

Two different dissolution tests were performed: one test compares the dissolution kinetics of two hollow fibres with the same geometry, the first made of Ti-CPG glass, the second made of BPh1 glass. Another test was performed on four identical single material fibres made using the BPh1, BPh2, BPh3 and BPh4 compositions.

These tests allowed assessing the solubility of the materials and the influence of composition changes on the dissolution kinetics. A trend in the dissolution time was observed as a function of the MgO concentration in the glass.

Dissolution test on hollow fibres

The hollow fibres used for this test presented a diameter of $205 \pm 5\,\mu$m. The test was performed on 15 mm-long sections of the fibres in order to compare the solubility in physiological conditions of the Ti-CPG and the BPh1 glasses. The test was performed using a volume/exposed surface ratio of $0.12\,\mathrm{ml/mm^2}$. The fibre's wall thickness and the pH of the solution were monitored as described in [28].

Fig.6.7.a displays the reduction of the hollow fibres wall as a function of time measured by optical microscopy (see Chapter 3). As it can be seen the BPh1 glass underwent complete dissolution within 21 days whilst in the same time the Ti-CPG experienced a reduction in the wall thickness of about 40 %. In both cases an almost linear dissolution profile can be observed, proving that dissolution is homogeneous throughout the tests.

The pH variation of PBS as a function of time for BPh1 and Ti-CPG glass is displayed in Fig.6.7.b. The pH value of PBS solution for the BPh1 test experienced a noticeable decrease in the first three days, followed by a rapid recovery during the following days. This is due to the faster dissolution of the BPh matrix and was not experienced for the Ti-CPG. However, in both cases the the pH values remained within the physiological range throughout the test.

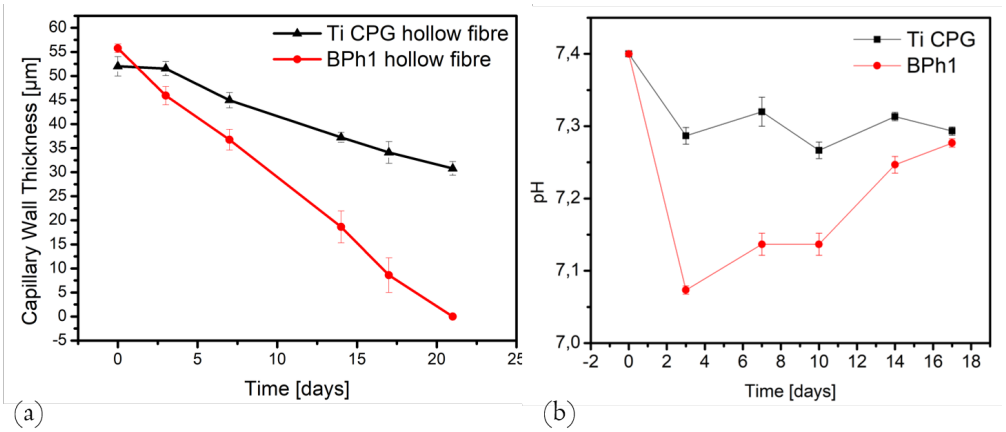

Fig. 6.7 (a) Reduction of the wall thickness of the BPh1 hollow fibre and the Ti-CPG as a function of the immersion time in PBS; (b) variation of *pH* in the PBS solution over time during the dissolution tests.

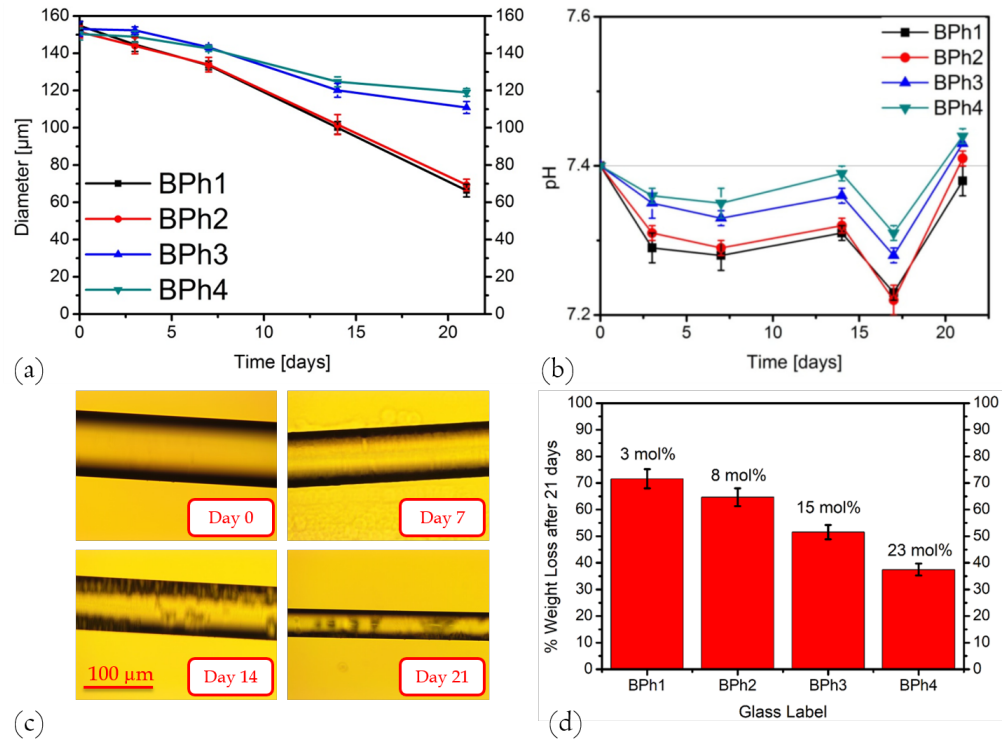

Fig. 6.8 (a) Diameter reduction of BPh1÷BPh4 glass fibres as a function of the immersion time in PBS; (b) variation of *pH* in the PBS solution over time; (c) an expample of BPH1 fibre undergoing dissolution; (d) weight loss of the samples after 21 days in PBS.

Dissolution test on single material fibres

Dissolution tests were performed on glass fibres made from the four different BPh1÷BPh4 compositions. The glasses were drawn into single material fibres with a diameter of 150±5 μm starting from cylindrical preforms of 11 mm in diameter. Two experiments were set up. In a first dissolution experiment, the decrease in diameter of the fibres was periodically monitored over the whole dissolution time. In a second experiment, the *pH* change of the solution during dissolution was monitored. The total weight loss was measured for each composition at the end of the experiment. The test was performed according to the procedure reported in [5] (see Chapter 3). An example of a BPh1 glass fibre undergoing dissolution in PBS can be seen in Fig.6.8.c.

The dissolution profile of the fibre, characterized through the reduction of the fibres diameter, is displayed in Fig.6.8.a. A clear difference in the dissolution time can be observed as a function of the composition, indicating that the BPh1 and BPh2 glasses undergo a faster dissolution in comparison to the BPh3 and BPh4. The trend is clearly highlighted by looking at the total weight loss of the material (see Fig.6.8.d). This suggests that MgO has a strengthening effect on the glass network.

The *pH* variation of the PBS solution during the test is depicted in Fig.6.8.b. Glasses undergoing faster dissolution experience a higher *pH* fluctuation, this is due to the fact that a higher amount of ions is released in a shorter time. However, in all cases the values measured are within the physiological range.

6.4 Discussion and conclusions

In this chapter the development and the full characterization of a new material is reported. For the first time to our knowledge an inorganic material was able to combine resorbability, biocompatibility and excellent optical properties. The material is suitable for crystal free fibre drawing and the possibility to tailor the refractive indices allows the design of different optical devices.

It is of interest to notice how the change in balancing just one component of the glass allowed modifying a wide range of properties, such as dissolution kinetics and refractive index. The same trend can be observed in relation to the mechanical properties, as shown in Chapter 7. In particular it is worthwhile noting that the

substitution of MgO to CaO in the glass matrix results in strengthening the glass network. This effect can be explained considering that Mg^{2+} and Ca^{2+} are glass network modifiers, able to to create a cross-linking between the non-bridging oxygens of different chains [46]. The strength of this bonds is related to the ionic radius of the atom, and results to be stronger for the smaller Mg^{2+} ion (ionic radius: 0.72 nm) than for the Ca^{2+} ion (ionic radius: 0.99 nm) [51]. This observation agrees with the thermal properties of the glasses, which show a slight increase in T_g with increasing MgO molar content. This is only an example of the possibilities opened by tuning the composition: the modification of other components in the glass may be used for increasing the photosensitivity of the material, or for introducing further functionalities (i.e. antibacterial or therapeutic properties).

The optical properties of the glass have overcome those of resorbable polymers in terms of transparency in the UV area. This has paved the way towards the application of CPGs in diverse fields, such as FBG inscription and TD-DOS.

In the next chapter will provide a detailed description of the fabrication and employment of inorganic resorbable optical fibres. The applications of such devices in time-domain diffuse optics experiments, inscription of fibre Bragg gratings and the development of hollow fibres for drug delivery are overviewed.

Chapter 7

Glass based resorbable optical fibres

Following the development of bioresorbable glasses with suitable optical properties, the second goal of this investigation was to demonstrate the first example of inorganic glass based resorbable optical devcice. In this chapter the fabrication and characterization of the resorbable waveguides developed during this Ph.D. program is reported and discussed, with particular detail on the fibres loss and modal properties.

Multi-mode and single-mode step-index fibres were manufactured and characterized, the core/cladding glass pairs were selected on the basis of previous optical characterization. BPh1 and BPh2 were chosen as core and cladding components of a single-mode fibre, due to the small value of numerical aperture ($NA = 0.08$). BPh1 and BPh4 were respectively chosen for the fabrication of the core and the cladding preforms of multi-mode optical fibres, providing an expected NA value of 0.15.

Light propagation experiments were also performed on the BPh1 hollow fibres, as a perspective use in photosensitive drug delivery and activation. The bioresorbable optical fibres were manufactured by preform drawing, where the core/cladding glass structured preform was assembled through the rod-in-tube technique.

7.1 Multi-mode optical fibers

Two multi-mode optical fibres were drawn: the first one served as a proof-of-concept experiment and was used for loss measurements and mechanical characterization (see Section 7.4), the second one was used for Time-domain Diffuse-Optics Spectroscopy

(TD-DOS) experiments in collaboration with Politecnico di Milano (see Section 7.4) [27].

7.1.1 Proof-of-concept for the fabrication of a resorbable inorganic optical fibre

This multi-mode optical fibre was fabricated by preform drawing, with the preform being obtained by rod-in-tube technique. A rod of BPh1 glass featuring a diameter of 4 mm was obtained by stretching of a 12 mm preform and used as the core of the fibre. The cladding was obtained by rotational casting using a BPh4 glass composition (see Chapter 3).

Fig.7.1 portrays the cross-section of the manufactured optical fibre. The diameter of the fibre is 125 μm and the core diameter is 43 μm. A good quality of the core/cladding interface was obtained. Fibre losses were measured by the cut-back technique using single-mode fibre pigtailed laser diode sources at 633 nm (QFLD-660-10S) and 1300 nm (Infineon SBM 52414x) as detailed in Chapter 3. Fig.7.4.b displays the results of the measurements. Attenuation loss coefficients of 6 dB/m and 15 dB/m were measured respectively at 1300 nm and 633 nm.

7.1.2 Multi-mode optical fibre for TD-DOS experiments

Time-domain diffuse optics is a spectroscopic technique that allows studying the composition of diffusive media by studying their absorption and scattering properties (see Section 7.5.2). In this technique, it is important to collect the highest possible amount of light, in order to have sufficient data to perform the desired analyses. This is a necessary requirement, as the photons that are collected and analysed are much less than those coming from the excitation source. For such reason it is important to have a fibre that features a large core and the highest possible numerical aperture.

This fibre was manufactured by following the same procedure of the previous one, however the core glass was doped with a small amount of SrO in order to further increase the refractive index. This resulted in increasing the numerical aperture of the fibre to a value of 0.17.

The fibre preform was drawn into three different diameters: two fibres with diameters of 150 and 300 μm respectively and a 600 μm cane waveguide. This corresponds to core sizes of 50, 100 and 200 μm respectively.

Fig7.2 depicts three typical sections of the optical fibres and the cane waveguide with different diameters. A defect located at the core/cladding interface of the 100 μm section can be observed by looking at Fig7.2.b. This resulted from a non-optimal adhesion of the core and cladding preforms. The presence of this defect, however, did not impair the waveguiding ability and the functionality of the fibre.

Cut-back measurements performed on different sections of the 100 μm-core fibre resulted in values of loss equal to 3.4 dB/m at 1300 nm and 4.1 dB/m at 633 μm.

7.2 Single mode optical fibre

Single-mode fibres are of interest for several applications in sensing and biosensing. In this work SM fibres have been developed to study the inscription of fiber Bragg gratings, as described in Section 7.5.1.

The single mode fibre was obtained by rod-in-tube method with the tubes being obtained by rotational casting. The same 4 mm-diameter BPh1 glass core rod used for the multi-mode fibre served as a core for this process. The procedure for the fabrication of single mode fibres involves the use of two identical cladding tubes, as depicted in Fig4.2 in Chapter 4.

A typical micrograph of the fibre cross-section is shown in Fig.7.1.a. The diameter of the fibre is 120 μm and the core diameter is 12 μm, as expected from the preform design and engineering. A homogeneous material and a good interface adhesion between core and cladding can be observed, thus demonstrating the thermo-mechanical compatibility of the two BPh1 and BPh2 glasses.

Fibre losses were measured by the cut-back technique at 633 nm and 1300 nm as done for the multi-mode fibres. Fig.7.5.b displays the results of the measurements. Attenuation loss coefficients of 1.9 dB/m and 4.7 dB/m were measured respectively at 1300 and 633 nm. These values are one to two orders of magnitude lower in the decibel scale than those published so far for bioresorbable waveguides [24, 165] and are in line with the typical loss values associated with phosphate glass optical fibres [102].

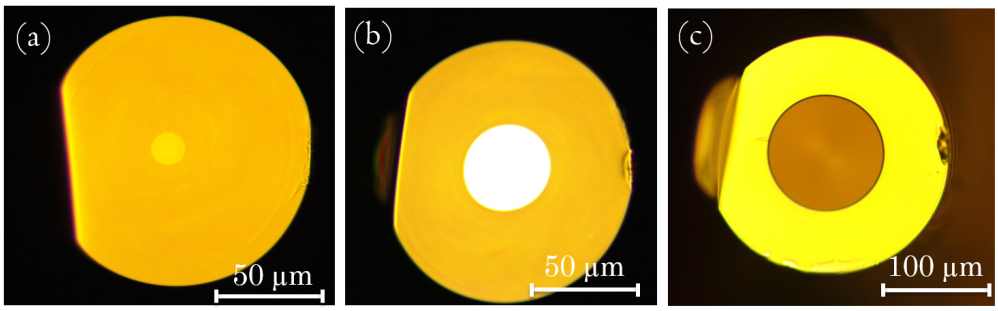

Fig. 7.1 Optical microscope pictures of different resorbable fibres: (a) Single-mode optical fibre; (b) proof-of-concept multi-mode optical fibre; (c) hollow fibre.

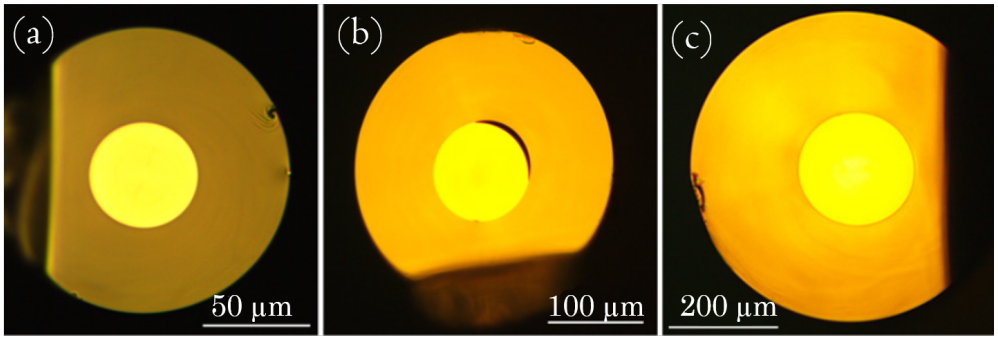

Fig. 7.2 Optical microscope pictures of multi-mode fibres and cane for TD-DOS: (a) 150 μm optical fibre; (b) 300 μm optical fibre; (c) 600 μm cane [27].

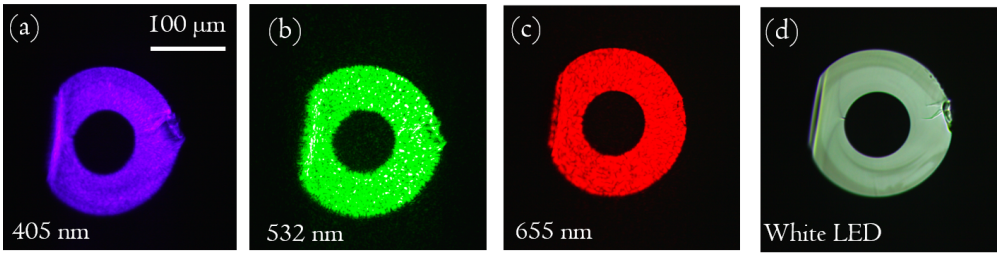

Fig. 7.3 Cleaved ends of the hollow fibre guiding visible light at (a) 405 nm, (b) 532 nm, (c) 650 nm, (d) white LED

The modal properties of the optical fibre were investigated by taking a set of near-field images of the fibre cross-section at the wavelengths of 633 and 1300 nm. The fibre operates in single-mode regime at a wavelength of 1300 nm, whilst multi-mode behaviour is observed at 633 nm (Fig.7.5.a). The estimated values of the V number, based on the refractive index measurements and the fibre size, confirm the observed behaviour: $V = 2.29$ at 1500 nm, $V = 2.44$ at 1300 nm, $V = 8.23$ at 633 nm This corresponds to 1 mode supported at 1500 nm, 2 modes supported at 1300 nm and approximately 33 modes supported at 633 nm.

7.3 Hollow glass fibre

The hollow fibre was drawn starting from a tube preform, as explained in Chapter 6. The main scope of these fibres is to be used as a drug delivery device. Besides, total internal reflection in the capillaries walls can be exploited to improve light propagation in tissues.

Light propagation experiments were performed on the 200 μm hollow fibre used for dissolution tests. The light guiding ability was assessed at 660 nm by launching a laser light through a 1 m-long section of the hollow fibre. The end facet of the fibre was observed by taking a set of near-field pictures of the cross section. A typical example is portrayed in Fig7.6.b. A loss value of 17 dB/m was measured at the wavelength of 660 nm. This value is higher than those measured on step-index fibres and is due to the absence of a core/cladding structure. However, it is still comparable to those achieved on polymeric materials [24, 165].

The UV-Vis spectra of the BPh glasses, depicted in Chapter 6, show that these glasses are transparent in the wavelength region from 260 to 2500 nm. This suggests that light guiding is possible in all the visible region and in the near UV. As a hands on demonstration of this hypothesis, a light guiding experiment was performed with three visible lasers operating in the red (650 ± 10 nm), green (532 ± 10 nm) and violet (405 ± 10 nm) region. The light was launched by end-face coupling the laser diodes to a cleaved end of the fibre, the second facet was observed though an optical microscope equipped with a camera. The end facet of the hollow fibre guiding visible light is portrayed in Fig.7.3. A picture of the fibre guiding white light from a LED source is also displayed as a comparison.

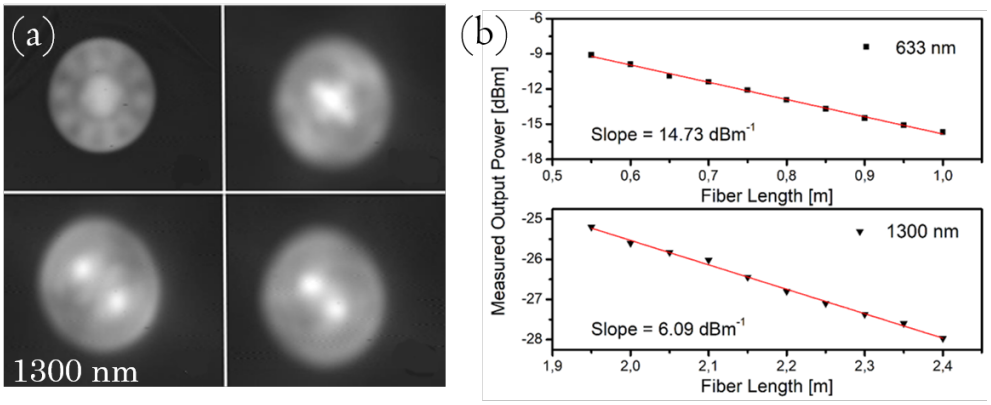

Fig. 7.4 (a) Near-field images of different modal structures on the proof-of-concept, multi-mode fibre, (b) loss of the multi-mode fibre at 633 nm and 1300 nm.

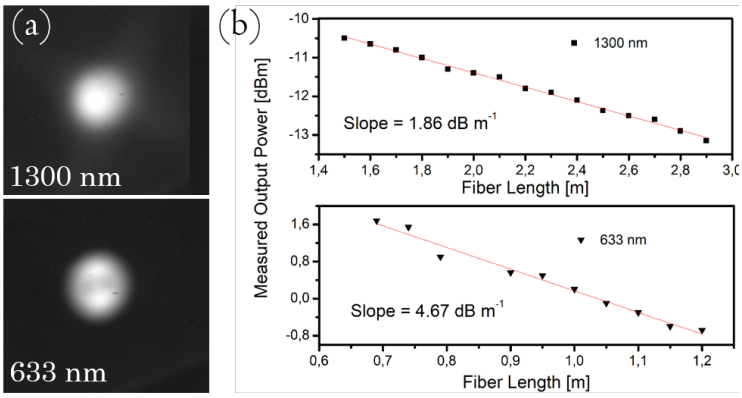

Fig. 7.5 (a) near field images of the single-mode optical fibre at 633 nm and 1300 nm. Higher order modes can be observed at 633 nm, (b) loss of the single-mode fibre at 1300 nm and 633 nm.

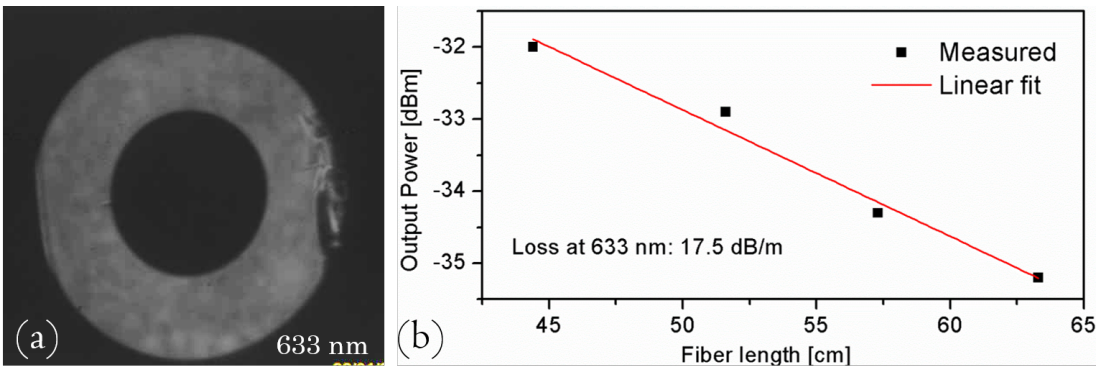

Fig. 7.6 Near field picture of the hollow fibre guiding light at 633 nm, (b) loss of the hollow fibre at 633 nm.

7.4 Mechanical properties of step-index and hollow fibres

The characterization of the mechanical properties of a biomedical device is fundamental in order to assess the reliability in clinical environment. The mechanical characterization of the optical and hollow fibres was carried out by the group of Prof. Vincenzo Sglavo at the University of Trento. An overview of the main results obtained from stress-strain measurements on the multi-mode proof-of concept-fibre and on the BPh1 hollow fibre is reported in this paragraph.

Samples of the length of 10, 60, 150 *mm* (15 samples per unit lenght) were tested to determine the Young's modulus (E) and the tensile strength (σ) of each fibre [32, 33]. The fibres were first tested in pristine conditions, subsequently the variation of fracture tensile stress was monitored during dissolution experiments in PBS.

Table 7.1 reports the values measured for the Young's modulus and the tensile strength of the pristine fibres (σ_0) and of the same fibres after a dissolution time in PBS of 675 h (σ_{675}). It can be noted that the multi-mode fibre shows higher modulus and resistance values in comparison to the hollow fibre. As the multi-mode fibre is mainly made of BPh4 glass, whilst the hollow fibre is made of BPh1 glass, it can be concluded that the increase of MgO concentration has a positive effect on the material's mechanical properties. Further mechanical tests on a BPh4 hollow fibre are currently ongoing and confirm this hypothesis.

The results obtained for this material are comparable with those measured by Sharmin et al. on single-material boro-phosphate fibres for biomedical applications [53] and with those reported for phosphate glass optical fibres [32, 33].

Table 7.1 Young's modulus and tensile fracture stress of the multi-mode fibre and the hollow fibre

	E [GPa]	σ_0 [MPa]	*St.Dev*	σ_{675} [MPa]	*St.Dev*
MM Optical fibre	55.8	350	100	280	50
BPh1 hollow fibre	39.9	225	60	100	15

7.5 Applications of resorbable optical fibres

Some perspective applications of resorbable optical fibres have been studied within the activity of this research group in collaboration with other institutions. Three main research lines have derived from the development of glass based resorbable optics:

- The single-mode fibres that were developed have been used for studying the photosensitivity of CPGs in the UV range and for the development of fibre Bragg grating sensors. This activity has been carried out in collaboration with the group of Dr.Stavros Pissadakis, at FORTH-IESL, Crete (Greece).
- High *NA* multi-mode optical fibres were employed in time-domain diffuse optics spectroscopy, as a perspective application for in-vivo imaging of biological tissues. This activity is carried out in collaboration with the group of Prof.Antonio Pifferi at Politecnico di Milano (Italy).
- Hollow fibres have been employed for the simultaneous delivery and excitation of photosensitive drugs in photodynamic therapy (PDT). This activity has been carried on in collaboration with the groups of Prof.Sonja Visentin and Prof.Claudia Barolo in University of Torino (Italy).

The following paragraphs overview the results obtained on this topics, as perspectives for future research activity.

7.5.1 Photosensitivity and fiber Bragg gratings

Fibre Bragg gratings are a well known and studied technique in optical sensing. They are made by inscribing (i.e. by using UV irradiation) a periodic pattern in the core of an optical fibre. When light is launched in a fibre containing a FBG, reflection at a very specific wavelength will be observed. The wavelength at which reflection occurs is strictly dependent on the pitch of the grating and of the effective refractive index of the fibres core.

Photosensitivity of phosphate glasses is a well known issue, in most cases FBGs have been written in phosphate glass single mode fibre by using laser light at 193 nm [194, 195]. In this work the inscription of a FBG in the single-mode resorbable fibre has been demonstrated in resorbable optical fibres by using the phase mask method

and an excimer-laser light at 193 nm as an irradiation source. An average refractive index change in the material of 5.8×10^{-4} was observed. A cleaved section of the FBG is portrayed in Fig.7.8.a [196].

The FBGs were tested in a dissolution environment (PBS) and the transmitted/reflected spectra showed clear changes after just 56 h of immersion in liquid. This result seemed to be incomparable with the dissolution of the optical fibre, that occurs on a longer time-scale. However, it was supposed that the irradiation with high intensity UV light increases the dissolution of the glass [196]. In order to confirm this hypothesis, study on the different dissolution kinetics of irradiated materials was conducted. A section of optical fibre was irradiated on a 200 μm periodic structure with the same parameters used for the FBG inscription. Subsequently a standard dissolution test in PBS was conducted (see Chapter 3). Results of observations at the optical fibre for different times are portrayed in Fig7.7, a dissolution rate of about 20 μm/day was measured on the irradiated sections of the fibre. This dissolution rate is an order of magnitude higher than the non-irradiated material.

A second dissolution experiment was conducted on a FBG sample. The dissolution occurred faster on areas undergoing higher irradiation, As confirmed by the SEM picture and the optical microscopy displayed in Fig.7.8.

7.5.2 Time-domain diffuse optics spectroscopy

In this research the fibres developed in Section 7.1 have been used for TD-DOS experiments. The fibres behaved comparably to standard silica fibres on the ex-vivo analysis of biological tissues. Fibres featuring core size of 50, 100 and 150 μm were tested, with optimal results being achieved on the 100 μm core fibre.

Diffuse optics spectroscopy is a technique that allows analysing the behaviour of light in highly diffusive media. This typically involves injecting a signal of NIR light in a sample and collecting the re-emitted light from another point in space. When the analyses is performed in the time-domain scheme it allows measuring the scattering and the absorption coefficients of a sample [159]. TD-DOS has been widely used for the analysis of biological samples as it conveys information on the composition, status and properties of a tissue [197].

During this work, a state-of-the-art set-up for TD-DOS was employed and resorbable fibres were used as a probe. At first, a series of experiments was conducted

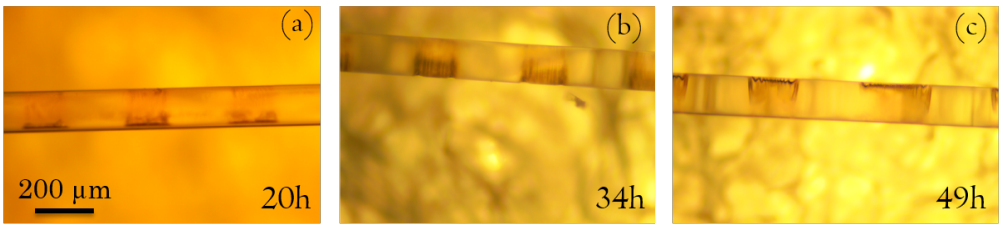

Fig. 7.7 different dissolution of irradiated and non-irradiated areas of an optical fibre after (a) 20 h, (b) 34 h, (c) 49 h of immersion in PBS.

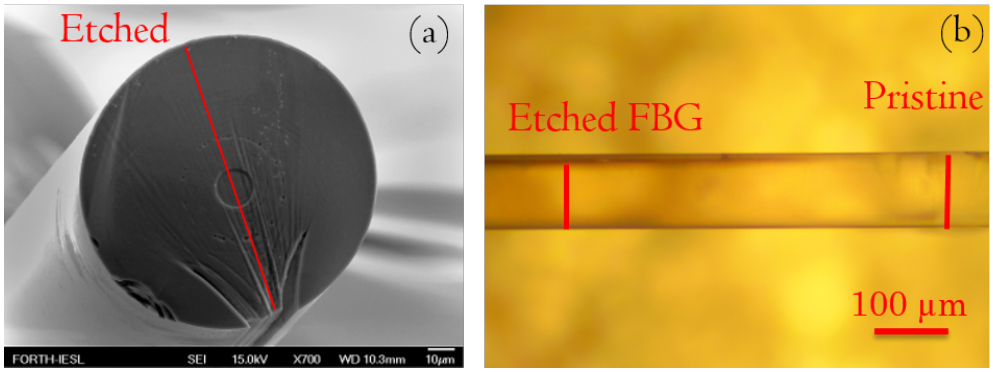

Fig. 7.8 (a) cleaved section of a fibre bragg grating after 5 h etching in water (credit: Dr. M. Konstantaki, FORTH), (b) a section of fibre being inscribed with a FBG undergoing dissolution in PBS.

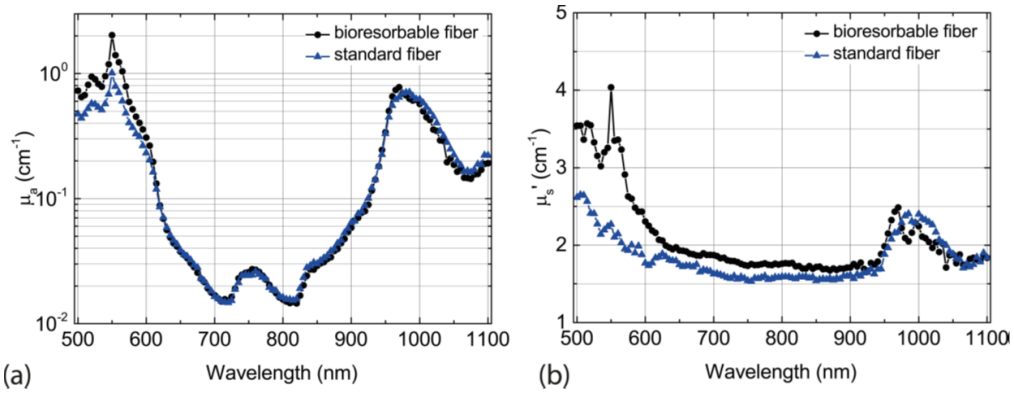

Fig. 7.9 Spectra of absorption coefficient (a) and reduced scattering (b) in a chicken breast measured by using standard silica or resorbable CPG fibres (credit: Dr. L. Di Sieno, FORTH) [27]. Copyright: Wiley.

on phantoms in order to characterize the response of the system. Finally the set-up was employed to measure the absorption and scattering coefficient in an ex-vivo experiment. A chicken breast was used as a sample. Fig.7.9 displays the measured values of absorption coefficient μ_a and the scattering coefficient μ_s measured ex-vivo by using resorbable CPG fibres in comparison to standard silica fibres [27].

Measurements were carried out over 24 h, and no degradation of the quality of the signal transmitted was observed.

7.5.3 Drug delivery through resorbable waveguides

The aim of this research is to develop a device able to perform the delivery of a photosensitive drug and at the same time guide the light necessary for its activation. This is particularly interesting for perspective use in photodynamic therapy. PDT is a cancer treatment that involves the administration of a photosensitive drug and subsequent exposure of the site to be treated to an adequate light source. The interaction between the drug and light generates strong cytotoxicity, responsible for the death of malignant cells [198]. The effectiveness of PDT is greatly determined by the possibility to reach with precision the treatment site, both with the photosensitizer and an opportune dose of light. In this framework a device able to be implanted locally is desirable. Moreover the resorbability of CPG eliminates the necessity of follow-up surgery, and paves the way towards the implementation of further diagnostic or therapeutic functionalities in the device.

The employment of hollow fibres for the controlled release of drugs has been studied in the past years [21, 20] and the results show the possibility to limit, or even totally avoid, the side effects of systemic drug administration. However, no considerations have been done so far with respect to the implementation of optical functionalities in the device.

This section describes the drug release tests performed on a BPh1 hollow fibre with a diameter of 220 μm, featuring the same properties of the hollow fibres used for mechanical, dissolution and light guiding experiments in Chapter 6. The release experiments are divided in two parts:

- In the **first part** release experiments have been performed on drugs with different chemical-physical and pharmacological profiles: theophylline, caffeine,

salicylic acid and procaine. The release kinetics of each chemical species were correlated to the influence of the interaction between the hollow fibre's surface and the corresponding molecular structure. It has been observed that some species have a more stable release with respect to others.

- In the **second part** Rose Bengal (see Fig.7.12.a) was selected as a promising photosensitizer, for its application in cancer PDT [199], antibacterial PDT [200] and photochemical tissue bonding [167]. In this case the fibre was functionalized with Trichloro(octadecyl)silane (TOS) obtaining a hydrophobic self-assembled monolayer on the internal surface of the fibre. This allowed decelerating the release kinetics, as requested for an effective clinical use of the device.

Release of non-photosensitive drugs

Fig7.10.a portrays the chemical structures of the drugs. 20 mM Stock solutions were prepared by dissolving the molecules in PBS (pH = 7.4, 2 mM). The hollow fibres were filled with each stock solution by capillary action and then cut into 2 cm-long sections. Ten sections per each drug release test were then soaked into 1 ml of clean PBS. After an initial waiting time of three minutes, the PBS solution containing the released drug was withdrawn for analysis by UV–Vis absorption spectroscopy (UH5300 Hitachi spectrophotometer) and then replaced with the same volume of fresh PBS. The procedure was repeated until complete release. The concentration of the released drug was then obtained by interpolating the appropriate calibration curve ($R^2 > 0.99$).

Different drugs were tested in order to assess the influence of different chemical structures on the interaction with the glass surface and thus on the release kinetics. At $pH = 7.4$, salicylic acid and procaine are completely in the anionic and cationic form, respectively, while theophylline and caffeine are in the neutral form. The extra methyl group in the caffeine molecule, compared to theophylline, reduces the tendency of the molecule to form hydrogen bonds, allowing to assess the influence of this interaction on the release kinetics.

Fig7.10.b displays the release profiles of the different drugs with respect to time. All drugs are released within 18 min, however ionized drugs are held for a longer time than non-ionized ones. This may be due either to the formation of hydrogen

bonding between the ionized molecules and the glass surface (charged negatively) or to the presence of electrostatic interactions between molecule and surface. Drugs with a neutral behaviour seem to react less with the glass surface and to be released more effectively. On this basis, it can be assumed that tailorable release kinetics can be obtained by an opportune surface modification of the capillary's wall, reducing the hydrophilic nature of the glass.

Release of Rose Bengal from surface-modified hollow fibres

A Trichloro(octadecyl)silane layer was applied on 2 cm-long sections of the fibre to reduce the hydrophilic nature of the glass. The following silanization protocol was used:

1. Alkaline piranha etching ($NH_4OH + H_2O_2 + H_2O$) for 10 min at room temperature.
2. Silanization of the glass by soaking the sample in a solution of TOS in hexane (10 μl in 25 ml for 1 h).
3. Final wash with abundant hexane, acetone and ethanol.

A flat sample of BPh1 glass was silanized according to the same protocol in order to assess the effectiveness of the silanization procedure. Contact angle measurements performed on a pristine and a silanized sample allowed assessing a clear change in the surface behaviour. Contact angle values on the silanized sample reached the value of 108° compared to a value of 35° measured on the pristine surface, this indicates a complete and compact deposition of the SAM. As a further confirmation of the effective deposition of the silane, AFM microscopy was performed in tapping mode both on the pristine and silanized sample. AFM morphology and phase measurements are displayed in Fig.7.11. Image analysis performed on a 1 μm^2 square area of pristine sample shows a value of roughness $R_{sq} = 0.56$ nm (see Fig.7.11.b). A value of $R_{sq} = 0.61$ nm was measured on the silanized sample (see Fig.7.11.f).

The release test were performed using a set of silanized hollow fibres and a set of pristine fibres, this second set being used as a control. The same procedure used for the non-photosensitive drug release test was applied. The Weibull equation reported in eq. 7.1 was used to fit the release data. The parameter "m" is the cumulative

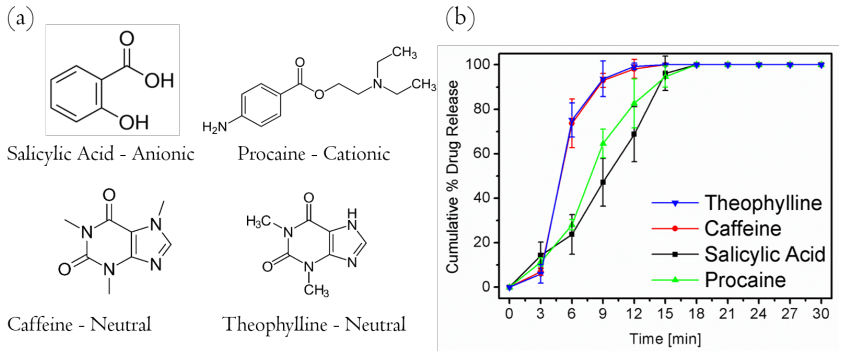

Fig. 7.10 (a) chemical structure and state of Salicylic Acid, Procaine, Caffeine and Teophylline in aqueous environment at pH = 7.4, (b) release profiles of the drugs in PBS [28].

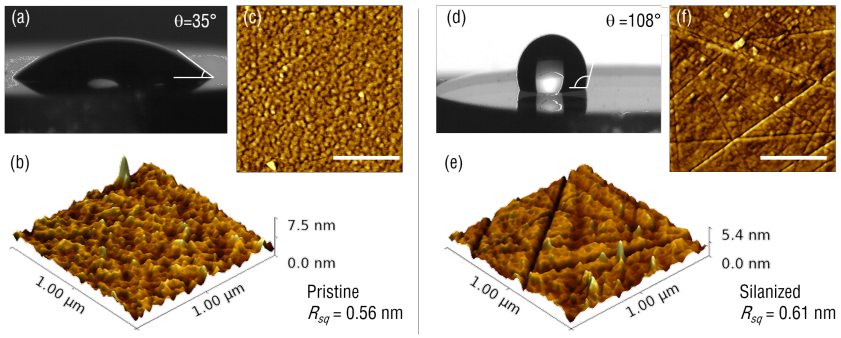

Fig. 7.11 Surface properties of the pristine and silanized glass surfaces analysed by contact angle measurement and AFM. (a)&(d) Bi-distilled water drop on a flat glass surface, (b)&(e) AFM topology of the same substrate, (c)&(f) AFM phase signal. Scale bars are 400nm.

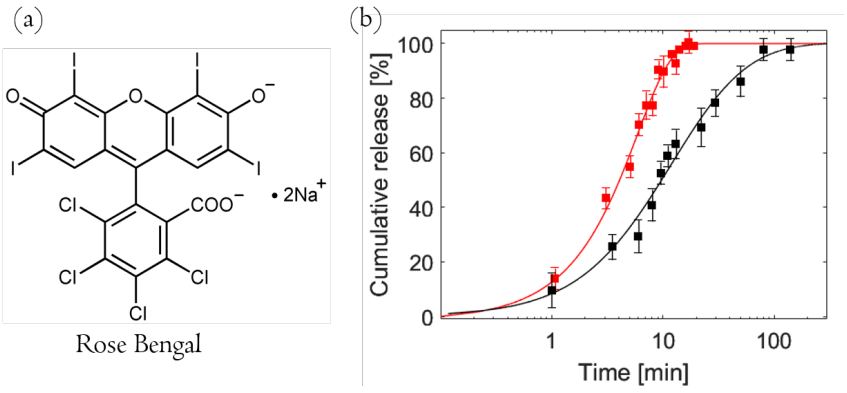

Fig. 7.12 (a) chemical structure of Rose Bengal, (b) release profiles of Rose bengal in PBS and fitting of the data with the Weibull's equation.

release, expressed in percentage or fraction, while "a" defines the time scale of the process. The exponent b is the shape factor of the equation and its value defines the behaviour of the function ($b = 1$ exponential, $b < 1$ parabolic, $b > 1$ sigmoid) [21, 201]. The parameter known as Weibull's modulus "T_d" is defined as in eq. 7.2 and represents the time at which 62.2% of the release process is complete.

$$m = 1 - \exp\left[\frac{-(t - T_i)^b}{a}\right] \tag{7.1}$$

$$a = (T_d)^b \tag{7.2}$$

Fig.7.12.b displays the release profiles of Rose Bengal for the silanized and non-silanized set of fibres. It can be noticed that the total release time increases from 10 to almost 100 min. The fitting with the Weibull's equation reveals in both sets a sigmoidal release pattern. It can be noted that 90% of the release is obtained within about 9 min for the non silanized set, whilst 70 min are needed for obtaining the same release with a silanized sample.

7.6 Discussion and conclusions

In this chapter the first examples of fully resorbable inorganic optical fibres have been presented and tested for different applications. The devices proved to behave as well as commercial silica-based fibres in time-domain diffuse optics experiments, they proved to be photosensitive and suitable for the inscription of fibre Bragg gratings. Preliminary results have been obtained regarding the functionalization of flat and curve surfaces, and the employment of hollow fibres in drug release experiments.

Overall calcium phosphate based fibres proved to outperform all resorbable devices manufactured so far, especially in terms of attenuation loss. This parameter has been reduced to values between 4 to 5 dB/m in the visible region. These are one to two orders of magnitude lower than those measured on cellulose, silks and hydrogels. Such low values have opened the possibility to use resorbable fibres in diffuse optics and generally in spectroscopy, as this applications were prevented in polymers due to the high loss. Moreover glasses are featured by a lower UV edge, allowing light guiding above the visible region, in the near UV range.

Studies on glass photosensitivity have paved the way towards the development of sensors and grating-based devices. Moreover they led to the evidence that glass dissolution kinetics can be modified by mean of intense UV irradiation. More studies are ongoing to understand and exploit this interesting phenomenon in future works.

Another aspect to be considered is the possibility to functionalize the material surface with desired molecules. An effective deposition of a TOS monolayer was obtained on a hollow fibre surface. However, this is only the first step towards the potential development of more complex surface structuring with enhanced properties, such as super-hydrophilic or super-hydrophobic structures.

Hollow fibres proved to be a promising medium to obtain a controlled release of photosensitizers, combined with an effective propagation of visible light, necessary for the drug's activation. This can be exploited in deep-tissue photodynamic therapy of cancer and infections.

It is likely that in the future multifunctional devices combining several of the functionalities described above may be developed and implemented, allowing developments in clinical practise and extending the field of application of light based therapies. The minimal impact of optical fibres on the human tissues opens the exciting prospect to access delicate and remote areas of the human body, including the brain.

Chapter 8

Conclusion

In this thesis, phosphate glasses have been studied along all their production process, starting from raw oxides and finally reaching the fabrication of a working devices. It is possible to understand how different compositions suite different applications, ranging from the development of high power lasers to the fabrication of implantable diagnostic and therapeutic devices. For the first time to the author's knowledge, good optical properties and bioresorbability have been combined in a single inorganic material, leading to the fabrication of resorbable waveguides with low loss and multiple functionalities.

A research line was followed for obtaining multiwatt power emission from a phosphate cane laser, exploring for the first time such geometry on this material. This configuration resembles the structure of an optical fibre, but shows a much larger diameter. It has the advantage to combine the shape stability of a solid state laser with the easy cooling of an optical fibre. Developing a cane laser requires fabricating core and cladding glasses with a perfect thermo-mechanical compatibility, as problems related to residual stress at the core-cladding interface become critical in this cases. This task was achieved by the developing an opportune glass composition and processing.

The employability of such fibres in spectroscopic techniques (time-domain diffuse optics), sensing and drug delivery was demonstrated, paving the way towards the use of resorbable devices different therapeutic or diagnostic techniques. At the moment, research is ongoing towards the development of multifunctional devices, able to perform at the same time a therapeutic and a diagnostic action. The in-vivo

testing of such devices is the next task to be accomplished in order to fully assess the employability of calcium phosphate glasses in resorbable optics. Hopefully, in future, this material will be exploited for the fabrication of minimally invasive medical devices, allowing some progress in the field of photomedicine.

In all these cases, the results achieved required an intense study of the materials compositions and processing. In particular the process for the fabrication of optical fibre preform proved to be critical for obtaining a well functioning device. The work performed on the extrusion of phosphate glasses allowed expanding the set of geometries available for optical fibre drawing and facilitating the development of asymmetrical structures. Finally, the minimization of interface stress in optical fibre and the optimization of the numerical aperture between core and cladding required a careful control of the glass composition. This resulted in the development of reliable and repeatable processing of the materials.

As a conclusion, phosphate glasses still have some unknown sides, and the range of their applications is vast. Additional studies can increase the functionalities of these materials, with advantageous applications in the optical and biomedical field.

Appendix A

List of acronyms and symbols

Acronyms

AFM Atomic Force Microscopy

ATR-FTIR Attenuated Reflectance Mode FTIR

CPG Calcium Phosphate Glass

CW Contiuous Wave

CVD Chemical Vapour Deposition

FBG Fibre Bragg Grating(s)

FTIR Fourier Transform Infrared Spectroscopy

ICF Inertial Confinement Fusion

IR Infra-Red

LIDAR Laser Imaging Detection and Ranging

MM Multi-mode

NIR Near Infra-Red

OC Output Coupler

ORC Optoelectronics Research Centre

PBS Phosphate Buffered Saline

PCF Photonic Crystal Fibre

PDT Photodynamic Therapy

RE Rare Earth(s)

SM Single Mode

TD-DOS Time-Domain Diffuse Optics Spectroscopy

TOS Trichloro(octadecyl) silane

UV Ultra-Violet

UV-Vis Ultra-Violet Visible

YAG Yttrium-Aluminium Garnet

Symbols

a_0 Optical loss value

CTE Coefficient of thermal expansion

E Young's modulus

g Laser gain

g_{th} Laser gain t the threshold point

k_{nonrad} Nonradiative decay rate

k_{mp} Multiphonon decay rate

k_{OH} Decay rate due to water absorption

k_{imp} Decay rate due to water impurities

I Beam intensity

k_{nonrad} Nonradiative decay rate

k_{mp} Multiphonon decay rate

k_{OH} Decay rate due to water absorption

k_{imp} Decay rate due to water impurities

K_I Fracture toughness

L Loss of the resonator

n Refractive Index

N_X Concentration of the element X [cm^{-3}]

N_0 Critical concentration for self quenching [cm^{-3}]

NA Numerical aperture

P_{th} Laser threshold pump power

T_g Glass transition temperature

T_s Glass softening temperature

T_x Glass crystallization temperature

V V-number

k_{nonrad} Nonradiative decay rate

k_{mp} Multiphonon decay rate

k_{OH} Decay rate due to water absorption

k_{imp} Decay rate due to water impurities

$v-P_2O_5$ Vitreous phosphorous pentoxide

α Absorption coefficient

η_s Laser slope efficiency

η_s Laser intrinsic slope efficiency

θ_c Critical angle for total internal reflection

ρ Density

σ tensile strength

σ_a Absorption cross-section

σ_e Emission cross-section

λ Wavelength

τ_m Measured fluorescence lifetime

$\tau(N)$ Fluorescence lifetime at the concentration N

τ_0 Lifetime at near-zero concentration

Appendix B

Publications resulting from this thesis

1. **E. Ceci-Ginistrelli**, C. Smith, D. Pugliese, J. Lousteau, N. G. Boetti, W. A. Clarkson, F. Poletti, D. Milanese "Nd-doped phosphate glass cane laser: From materials fabrication to power scaling tests" *Journal of Alloys and Compounds*,vol. 722, pp. 599-605, 2017.

2. L. Di Sieno, N. G. Boetti, A. Dalla Mora, D. Pugliese, A. Farina, S. K. Venkata Sekar, **E. Ceci-Ginistrelli**, D. Janner, A. Pifferi, D. Milanese "Towards the use of bioresorbable fibers in time-domain diffuse optics" *Journal of Biophotonics*, 2017, DOI: 10.1002/jbio.201600275 (in press).

3. **E. Ceci-Ginistrelli**, C. Pontremoli, D. Pugliese, N. Barbero, N. G. Boetti, C. Barolo, S. Visentin, D. Milanese "Drug release kinetics from biodegradable UV-transparent hollow calcium-phosphate glass fibers" *Materials Letters*, vol. 191, pp. 116-118, 2017.

4. **E. Ceci-Ginistrelli**, D. Pugliese, N. G. Boetti, G. Novajra, A. Ambrosone, J. Lousteau, C. Vitale-Brovarone, S. Abrate, D. Milanese "Novel biocompatible and resorbable UV-transparent phosphate glass based optical fiber" *Optical Materials Express*, vol. 6, pp. 2040-2051, 2016.

5. D. Pugliese, N. Boetti, J. Lousteau, **E. Ceci Ginistrelli**, E. Bertone, F. Geobaldo, D. Milanese, "Concentration quenching in an Er^{3+} doped phosphate glass for compact optical lasers and amplifiers," *Journal of Alloys and Compounds*, vol. 657, pp. 678-683, 2016.

6. Boetti N.G., Pugliese D., **Ceci Ginistrelli E.**, Lousteau J., Janner, D., Milanese, D.,"Recent advances in highly doped phosphate glass fibers for compact laser and amplifiers [Invited]", *Applied Sciences*, vol. 7, pp. 1295, 2017.

7. Pugliese, D., Konstantaki, M., Konidakis, I., **Ceci Ginistrelli E.**, Boetti N.G., Milanese, D., Pissadakis, S., "Bioresorbable optical fiber Bragg gratings", *Optics Letters*. vol. 43, pp. 671-674, 2018.

8. **Ceci Ginistrelli E.**, Pugliese, D., Boetti, N.G., Bertiond, C., Tortello, M., Sglavo, V.M., Barbero, N., Mannelli, I., Visentin, S., Barolo, C., Janner, D., Milanese, D., "Multifunctional and bioresorbable hollow fibre for local drug and light delivery" (in preparation).

References

[1] Richard K Brow. Review: the structure of simple phosphate glasses. *Journal of Non-Crystalline Solids*, 263:1 – 28, 2000.

[2] H. Bach and N. Neuroth. *The Properties of Optical Glass*. Schott Series on Glass and Glass Ceramics. Springer Berlin Heidelberg, 1998.

[3] Doris Ehrt. Phosphate and fluoride phosphate optical glasses—properties, structure and applications. *Physics and Chemistry of Glasses-European Journal of Glass Science and Technology Part B*, 56(6):217–234, 2015.

[4] Edoardo Ceci-Ginistrelli, Callum Smith, Diego Pugliese, Joris Lousteau, Nadia G. Boetti, W. Andrew Clarkson, Francesco Poletti, and Daniel Milanese. Nd-doped phosphate glass cane laser: from materials fabrication to power scaling tests. *Journal of Alloys and Compounds*, 722:599 – 605, 2017.

[5] Edoardo Ceci-Ginistrelli, Diego Pugliese, Nadia G. Boetti, Giorgia Novajra, Annarita Ambrosone, Joris Lousteau, Chiara Vitale-Brovarone, Silvio Abrate, and Daniel Milanese. Novel biocompatible and resorbable uv-transparent phosphate glass based optical fiber. *Opt. Mater. Express*, 6(6):2040–2051, Jun 2016.

[6] Pablo Lopez-Iscoa, Laeticia Petit, Jonathan Massera, Davide Janner, Nadia G Boetti, Diego Pugliese, Sonia Fiorilli, Chiara Novara, Fabrizio Giorgis, and Daniel Milanese. Effect of the addition of al 2 o 3, tio 2 and zno on the thermal, structural and luminescence properties of er 3+-doped phosphate glasses. *Journal of Non-Crystalline Solids*, 460:161–168, 2017.

[7] Nadia Giovanna Boetti, Diego Pugliese, Edoardo Ceci-Ginistrelli, Joris Lousteau, Davide Janner, and Daniel Milanese. Highly doped phosphate glass fibers for compact lasers and amplifiers: A review. *Applied Sciences*, 7(12), 2017.

[8] JH Campbell, TI Suratwala, CB Thorsness, JS Hayden, AJ Thorne, JM Cimino, AJ Marker Iii, K Takeuchi, M Smolley, and GF Ficini-Dorn. Continuous melting of phosphate laser glasses. *Journal of Non-crystalline solids*, 263:342–357, 2000.

[9] Paul R Ehrmann and John H Campbell. Nonradiative energy losses and radiation trapping in neodymium-doped phosphate laser glasses. *Journal of the American Ceramic Society*, 85(5):1061–1069, 2002.

[10] Diego Pugliese, Nadia G Boetti, Joris Lousteau, Edoardo Ceci-Ginistrelli, Elisa Bertone, Francesco Geobaldo, and Daniel Milanese. Concentration quenching in an er-doped phosphate glass for compact optical lasers and amplifiers. *Journal of Alloys and Compounds*, 657:678–683, 2016.

[11] Nadia Giovanna Boetti, Joris Lousteau, Davide Negro, Emanuele Mura, Gerardo Cristian Scarpignato, Guido Perrone, S Abrate, and Daniel Milanese. Solar pumping of solid state lasers for space mission: a novel approach. *European Space Agency*, 2012.

[12] Emanuele Mura. *Phosphate Optical Fibers for Infrared Fiber Lasers*. PhD thesis, Politecnico di Torino, Department of Applied Science and Tecology, 2013.

[13] Nadia G. Boetti, Edoardo Ceci-Ginistrelli, Diego Pugliese, Giorgia Novajra, Chiara Vitale-Brovarone, Joris Lousteau, Silvio Abrate, and Daniel Milanese. Bioresorbable calcium-phosphate optical fiber. *Advanced Photonics 2016 (IPR, NOMA, Sensors, Networks, SPPCom, SOF)*, page JTu4A.27, 2016.

[14] Joris Lousteau, Gerardo Scarpignato, Giorgos S. Athanasiou, Emanuele Mura, Nadia Boetti, Massimo Olivero, Trevor Benson, Phillip Sewell, Silvio Abrate, and Daniel Milanese. Photonic bandgap confinement in an all-solid tellurite-glass photonic crystal fiber. *Opt. Lett.*, 37(23):4922–4924, Dec 2012.

[15] Emanuele Mura, Gerardo Cristian Scarpignato, Joris Lousteau, Nadia Giovanna Boetti, S Abrate, and Daniel Milanese. Yb-doped phosphate double-cladding optical fiber laser for high-power applications. In *Proc. SPIE*. SPIE-The International Society for Optical Engineering, 2013.

[16] E. Roeder. Extrusion of glass. *Journal of Non-Crystalline Solids*, 5(5):377 – 388, 1971.

[17] Heike Ebendorff-Heidepriem, Juliane Schuppich, Alastair Dowler, Luis Lima-Marques, and Tanya M Monro. 3d-printed extrusion dies: a versatile approach to optical material processing. *Optical Materials Express*, 4(8):1494–1504, 2014.

[18] C. Vitale-Brovarone, G. Novajra, J. Lousteau, D. Milanese, S. Raimondo, and M. Fornaro. Phosphate glass fibres and their role in neuronal polarization and axonal growth direction. *Acta Biomaterialia*, 8(3):1125 – 1136, 2012.

[19] C. Vitale-Brovarone, G. Novajra, D. Milanese, J. Lousteau, and J.C. Knowles. Novel phosphate glasses with different amounts of tio2 for biomedical applications. *Materials Science and Engineering: C*, 31(2):434 – 442, 2011.

[20] G. Novajra, J. Lousteau, D. Milanese, and C. Vitale-Brovarone. Resorbable hollow phosphate glass fibres as controlled release systems for biomedical applications. *Materials Letters*, 99:125 – 127, 2013.

[21] G. Novajra, C. Tonda-Turo, C. Vitale-Brovarone, G. Ciardelli, S. Geuna, and S. Raimondo. Novel systems for tailored neurotrophic factor release based on hydrogel and resorbable glass hollow fibers. *Materials Science and Engineering: C*, 36:25 – 32, 2014.

[22] Alexandre Dupuis, Ning Guo, Yan Gao, Nicolas Godbout, Suzanne Lacroix, Charles Dubois, and Maksim Skorobogatiy. Prospective for biodegradable microstructured optical fibers. *Optics letters*, 32(2):109–111, 2007.

[23] Amy K. Manocchi, Peter Domachuk, Fiorenzo G. Omenetto, and Hyunmin Yi. Facile fabrication of gelatin-based biopolymeric optical waveguides. *Biotechnology and Bioengineering*, 103(4):725–732, 2009.

[24] Sara T. Parker, Peter Domachuk, Jason Amsden, Jason Bressner, Jennifer A. Lewis, David L. Kaplan, and Fiorenzo G. Omenetto. Biocompatible silk printed optical waveguides. *Advanced Materials*, 21(23):2411–2415, 2009.

[25] Jingjing Guo, Xinyue Liu, Nan Jiang, Ali K. Yetisen, Hyunwoo Yuk, Changxi Yang, Ali Khademhosseini, Xuanhe Zhao, and Seok-Hyun Yun. Highly stretchable, strain sensing hydrogel optical fibers. *Advanced Materials*, 28(46):10244–10249, 2016.

[26] Nilay J Lakhkar, Jeong-Hui Park, Nicola J Mordan, Vehid Salih, Ivan B Wall, Hae-Won Kim, Scott P King, John V Hanna, Richard A Martin, Owen Addison, et al. Titanium phosphate glass microspheres for bone tissue engineering. *Acta biomaterialia*, 8(11):4181–4190, 2012.

[27] Laura Di Sieno, Nadia G. Boetti, Alberto Dalla Mora, Diego Pugliese, Andrea Farina, Sanathana Konugolu Venkata Sekar, Edoardo Ceci-Ginistrelli, Davide Janner, Antonio Pifferi, and Daniel Milanese. Towards the use of bioresorbable fibers in time-domain diffuse optics. *Journal of Biophotonics*, 2017.

[28] Edoardo Ceci-Ginistrelli, Carlotta Pontremoli, Diego Pugliese, Nadia Barbero, Nadia G. Boetti, Claudia Barolo, Sonja Visentin, and Daniel Milanese. Drug release kinetics from biodegradable uv-transparent hollow calcium-phosphate glass fibers. *Materials Letters*, 191:116 – 118, 2017.

[29] Robert Adair, LL Chase, and Stephen A Payne. Nonlinear refractive-index measurements of glasses using three-wave frequency mixing. *JOSA B*, 4(6):875–881, 1987.

[30] Nadia Giovanna Boetti, Joris Lousteau, Emanuele Mura, Gerardo Cristian Scarpignato, and Daniel Milanese. Nd 3+ doped phosphate glass optical fibre lasers. In *Transparent Optical Networks (ICTON), 2013 15th International Conference on*, pages 1–5. IEEE, 2013.

[31] Nadia Giovanna Boetti, Joris Lousteau, Joris Lousteau, Emanuele Mura, Silvio Abrate, and Daniel Milanese. Cw cladding pumped phosphate glass fibre laser operating at 1.054 micron. *16th International Conference on Transparent Optical Networks*, page 6876634, 2014.

[32] Emanuele Mura, Joris Lousteau, Daniel Milanese, Silvio Abrate, and Vincenzo M. Sglavo. Phosphate glasses for optical fibers: Synthesis, characterization and mechanical properties. *Journal of Non-Crystalline Solids*, 362:147 – 151, 2013.

[33] Vincenzo M. Sglavo, Emanuele Mura, Daniel Milanese, and Joris Lousteau. Mechanical properties of phosphate glass optical fibers. *International Journal of Applied Glass Science*, 5(1):57–64, 2014.

[34] Edgar D Zanotto and John C Mauro. The glassy state of matter: Its definition and ultimate fate. *Journal of Non-Crystalline Solids*, 2017.

[35] John H Campbell, Joseph S Hayden, and Alex Marker. High-power solid-state lasers: a laser glass perspective. *International Journal of Applied Glass Science*, 2(1):3–29, 2011.

[36] J.H Campbell and T.I Suratwala. Nd-doped phosphate glasses for high-energy/high-peak-power lasers. *Journal of Non-Crystalline Solids*, 263:318 – 341, 2000.

[37] JH Campbell, EP Wallerstein, JS Hayden, DL Sapak, DE Warrington, AJ Marker III, H Toratani, H Meissner, S Nakajima, and T Izumitani. Elimination of platinum inclusions in phosphate laser glasses. Technical report, Lawrence Livermore National Lab., CA (USA), 1989.

[38] John H Campbell, Edward P Wallerstein, Joseph S Hayden, David L Sapak, David E Warrington, and AJ Marker. Effects of melting conditions on platinum-inclusion content in phosphate laser glasses. *Glass science and technology*, 68(1):11–21, 1995.

[39] Bor-Chyuan Hwang, Shibin Jiang, Tao Luo, Jason Watson, Gino Sorbello, and Nasser Peyghambarian. Cooperative upconversion and energy transfer of new high er 3+-and yb 3+–er 3+-doped phosphate glasses. *JOSA B*, 17(5):833–839, 2000.

[40] T Ohtsuki, S Honkanen, SI Najafi, and N Peyghambarian. Cooperative upconversion effects on the performance of er 3+-doped phosphate glass waveguide amplifiers. *JOSA B*, 14(7):1838–1845, 1997.

[41] J Burnie, T Gilchrist, SRI Duff, CF Drake, NGL Harding, and AJ Malcolm. Controlled release glasses (crg) for biomedical uses. *Biomaterials*, 2(4):244–246, 1981.

[42] Larry L Hench and Julia M Polak. Third-generation biomedical materials. *Science*, 295(5557):1014–1017, 2002.

[43] Larry L Hench. *An introduction to bioceramics*. World Scientific Publishing Co Inc, 2013.

[44] SS Das, BP Baranwal, CP Gupta, and Punita Singh. Characteristics of solid-state batteries with zinc/cadmium halide-doped silver phosphate glasses as electrolytes. *Journal of power sources*, 114(2):346–351, 2003.

[45] Steve W Martin. Ionic conduction in phosphate glasses. *Journal of the American Ceramic Society*, 74(8):1767–1784, 1991.

[46] Arun K Varshneya. *Fundamentals of inorganic glasses*. Elsevier, 2013.

[47] William Houlder Zachariasen. The atomic arrangement in glass. *Journal of the American Chemical Society*, 54(10):3841–3851, 1932.

[48] Gunnar Hägg. The vitreous state. *The Journal of Chemical Physics*, 3(1).

[49] Alexander Hoppe, Nusret S Güldal, and Aldo R Boccaccini. A review of the biological response to ionic dissolution products from bioactive glasses and glass-ceramics. *Biomaterials*, 32(11):2757–2774, 2011.

[50] Masayuki Yamane and Yoshiyuki Asahara. *Glasses for photonics*. Cambridge University Press, 2000.

[51] BC Bunker, GW Arnold, and J Ao Wilder. Phosphate glass dissolution in aqueous solutions. *Journal of Non-Crystalline Solids*, 64(3):291–316, 1984.

[52] Daniela Carta, Dong Qiu, Paul Guerry, Ifty Ahmed, Ensanya A Abou Neel, Jonathan C Knowles, Mark E Smith, and Robert J Newport. The effect of composition on the structure of sodium borophosphate glasses. *Journal of Non-Crystalline Solids*, 354(31):3671–3677, 2008.

[53] Nusrat Sharmin, Andrew J Parsons, Chris D Rudd, and Ifty Ahmed. Effect of boron oxide addition on fibre drawing, mechanical properties and dissolution behaviour of phosphate-based glass fibres with fixed 40, 45 and 50 mol% p_2o_5. *Journal of biomaterials applications*, 29(5):639–653, 2014.

[54] YW Lee, S Sinha, MJF Digonnet, RL Byer, and S Jiang. Measurement of high photodarkening resistance in heavily yb3+-doped phosphate fibres. *Electronics letters*, 44(1):14–16, 2008.

[55] Mark Fox. *Optical properties of solids*. AAPT, 2002.

[56] B Karmakar, P Kundu, and RN Dwivedi. Effect of vacuum dehydroxylation on the uv transparency and structure of metaphosphate glasses. *Materials Letters*, 47(6):371–375, 2001.

[57] Samir Y Marzouk and Fatma H Elbatal. Ultraviolet–visible absorption of gamma-irradiated transition metal ions doped in sodium metaphosphate glasses. *Nuclear Instruments and Methods in Physics Research Section B: Beam Interactions with Materials and Atoms*, 248(1):90–102, 2006.

[58] Ping-Yu Shih and Han-Min Shiu. Properties and structural investigations of uv-transmitting vitreous strontium zinc metaphosphate. *Materials Chemistry and Physics*, 106(2):222–226, 2007.

[59] D Ehrt, P Ebeling, and U Natura. Uv transmission and radiation-induced defects in phosphate and fluoride–phosphate glasses. *Journal of Non-Crystalline Solids*, 263:240–250, 2000.

[60] MA Marzouk, FH ElBatal, and AM Abdelghany. Ultraviolet and infrared absorption spectra of cr 2 o 3 doped–sodium metaphosphate, lead metaphosphate and zinc metaphosphate glasses and effects of gamma irradiation: a comparative study. *Spectrochimica Acta Part A: Molecular and Biomolecular Spectroscopy*, 114:658–667, 2013.

[61] M Weber, J Lynch, D Blackburn, and D Cronin. Dependence of the stimulated emission cross section of yb 3+ on host glass composition. *IEEE Journal of quantum electronics*, 19(10):1600–1608, 1983.

[62] MJ Weber. Science and technology of laser glass. *Journal of Non-Crystalline Solids*, 123(1-3):208–222, 1990.

[63] JN Sandoe, PH Sarkies, and S Parke. Variation of er3+ cross section for stimulated emission with glass composition. *Journal of Physics D: Applied Physics*, 5(10):1788, 1972.

[64] JF Philipps, T Töpfer, Heike Ebendorff-Heidepriem, D Ehrt, and R Sauerbrey. Spectroscopic and lasing properties of er3+: Yb3+-doped fluoride phosphate glasses. *Applied Physics B: Lasers and Optics*, 72(4):399–405, 2001.

[65] Michel JF Digonnet. *Rare-earth-doped fiber lasers and amplifiers, revised and expanded*. CRC press, 2001.

[66] Schott.inc. www.schott.com.

[67] Kigre.inc. www.kigre.com.

[68] Rudiger Paschotta, Johan Nilsson, Anne C Tropper, and David C Hanna. Ytterbium-doped fiber amplifiers. *IEEE Journal of quantum electronics*, 33(7):1049–1056, 1997.

[69] Zhuping Liu, Changhong Qi, Shixun Dai, Yasi Jiang, and Lili Hu. Spectra and laser properties of er3+, yb3+: phosphate glasses. *Optical Materials*, 21(4):789–794, 2003.

[70] MJ Weber, D Milam, WL Smith, et al. Nonlinear refractive index of glasses and crystals. *Opt. Eng*, 17(5):463–469, 1978.

[71] D Heiman, RW Hellwarth, and D_S Hamilton. Raman scattering and nonlinear refractive index measurements of optical glasses. *Journal of Non-Crystalline Solids*, 34(1):63–79, 1979.

[72] S Yoo, C Basu, AJ Boyland, C Sones, J Nilsson, JK Sahu, and D Payne. Photodarkening in yb-doped aluminosilicate fibers induced by 488 nm irradiation. *Optics letters*, 32(12):1626–1628, 2007.

[73] R Paschotta, Johan Nilsson, PR Barber, JE Caplen, Anne C Tropper, and David C Hanna. Lifetime quenching in yb-doped fibres. *Optics Communications*, 136(5-6):375–378, 1997.

[74] Stefano Taccheo, Hrvoje Gebavi, Achille Monteville, Olivier Le Goffic, David Landais, David Mechin, Denis Tregoat, Benoit Cadier, Thierry Robin, Daniel Milanese, et al. Concentration dependence and self-similarity of photodarkening losses induced in yb-doped fibers by comparable excitation. *Optics express*, 19(20):19340–19345, 2011.

[75] Riccardo Piccoli, Hrvoje Gebavi, Stefano Taccheo, Laurent Lablonde, Benoit Cadier, Thierry Robin, Achille Monteville, Olivier Le Goffic, David Landais, David Mechin, et al. Photodarkening mitigation in yb-doped fiber lasers by 405 nm irradiation. In *Advanced Solid State Lasers*, pages AM2A–6. Optical Society of America, 2013.

[76] Hrvoje Gebavi, Stefano Taccheo, Laurent Lablonde, Benoit Cadier, Thierry Robin, David Méchin, and Denis Tregoat. Mitigation of photodarkening phenomenon in fiber lasers by 633 nm light exposure. *Optics letters*, 38(2):196–198, 2013.

[77] Tino Eidam, Stefan Hanf, Enrico Seise, Thomas V Andersen, Thomas Gabler, Christian Wirth, Thomas Schreiber, Jens Limpert, and Andreas Tünnermann. Femtosecond fiber cpa system emitting 830 w average output power. *Optics letters*, 35(2):94–96, 2010.

[78] Cesar Jauregui, Jens Limpert, and Andreas Tünnermann. High-power fibre lasers. *Nature photonics*, 7(11):861, 2013.

[79] Arlee V Smith and Jesse J Smith. Mode instability in high power fiber amplifiers. *Optics express*, 19(11):10180–10192, 2011.

[80] Hans-Jürgen Otto, Norbert Modsching, Cesar Jauregui, Jens Limpert, and Andreas Tünnermann. Impact of photodarkening on the mode instability threshold. *Optics express*, 23(12):15265–15277, 2015.

[81] E. Snitzer. Optical maser action of nd^{+3} in a barium crown glass. *Phys. Rev. Lett.*, 7:444–446, Dec 1961.

[82] Dawei Liang, Joana Almeida, Cláudia R Vistas, Mariana Oliveira, Filipe Gonçalves, and Emmanuel Guillot. High-efficiency solar-pumped tem 00-mode nd: Yag laser. *Solar Energy Materials and Solar Cells*, 145:397–402, 2016.

[83] R Bouadjemine, D Liang, J Almeida, S Mehellou, CR Vistas, A Kellou, and E Guillot. Stable tem00-mode nd: Yag solar laser operation by a twisted fused silica light-guide. *Optics & Laser Technology*, 97:1–11, 2017.

[84] Kohei Nogata, Takenobu Suzuki, and Yasutake Ohishi. Quantum efficiency of nd 3+-doped phosphate glass under simulated sunlight. *Optical Materials*, 35(11):1918–1921, 2013.

[85] Nadia G Boetti, Davide Negro, Joris Lousteau, Francesca S Freyria, Barbara Bonelli, Silvio Abrate, and Daniel Milanese. Spectroscopic investigation of nd 3+ single doped and eu 3+/nd 3+ co-doped phosphate glass for solar pumped lasers. *Journal of Non-Crystalline Solids*, 377:100–104, 2013.

[86] Longfei Wang, Dongbing He, Suya Feng, Chunlei Yu, Lili Hu, and Danping Chen. Seven-core neodymium-doped phosphate all-solid photonic crystal fibers. *Laser Physics*, 26(1):015104, 2016.

[87] KJ Malone, Norman A Sanford, and Joseph S Hayden. Integrated optic laser emitting at 906, 1057, and 1358 nm. *Electronics Letters*, 29(8):691–693, 1993.

[88] Yin-Wen Lee, Michel JF Digonnet, Supriyo Sinha, Karel E Urbanek, Robert L Byer, and Shibin Jiang. High-power yb/sup 3+ -doped phosphate fiber amplifier. *IEEE Journal of Selected Topics in Quantum Electronics*, 15(1):93–102, 2009.

[89] Zhenhua Yu, Wei Shi, Xinzheng Dong, Jinhui Li, and Yizhu Zhao. High power all fiber-based ultrafast lasers. In *International Symposium on Ultrafast Phenomena and Terahertz Waves*, pages IW1C–4. Optical Society of America, 2016.

[90] Emmanuel Desurvire, Jay R Simpson, and PC Becker. High-gain erbium-doped traveling-wave fiber amplifier. *Optics Letters*, 12(11):888–890, 1987.

[91] Ch Basavapoornima, K Linganna, CR Kesavulu, S Ju, BH Kim, W-T Han, and CK Jayasankar. Spectroscopic and pump power dependent upconversion studies of er 3+-doped lead phosphate glasses for photonic applications. *Journal of Alloys and Compounds*, 699:959–968, 2017.

[92] JF Massicott, MC Brierley, R Wyatt, ST Davey, and D Szebesta. Low threshold, diode pumped operation of a green, er/sup 3+/doped fluoride fibre laser. *Electronics Letters*, 29(24):2119–2120, 1993.

[93] R Brede, E Heumann, J Koetke, T Danger, G Huber, and B Chai. Green upconversion laser emission in er-doped crystals at room temperature. *Applied physics letters*, 63(15):2030–2031, 1993.

[94] SY Moustafa, MR Sahar, and SK Ghoshal. Spectroscopic attributes of er 3+ ions in antimony phosphate glass incorporated with ag nanoparticles: Judd-ofelt analysis. *Journal of Alloys and Compounds*, 712:781–794, 2017.

[95] T Schweizer, Domink J Brady, and Daniel William Hewak. Fabrication and spectroscopy of erbium doped gallium lanthanum sulphide glass fibres for mid-infrared laser applications. *Optics Express*, 1(4):102–107, 1997.

[96] Andrea Ravagli, Christopher Craig, Ghada A Alzaidy, Paul Bastock, and Daniel W Hewak. Optical, thermal, and mechanical characterization of ga2se3-added gls glass. *Advanced Materials*, 2017.

[97] VP Gapontsev, SM Matitsin, AA Isineev, and VB Kravchenko. Erbium glass lasers and their applications. *Optics & Laser Technology*, 14(4):189–196, 1982.

[98] Renata Reisfeld and Christian K Jørgensen. Excited state phenomena in vitreous materials. *Handbook on the physics and chemistry of rare earths*, 9:1–90, 1987.

[99] John Caird, Vivek Agrawal, Andy Bayramian, Ray Beach, Jerry Britten, Diana Chen, Robert Cross, Christopher Ebbers, Alvin Erlandson, Michael Feit, et al. Nd: glass laser design for laser icf fission energy (life). *Fusion science and technology*, 56(2):607–617, 2009.

[100] J.H Campbell. Recent advances in phosphate laser glasses for high power applications. *P. Klocek(Ed.)*, Inorganic Optical Materials, SPIE:3–39, 1996.

[101] Fei Yang, Qing Ye, Zhengqing Pan, Dijun Chen, Haiwen Cai, Ronghui Qu, Zhongmin Yang, and Qinyuan Zhang. 100-mw linear polarization single-frequency all-fiber seed laser for coherent doppler lidar application. *Optics Communications*, 285(2):149–152, 2012.

[102] Y. W. Lee, S. Sinha, M. J. F. Digonnet, R. L. Byer, and S. Jiang. 20 w single-mode yb3+-doped phosphate fiber laser. *Opt. Lett.*, 31(22):3255–3257, Nov 2006.

[103] CB Layne, WH Lowdermilk, and M Jp Weber. Multiphonon relaxation of rare-earth ions in oxide glasses. *Physical Review B*, 16(1):10, 1977.

[104] PR Ehrmann, K Carlson, JH Campbell, Carol A Click, and Richard K Brow. Neodymium fluorescence quenching by hydroxyl groups in phosphate laser glasses. *Journal of non-crystalline solids*, 349:105–114, 2004.

[105] A Speghini, R Francini, A Martinez, M Tavernese, and M Bettinelli. Spectroscopic properties of er 3+, yb 3+ and er 3+/yb 3+ doped metaphosphate glasses. *Spectrochimica Acta Part A: Molecular and Biomolecular Spectroscopy*, 57(10), 2001.

[106] H Ebendorff-Heidepriem, W Seeber, and D Ehrt. Spectroscopic properties of nd3+ ions in phoshate glasses. *Journal of non-crystalline solids*, 183(1-2):191–200, 1995.

[107] SE Stokowski and D Krashkevich. Transition-metal ions in nd-doped glasses: spectra and effects on nd fluorescence. *MRS Online Proceedings Library Archive*, 61, 1985.

[108] Yingchao Yan, Anne Jans Faber, and Henk De Waal. Luminescence quenching by oh groups in highly er-doped phosphate glasses. *Journal of Non-Crystalline Solids*, 181(3):283–290, 1995.

[109] Laëtitia Petit, Thierry Cardinal, Jean-Jacques Videau, Etienne Durand, L Canioni, M Martines, Y Guyot, and G Boulon. Effect of niobium oxide introduction on erbium luminescence in borophosphate glasses. *Optical Materials*, 28(3):172–180, 2006.

[110] F Auzel, F Bonfigli, S Gagliari, and G Baldacchini. The interplay of self-trapping and self-quenching for resonant transitions in solids; role of a cavity. *Journal of luminescence*, 94:293–297, 2001.

[111] F Auzel, G Baldacchini, L Laversenne, and G Boulon. Radiation trapping and self-quenching analysis in yb 3+, er 3+, and ho 3+ doped y 2 o 3. *Optical Materials*, 24(1):103–109, 2003.

[112] P Babu, Hyo Jin Seo, Kyoung Hyuk Jang, R Balakrishnaiah, CK Jayasankar, Ki-Soo Lim, and V Lavín. Optical spectroscopy, 1.5 μm emission, and upconversion properties of er 3+-doped metaphosphate laser glasses. *JOSA B*, 24(9):2218–2228, 2007.

[113] F Rivera-López, P Babu, L Jyothi, UR Rodríguez-Mendoza, IR Martín, CK Jayasankar, and V Lavín. Er 3+–yb 3+ codoped phosphate glasses used for an efficient 1.5 μm broadband gain medium. *Optical Materials*, 34(8):1235–1240, 2012.

[114] V Venkatramu, R Vijaya, SF León-Luis, P Babu, CK Jayasankar, V Lavín, and LJ Dhareshwar. Optical properties of yb 3+-doped phosphate laser glasses. *Journal of Alloys and Compounds*, 509(16):5084–5089, 2011.

[115] S Taccheo, P Laporta, and C Svelto. Widely tunable single-frequency erbium–ytterbium phosphate glass laser. *Applied physics letters*, 68(19):2621–2623, 1996.

[116] J Andrew Hutchinson and Toomas H Allik. Diode array-pumped er, yb: Phosphate glass laser. *Applied physics letters*, 60(12):1424–1426, 1992.

[117] Shibin Jiang, Tao Luo, Bor-Chyuan Hwang, Fred Smekatala, Karine Seneschal, Jacques Lucas, and Nasser Peyghambarian. Er 3+-doped phosphate glasses for fiber amplifiers with high gain per unit length. *Journal of non-crystalline solids*, 263:364–368, 2000.

[118] Peter Hofmann, Christian Voigtländer, Stefan Nolte, N Peyghambarian, and Axel Schülzgen. 550-mw output power from a narrow linewidth all-phosphate fiber laser. *Journal of Lightwave Technology*, 31(5):756–760, 2013.

[119] Karine Seneschal, Frédéric Smektala, Bruno Bureau, Marie Le Floch, Shibin Jiang, Tao Luo, Jacques Lucas, and Nasser Peyghambarian. Properties and structure of high erbium doped phosphate glass for short optical fibers amplifiers. *Materials research bulletin*, 40(9):1433–1442, 2005.

[120] Marcio Luis Ferreira Nascimento and Noelio Oliveira Dantas. Assessment of glass-forming ability and the effect of la 2 o 3 on crystallization mechanism of barium–lead–zinc phosphate glasses. *Materials Letters*, 61(3):912–916, 2007.

[121] Richard A Martin and Jonathan C Knight. Silica-clad neodymium-doped lanthanum phosphate fibers and fiber lasers. *IEEE photonics technology letters*, 18(4):574–576, 2006.

[122] Qianwen Yin, Shuai Kang, Xue Wang, Shunguang Li, Dongbing He, and Lili Hu. Effect of pbo on the spectral and thermo-optical properties of nd 3+-doped phosphate laser glass. *Optical Materials*, 66:23–28, 2017.

[123] Elias Snitzer. Cylindrical dielectric waveguide modes. *JOSA*, 51(5):491–498, 1961.

[124] Nadia Giovanna Boetti, Gerardo Cristian Scarpignato, Joris Lousteau, Diego Pugliese, Lionel Bastard, Jean-Emmanuel Broquin, and Daniel Milanese. High concentration yb-er co-doped phosphate glass for optical fiber amplification. *Journal of Optics*, 17(6):065705, 2015.

[125] LG Baikova, Yu K Fedorov, VP Pukh, LV Tikhonova, TP Kazannikova, AB Sinani, and SI Nikitina. The influence of silicon oxide on the mechanical properties of metaphosphate glasses. *Glass Physics and Chemistry*, 30(5):420–424, 2004.

[126] Guang Zhang, Meng Wang, Chunlei Yu, Qinling Zhou, Jianrong Qiu, Lili Hu, Danping Chen, et al. Efficient generation of watt-level output from short-length nd-doped phosphate fiber lasers. *IEEE Photonics Technology Letters*, 23(5):350, 2011.

[127] G Zhang, CL Yu, M Wang, QL Zhou, JR Qiu, LL Hu, and DP Chen. Local-cooled watt-level nd-doped phosphate single-mode fiber laser. *Laser Physics*, 22(7):1235–1239, 2012.

[128] T Qiu, L Li, A Schulzgen, VL Temyanko, T Luo, S Jiang, A Mafi, JV Moloney, and N Peyghambarian. Generation of 9.3-w multimode and 4-w single-mode output from 7-cm short fiber lasers. *IEEE photonics technology letters*, 16(12):2592–2594, 2004.

[129] Mirko Tiegel, Andreas Herrmann, Christian Rüssel, Jörg Körner, Diethard Klöpfel, Joachim Hein, and Malte C Kaluza. Magnesium aluminosilicate glasses as potential laser host material for ultrahigh power laser systems. *Journal of Materials Chemistry C*, 1(33):5031–5039, 2013.

[130] David A Porter, Kenneth E Easterling, and Mohamed Sherif. *Phase Transformations in Metals and Alloys, (Revised Reprint)*. CRC press, 2009.

[131] Biological evaluation of medical devices - identification and quantification of degradation products from ceramics. Standard, ISO, 2001.

[132] D Findlay and RA Clay. The measurement of internal losses in 4-level lasers. *Physics Letters*, 20(3):277–278, 1966.

[133] John A Caird, Stephen A Payne, PR Staber, AJ Ramponi, LL Chase, and William F Krupke. Quantum electronic properties of the na/sub 3/ga/sub 2/li/sub 3/f/sub 12: Cr/sup 3+/laser. *IEEE journal of quantum electronics*, 24(6):1077–1099, 1988.

[134] David J. Richardson, John Nilsson, and William A. Clarkson. High power fiber lasers: current status and future perspectives. *Journal of the Optical Society of America B*, 27(11):63–92, November 2010.

[135] Junjie Luo, Luke J Gilbert, Douglas A Bristow, Robert G Landers, Jonathan T Goldstein, Augustine M Urbas, and Edward C Kinzel. Additive manufacturing of glass for optical applications. In *Proc. SPIE*, volume 9738, page 97380Y, 2016.

[136] Frederik Kotz, Karl Arnold, Werner Bauer, Dieter Schild, Nico Keller, Kai Sachsenheimer, Tobias M Nargang, Christiane Richter, Dorothea Helmer, and Bastian E Rapp. Three-dimensional printing of transparent fused silica glass. *Nature*, 544(7650):337–339, 2017.

[137] D. C. Tran, C. F. Fisher, and G. H. Sigel. Fluoride glass preforms prepared by a rotational casting process. *Electronics Letters*, 18(15):657–658, July 1982.

[138] E. Roeder. Flow behaviour of glass during extrusion. *Journal of Non-Crystalline Solids*, 7(2):203 – 220, 1972.

[139] Heike Ebendorff-Heidepriem and Tanya M. Monro. Extrusion of complex preforms for microstructured optical fibers. *Opt. Express*, 15(23):15086–15092, Nov 2007.

[140] Heike Ebendorff-Heidepriem and Tanya M. Monro. Analysis of glass flow during extrusion of optical fiber preforms. *Opt. Mater. Express*, 2(3):304–320, Mar 2012.

[141] J. Lousteau, H. Bookey, X. Jiang, C. Hill, A. Kar, and A. Jha. Fabrication of multicore tellurite glass optical fibres. In *2007 9th International Conference on Transparent Optical Networks*, volume 2, pages 305–308, July 2007.

[142] J. Lousteau, G. Jose, D. Furniss, A.B. Seddon, T.M. Benson, and A. Jha. A novel approach for the fabrication of planar waveguides from heavy metal oxide glasses. *Journal of Non-Crystalline Solids*, 355(37):1973 – 1979, 2009. Non-Oxide and New Optical Glasses 16.

[143] D Furniss, JD Shephard, and AB Seddon. A novel approach for drawing optical fibers from disparate core/clad. glasses. *Journal of non-crystalline solids*, 213:141–146, 1997.

[144] Charles J Koester and Elias Snitzer. Amplification in a fiber laser. *Applied optics*, 3(10):1182–1186, 1964.

[145] ALF Novais, NO Dantas, I Guedes, and MVD Vermelho. Spectroscopic properties of highly nd-doped lead phosphate glass. *Journal of Alloys and Compounds*, 648:338–345, 2015.

[146] Yongdan Hu, Shibin Jiang, Tao Luo, Karine Seneschal, Mike Morrell, Frédéric Smektala, Seppo Honkanen, Jacques Lucas, and N Peyghambarian. Performance of high-concentration er/sup 3+/-yb/sup 3+/-codoped phosphate fiber amplifiers. *IEEE Photonics Technology Letters*, 13(7):657–659, 2001.

[147] Fengxiao Wang, Feng Song, Shuangxin An, Wenshun Wan, Hao Guo, Shujing Liu, and Jianguo Tian. Er3+/yb3+-codoped phosphate glass for short-length high-gain fiber lasers and amplifiers. *Appl. Opt.*, 54(5):1198–1205, Feb 2015.

[148] Shuai Kang, Xue Wang, Wenbin Xu, Xin Wang, Dongbing He, and Lili Hu. Effect of b2o3 content on structure and spectroscopic properties of neodymium-doped calcium aluminate glasses. *Optical Materials*, 66:287 – 292, 2017.

[149] Yasser B. Saddeek, A.A. El-Maaref, K.A. Aly, M.M. ElOkr, and A.A. showahy. Investigations on spectroscopic and elasticity studies of nd2o3 doped canp phosphate glasses. *Journal of Alloys and Compounds*, 694:325 – 332, 2017.

[150] Longfei Wang, Hui Liu, Dongbing He, Chunlei Yu, Lili Hu, Jianrong Qiu, and Danping Chen. Phosphate single mode large mode area all-solid photonic crystal fiber with multi-watt output power. *Applied Physics Letters*, 104(13):131111, 2014.

[151] Longfei Wang, Wentao Li, Qiuchun Sheng, Qinling Zhou, Lei Zhang, Lili Hu, Jianrong Qiu, and Danping Chen. All-solid silicate photonic crystal fiber laser with 13.1 w output power and 64.5% slope efficiency. *Journal of Lightwave Technology*, 32(6):1116–1119, 2014.

[152] Nadia G. Boetti, Diego Pugliese, Edoardo Ceci-Ginistrelli, Joris Lousteau, Francesco Poletti, and Daniel Milanese. Nd 3+ doped phosphate glass waveguides for pulsed laser applications. In *Lasers Congress 2016 (ASSL, LSC, LAC)*, page JTu2A.10. Optical Society of America, 2016.

[153] John I Peterson and Gerald G Vurek. Fiber-optic sensors for biomedical applications. *Science*, 224:123–128, 1984.

[154] Ioannis N Papadopoulos, Salma Farahi, Christophe Moser, and Demetri Psaltis. High-resolution, lensless endoscope based on digital scanning through a multimode optical fiber. *Biomedical optics express*, 4(2):260–270, 2013.

[155] M. Barozzi, A. Manicardi, A. Vannucci, A. Candiani, M. Sozzi, M. Konstantaki, S. Pissadakis, R. Corradini, S. Selleri, and A. Cucinotta. Optical fiber sensors for label-free dna detection. *Journal of Lightwave Technology*, 35(16):3461–3472, Aug 2017.

[156] Angela Leung, P. Mohana Shankar, and Raj Mutharasan. A review of fiber-optic biosensors. *Sensors and Actuators B: Chemical*, 125(2):688 – 703, 2007.

[157] Charles H Camp Jr and Marcus T Cicerone. Chemically sensitive bioimaging with coherent raman scattering. *Nature Photonics*, 9(5):295–305, 2015.

[158] AP Gibson, JC Hebden, and Simon R Arridge. Recent advances in diffuse optical imaging. *Physics in medicine and biology*, 50(4):R1, 2005.

[159] Antonio Pifferi, Davide Contini, Alberto Dalla Mora, Andrea Farina, Lorenzo Spinelli, and Alessandro Torricelli. New frontiers in time-domain diffuse optics, a review. *Journal of biomedical optics*, 21(9):091310–091310, 2016.

[160] Alexandre Dupuis, Yan Gao, Ning Guo, Elio Pone, Nicolas Godbout, Suzanne Lacroix, Charles Dubois, and Maksim Skorobogatiy. Biodegradable, double-core, porous optical fiber for sensing applications. In *Optical Fiber Sensors*, page WA2. Optical Society of America, 2006.

[161] Matjaž Humar, Sheldon J. J. Kwok, Myunghwan Choi, Ali K. Yetisen, Sangyeon Cho, and Seok-Hyun Yun. Toward biomaterial-based implantable photonic devices. *Nanophotonics*, 6(2):414–434, 2017.

[162] Hu Tao, Jana M. Kainerstorfer, Sean M. Siebert, Eleanor M. Pritchard, Angelo Sassaroli, Bruce J. B. Panilaitis, Mark A. Brenckle, Jason J. Amsden, Jonathan Levitt, Sergio Fantini, David L. Kaplan, and Fiorenzo G. Omenetto. Implantable, multifunctional, bioresorbable optics. *Proceedings of the National Academy of Sciences*, 109(48):19584–19589, 2012.

[163] Xin Qiao, Zhigang Qian, Junjie Li, Hongji Sun, Yao Han, Xiaoxia Xia, Jin Zhou, Chunlan Wang, Yan Wang, and Changyong Wang. Synthetic engineering of spider silk fiber as implantable optical waveguides for low-loss light guiding. *ACS Applied Materials & Interfaces*, 9(17):14665–14676, 2017.

[164] Sami Kujala, Anna Mannila, Lasse Karvonen, Khanh Kieu, and Zhipei Sun. Natural silk as a photonics component: a study on its light guiding and nonlinear optical properties. *Scientific Reports*, 6:22358, Mar 2016. Article.

[165] Myunghwan Choi, Jin Woo Choi, Seonghoon Kim, Sedat Nizamoglu, Sei Kwang Hahn, and Seok Hyun Yun. Light-guiding hydrogels for cell-based sensing and optogenetic synthesis in vivo. *Nature Photonics*, 7(12):987–994, Dec 2013. Article.

[166] Myunghwan Choi, Matjaž Humar, Seonghoon Kim, and Seok-Hyun Yun. Step-index optical fiber made of biocompatible hydrogels. *Advanced Materials*, 27(27):4081–4086, 2015.

[167] Sedat Nizamoglu, Malte C. Gather, Matjaž Humar, Myunghwan Choi, Seonghoon Kim, Ki Su Kim, Sei Kwang Hahn, Giuliano Scarcelli, Mark Randolph, Robert W. Redmond, and Seok Hyun Yun. Bioabsorbable polymer

optical waveguides for deep-tissue photomedicine. *Nature Communications*, 7:10374, 2016.

[168] Maziar Montazerian and Edgar D Zanotto. A guided walk through larry hench's monumental discoveries. *Journal of Materials Science*, pages 1–38, 2017.

[169] Jonathan C Knowles. Phosphate based glasses for biomedical applications. *Journal of Materials Chemistry*, 13(10):2395–2401, 2003.

[170] Nilay J Lakhkar, In-Ho Lee, Hae-Won Kim, Vehid Salih, Ivan B Wall, and Jonathan C Knowles. Bone formation controlled by biologically relevant inorganic ions: role and controlled delivery from phosphate-based glasses. *Advanced drug delivery reviews*, 65(4):405–420, 2013.

[171] Robert M Moss, David M Pickup, Ifty Ahmed, Jonathan C Knowles, Mark E Smith, and Robert J Newport. Structural characteristics of antibacterial bioresorbable phosphate glass. *Advanced Functional Materials*, 18(4):634–639, 2008.

[172] EA Abou Neel, I Ahmed, J Pratten, SN Nazhat, and JC Knowles. Characterisation of antibacterial copper releasing degradable phosphate glass fibres. *Biomaterials*, 26(15):2247–2254, 2005.

[173] EA Abou Neel and JC Knowles. Physical and biocompatibility studies of novel titanium dioxide doped phosphate-based glasses for bone tissue engineering applications. *Journal of Materials Science: Materials in Medicine*, 19(1):377–386, 2008.

[174] R Govindan, G Suresh Kumar, and EK Girija. Polymer coated phosphate glass/hydroxyapatite composite scaffolds for bone tissue engineering applications. *RSC Advances*, 5(74):60188–60198, 2015.

[175] Oana Bretcanu, Francesco Baino, Enrica Verné, and Chiara Vitale-Brovarone. Novel resorbable glass-ceramic scaffolds for hard tissue engineering: from the parent phosphate glass to its bone-like macroporous derivatives. *Journal of biomaterials applications*, 28(9):1287–1303, 2014.

[176] Melba Navarro, Sergio del Valle, Salvador Martinez, Stefania Zeppetelli, Luigi Ambrosio, Josep Anton Planell, and Maria Pau Ginebra. New macroporous calcium phosphate glass ceramic for guided bone regeneration. *Biomaterials*, 25(18):4233–4241, 2004.

[177] Frank F Sene, José R Martinelli, and Emico Okuno. Synthesis and characterization of phosphate glass microspheres for radiotherapy applications. *Journal of Non-Crystalline Solids*, 354(42):4887–4893, 2008.

[178] Francesco Baino, Giorgia Novajra, Valentina Miguez-Pacheco, Aldo R Boccaccini, and Chiara Vitale-Brovarone. Bioactive glasses: special applications outside the skeletal system. *Journal of Non-Crystalline Solids*, 432:15–30, 2016.

[179] Ensanya A Abou Neel, David M Pickup, Sabeel P Valappil, Robert J Newport, and Jonathan C Knowles. Bioactive functional materials: a perspective on phosphate-based glasses. *Journal of Materials Chemistry*, 19(6):690–701, 2009.

[180] LA Jeans, T Gilchrist, and D Healy. Peripheral nerve repair by means of a flexible biodegradable glass fibre wrap: a comparison with microsurgical epineurial repair. *Journal of Plastic, Reconstructive & Aesthetic Surgery*, 60(12):1302–1308, 2007.

[181] Na-Young Joo, Jonathan C Knowles, Gil-Su Lee, Jong-Wan Kim, Hae-Won Kim, Young-Jin Son, and Jung Keun Hyun. Effects of phosphate glass fiber–collagen scaffolds on functional recovery of completely transected rat spinal cords. *Acta biomaterialia*, 8(5):1802–1812, 2012.

[182] M Bitar, JC Knowles, MP Lewis, and V Salih. Soluble phosphate glass fibres for repair of bone-ligament interface. *Journal of Materials Science: Materials in Medicine*, 16(12):1131–1136, 2005.

[183] Andrew J Parsons, Ifty Ahmed, Papia Haque, Ben Fitzpatrick, Muhammad IK Niazi, Gavin S Walker, and Chris D Rudd. Phosphate glass fibre composites for bone repair. *Journal of Bionic Engineering*, 6(4):318–323, 2009.

[184] Montse Charles-Harris, Sergio del Valle, Emilie Hentges, Pierre Bleuet, Damien Lacroix, and Josep A Planell. Mechanical and structural characterisation of completely degradable polylactic acid/calcium phosphate glass scaffolds. *Biomaterials*, 28(30):4429–4438, 2007.

[185] R Shah, ACM Sinanan, JC Knowles, NP Hunt, and MP Lewis. Craniofacial muscle engineering using a 3-dimensional phosphate glass fibre construct. *Biomaterials*, 26(13):1497–1505, 2005.

[186] Yong Zhang and Miqin Zhang. Synthesis and characterization of macroporous chitosan/calcium phosphate composite scaffolds for tissue engineering. *Journal of Biomedical Materials Research Part A*, 55(3):304–312, 2001.

[187] I Ahmed, D Ready, M Wilson, and JC Knowles. Antimicrobial effect of silver-doped phosphate-based glasses. *Journal of Biomedical Materials Research Part A*, 79(3):618–626, 2006.

[188] Sabeel P Valappil, Jonathan C Knowles, and Michael Wilson. Effect of silver-doped phosphate-based glasses on bacterial biofilm growth. *Applied and environmental microbiology*, 74(16):5228–5230, 2008.

[189] AM Mulligan, M Wilson, and JC Knowles. The effect of increasing copper content in phosphate-based glasses on biofilms of streptococcus sanguis. *Biomaterials*, 24(10):1797–1807, 2003.

[190] Rishma Shah, Derren Ready, Jonathan C Knowles, Nigel P Hunt, and Mark P Lewis. Sequential identification of a degradable phosphate glass scaffold for skeletal muscle regeneration. *Journal of tissue engineering and regenerative medicine*, 8(10):801–810, 2014.

[191] Francis A Jenkins and Harvey E White. *Fundamentals of optics*. New York: McGraw-Hill, 1957.

[192] Fatma H ElBatal and Amany ElKheshen. Preparation and characterization of some substituted bioglasses and their ceramic derivatives from the system sio 2–na 2 o–cao–p 2 o 5 and effect of gamma irradiation. *Materials Chemistry and Physics*, 110(2):352–362, 2008.

[193] Maria Konstantaki, Stavros Pissadakis, Diego Pugliese, Edoardo Ceci-Ginistrelli, Nadia G Boetti, and Daniel Milanese. Bragg grating uv inscription in a bioresorbable phosphate glass optical fiber. In *Transparent Optical Networks (ICTON), 2016 18th International Conference on*, pages 1–4. IEEE, 2016.

[194] J Albert, A Schülzgen, VL Temyanko, S Honkanen, and N Peyghambarian. Strong bragg gratings in phosphate glass single mode fiber. *Applied physics letters*, 89(10):101127, 2006.

[195] J Canning, MG Sceats, HG Inglis, and P Hill. Transient and permanent gratings in phosphosilicate optical fibers produced by the flash condensation technique. *Optics letters*, 20(21):2189–2191, 1995.

[196] Diego Pugliese, Maria Konstantaki, Ioannis Konidakis, Edoardo Ceci-Ginistrelli, Nadia G Boetti, Daniel Milanese, and Stavros Pissadakis. Bioresorbable optical fiber bragg gratings. *Optics Letters*, 43(4):671–674, 2018.

[197] Sanathana Konugolu Venkata Sekar, Alberto Dalla Mora, Ilaria Bargigia, Edoardo Martinenghi, Claus Lindner, Parisa Farzam, Marco Pagliazzi, Turgut Durduran, Paola Taroni, Antonio Pifferi, et al. Broadband (600–1350 nm) time-resolved diffuse optical spectrometer for clinical use. *IEEE Journal of Selected Topics in Quantum Electronics*, 22(3):406–414, 2016.

[198] Dennis E.J.G.J. Dolmans, Dai Fukumura, and Rakesh K. Jain. Photodynamic therapy for cancer. *Nature Reviews Cancer*, pages 380–387, May 2003.

[199] Beike Wang, Jia-Hong Wang, Qian Liu, Hao Huang, Ming Chen, Kaiyang Li, Chengzhang Li, Xue-Feng Yu, and Paul K Chu. Rose-bengal-conjugated gold nanorods for in vivo photodynamic and photothermal oral cancer therapies. *Biomaterials*, 35(6):1954–1966, 2014.

[200] Michael R Hamblin and Tayyaba Hasan. Photodynamic therapy: a new antimicrobial approach to infectious disease? *Photochemical & Photobiological Sciences*, 3(5):436–450, 2004.

[201] Paulo Costa and José Manuel Sousa Lobo. Modeling and comparison of dissolution profiles. *European Journal of Pharmaceutical Sciences*, 13(2):123 – 133, 2001.